UTILIZATION OF MOUSE TUBAL EPITHELIAL ORGANOIDS TO STUDY GENE COMBINATIONS OF HIGH GRADE SEROUS OVARIAN CARCINOMA AND CELL OF ORIGIN

A Dissertation

Presented to the faculty of the Graduate School

of Cornell University

In partial fulfillment of the requirements for the degree of

Doctor of Philosophy

By

Daryl James Phuong

August 2025

UTILIZATION OF MOUSE TUBAL EPITHELIAL ORGANOIDS TO STUDY GENE COMBINATIONS OF HIGH GRADE SEROUS OVARIAN CARCINOMA AND CELL OF ORIGIN

Daryl James Phuong, PhD

Cornell University 2025

By 2050, ovarian cancer deaths are projected to exceed 350,000 annually, a 70% increase from 2022. Of these, 70% will be high-grade serous ovarian carcinoma (HGSC), the most aggressive subtype. Understanding HGSC is crucial for improving patient outcomes, but research has been hindered by a lack of recurrent mutations aside from *TP53* and challenges related to the homologous recombination deficiency of HGSC, which can lead to significant genome loss. In my studies, I demonstrate that tubal epithelial (TE) organoids from the mouse uterine tube can be used in combinatorial screening to identify HGSC drivers and cell of origin. Using CRISPR knockout libraries, we found that *Map2k4* mutations primarily form papillary tumor phenotypes, while *Nf1* mutations lead to mesenchymal phenotypes. *Map2k4* mutations were more sensitive to paclitaxel and resistant to trametinib. Additionally, TE organoid models closely reflect their *in vivo* counterparts, with SLC1A3+ cells more likely to form organoids and exhibit ciliation. These findings highlight the potential of TE organoid models for studying HGSC genetic drivers and the cell of origin. Overall, I demonstrate the potential of this system for use in future human studies, particularly in exploring spontaneous mutations caused by tumor promoting environmental factors. These findings could lead to the development of a more thorough diagnostic and prognostic pipeline and database that help monitor and improve patient survival.

BIOGRAPHICAL SKETCH

Daryl J. Phuong was born and raised in Seattle, Washington and is the oldest of three brothers. He attended Aviation High School where he developed a love for STEM and project based learning. He then attended the University of Washington (Seattle) where he obtained a B.S. in biochemistry and chemistry. While at the University of Washington he performed undergraduate research under the mentorship of Dr. Ashley George in the lab of Dr. Susan Brockerhoff where he studied photoreceptors in zebrafish. He knew he wanted to have a career in science when he first imaged a live beating fluorescent zebrafish heart. He then worked in the lab of Dr. Jaisri Lingappa where he worked on recombinantly expressing the HIV-1 Gag protein and human ABCE1 proteins to identify the binding sites. While there, he mastered the art of plasmid cloning and cloned over 1000 plasmids. After building a strong foundation in molecular biology and biochemistry, Daryl was inspired by his post-doctoral mentors to pursue graduate studies at Cornell University in the biochemistry, molecular and cell biology program. At Cornell, Daryl joined the labs of Dr. John Schimenti and Dr. Alexander Nikitin, where he worked on projects related to identifying the genetic drivers of high grade serous ovarian carcinoma.

ACKNOWLEDGEMENTS

This dissertation was only accomplished under the guidance and mentorship of Dr. John Schimenti and Dr. Alexander Nikitin. John and Alex have taught me to become a more independent scientist and have provided both insight and resources into helping me make these challenging experiments possible. They have also helped me to develop strong mentoring and collaboration skills by allowing me the opportunity to roam and work on different projects with different individuals and lab groups. Throughout my whole PhD, they have provided me all possible opportunities that a graduate student could have. I also thank Dr. Andrew White for his challenging questions and insightful perspectives on my progress and results.

I would also like to thank Ryan C. James for his assistance and deep insight throughout my graduate school years. Ryan and I became close friends shortly after I joined the Schimenti lab and have helped each other immensely on projects and scientific discussion for which I am truly grateful. I would like to thank my friends and collaborators Yiwen Qin, Leanne R. Donahue, Leah Simon, Stephanie Tanis and Anna Wood who were always supportive.

Dr. Andrea Flesken-Nikitin, Coulter Q. Ralston, Matalin G. Pirtz and Dr. Christopher S. Ashe have been instrumental to my success. They provided a lot of ovarian cancer, computational and histological assistance and expertise during the creation of this dissertation. Without their help, many of these experiments would not be successful. I appreciate the deep knowledge and refreshing perspectives on techniques, models and hypothesis that I often overlook.

I would like to thank Dr. Jaisri R. Lingappa, Dr. Jonathan Reed, Dr. Motoko Tanaka and Dr. Brook Barajas for mentoring and inspiring me to attend graduate school. Without their support and motivation, I would not have been able to troubleshoot and design such complex experiments during my graduate studies and become such a strong independent scientist.

Finally, I would like to thank my parents Long Phuong and Cynthia Wang, and my brothers Michael and Brian Phuong who have supported me throughout my graduate studies and are always willing to lend an ear or a helping hand. I would especially like to thank my parents who instilled a strong work ethic and have always allowed me the freedom to chase my dreams.

Table of Contents

Chapter 1: Aggressive Serous Carcinomas of the Female Reproductive Tract: Cancer-Prone Cell States and Genetic Drivers

The following chapter is adapted from a manuscript submitted to *Cancers* (https://doi.org/10.3390/cancers17040604)

Conceptualization, D.J.P., M.G.P., C.Q.R., A.F.-N. and A.Y.N.; writing—original draft preparation, D.J.P., M.G.P. and C.Q.R.; writing—review and editing, all authors; visualization, D.J.P., M.G.P. and C.Q.R.; supervision, B.D.C., J.C.S., A.F.-N. and A.Y.N.; funding acquisition, M.G.P., C.Q.R., J.C.S. and A.Y.N. All authors have read and agreed to the published version of the manuscript.

Authors: Daryl J. Phuong, Matalin G. Pirtz, Coulter Q. Ralston, Benjamin D. Cosgrove, John C. Schimenti, Andrea Flesken-Nikitin, and Alexander Yu. Nikitin.

1.1 Abstract

In 2025, gynecological cancers are projected to account for approximately 10% of cancer-related deaths in women. High-grade serous ovarian carcinoma (HGSC) and serous endometrial carcinoma (SEC) are the most lethal gynecological cancer subtypes. Both malignancies commonly have *TP53* mutations, alterations of the RB1 pathway, and numerous secondary mutations. Both carcinoma types consist of poorly differentiated and highly heterogeneous cell populations at the time of detection. Latent development and rapid progression of HGSC and SEC impede the identification of definitive cells of origin and genetic drivers. Here, we review our current knowledge about cancer-prone cell states and genetic drivers. We also discuss how emerging transcriptomic and genetic tools applied to contemporary model systems may facilitate the identification of novel targets for timely detection and therapeutic intervention.

1.2 Introduction

Cancers of the ovary and uterine corpus contribute to approximately 10% of cancer-related deaths in women today (1). High-grade serous ovarian carcinoma (HGSC) and serous endometrial carcinoma (SEC) are among the most aggressive forms of cancer affecting women. They currently account for 80% of ovarian and 40% of uterine cancer-related deaths, respectively (2,3). HGSC is the most aggressive and prevalent subtype of ovarian cancer. Consequently, HGSC is most often detected in advanced stages with a 5-year survival rate of 32%; however, patients diagnosed during early stages of HGSC have a 5-year survival rate of 71% (4). Furthermore, HGSC contributes to a significant proportion of cancer-related deaths despite a relatively low incidence rate affecting only 1.3% of women(4). SEC is slightly more common than HGSC, as uterine cancers are the fourth most common cancer among women in the US, and about 10% of those cases are diagnosed as SEC (2,3). Similarly to HGSC, the overall five-year survival rate for SEC is about 30-40%, but significantly improves when identified early to as high as 80% (5). Furthermore, for poorly understood reasons, mortality rate increased in SEC patients over past decade (6,7).

Improved understanding of the key molecular and cellular mechanisms involved in the initiation and progression of these malignancies offers promise for the identification of new diagnostic markers and targets for early treatment and prevention. Unfortunately, HGSC progresses latently and commonly remain undetected until advanced stages of neoplastic progression, after the disease has spread. Although SEC can be detected earlier than HGSC due to abnormal bleeding, 30-50% of cases are nevertheless diagnosed at stage III or IV, specifically, when disease has spread to areas outside of the uterus (8–13). At

detection, these malignancies consist of poorly differentiated and highly heterogeneous cell populations. Such cells are insufficiently reminiscent of their cell of origin and contain numerous mutations of unproven importance for carcinogenesis. As a result, advancements in early detection and intervention methods have been hindered.

During recent years some progress has been made in the identification of putative precursor lesions of HGSC and SEC. However, further cell fate studies are required to definitively link these lesions to overt carcinomas. Furthermore, modeling of early cancer stages is complicated by our insufficient knowledge about normal cell lineages of target tissues and genetic cancer drivers critical for the transformation of individual states of cell differentiation.

In this review, we summarize current knowledge surrounding cancer-prone cell states and genetic drivers. We also discuss how new interdisciplinary approaches may improve our comparative understanding of early mechanisms of HGSC and SEC formation, thereby unraveling new prognostic and diagnostic tools and therapeutic modalities.

1.3 Cancer-prone cell states

1.3.1 Precancerous lesions

There is substantial evidence that HGSC can originate from either the ovarian surface epithelium (OSE) or the tubal epithelium (TE) of the uterine tube, also known as fallopian tube in humans and oviduct in various animals (4,14–18). Historically, HGSC was believed to originate from the ovarian inclusion cysts lined by OSE (18). However, studies of familial HGSC cases discovered serous tubal intraepithelial carcinoma (STIC) lesions to be a common neoplastic precursor (4,19–21). STICs exclusively form in the distal TE where they present as lesions lacking ciliation and expressing PAX8 (22). These lesions

are characterized by dysplastic epithelial cells with the loss of cell polarity, high proliferative index, and *TP53* missense or null mutations presented as increased p53 (also known as TP53 in humans and TRP53 in mice) accumulation or its total absence, respectively. Thus, clinical identification of STICs relies on hematoxylin and eosin staining, aberrant p53 immunostaining patterns, and increased number of $Ki67^+$ neoplastic cells (23). It is possible that STICs are preceded by the formation of "p53 signatures", areas of a single layer of consecutive $PAX8^+$ cells that contain aberrant p53 expression but lack cellular atypia and show a low proliferative index (20,22). The extent of STIC and p53 signature contributions to sporadic non-familiar cases remains debatable. Thus, it is currently hypothesized that many cases originate in the TE, but both sites contribute to the HGSC pathogenesis (17,18).

1.3.2 Ovarian surface epithelium

The OSE presents as a single layer of squamous epithelium capable of regeneration after ovulation (24). The inactivation of *Trp53* (mouse homologue of human *TP53*) and accompanying genes, such as tumor suppressor *Rb1*, in 2D and 3D OSE cell cultures are sufficient to drive tumor formation when reimplanted within mice (14,25). Similarly, intravital inactivation of *Trp53* and *Rb1* in OSE leads to the formation of HGSC (26). Consistent with these observations, it has been reported that a gene signature indicative of OSE origin is associated with poor outcomes, and such tumors are both more resistant to chemotherapy and predisposed to a suboptimal debulking surgery as compared to TE-derived HGSC (16). However, other studies claim that the mesenchymal subtype, typically associated with a poor prognosis, could be connected to diverse cell states present in TE cell lineages (15,27). Inconsistency between reported gene signatures and the course of

diseases in different studies suggests that the current stratifications of HGSC, according to their molecular profiles alone, are imprecise.

Further studies have identified OSE stem/progenitor cells as the main source of long-term OSE regeneration. Such cells are mainly located in the ovarian hilum region and are characterized by the expression of *Aldh1*$^{+}$, *Lgr5*$^{+}$, *Lefl*$^{+}$, *Cd133*$^{+}$, and *Krt6b*$^{+}$ (28,29) (**Figure 1**). Compared to more differentiated OSE cells, stem/progenitor cells are more easily transformed by the inactivation of *Trp53* and *Rb1* and form HGSC (28–30). These findings support the notion that OSE cells in a stem/progenitor state have a high propensity for malignant transformation, similar to cancer-prone stem cells of the hematopoietic system, intestinal tract, and skin (28,31,32). Further evaluation of specific differentiation states of human OSE may shed more light on the potential contribution of OSE subpopulations to HGSC formation.

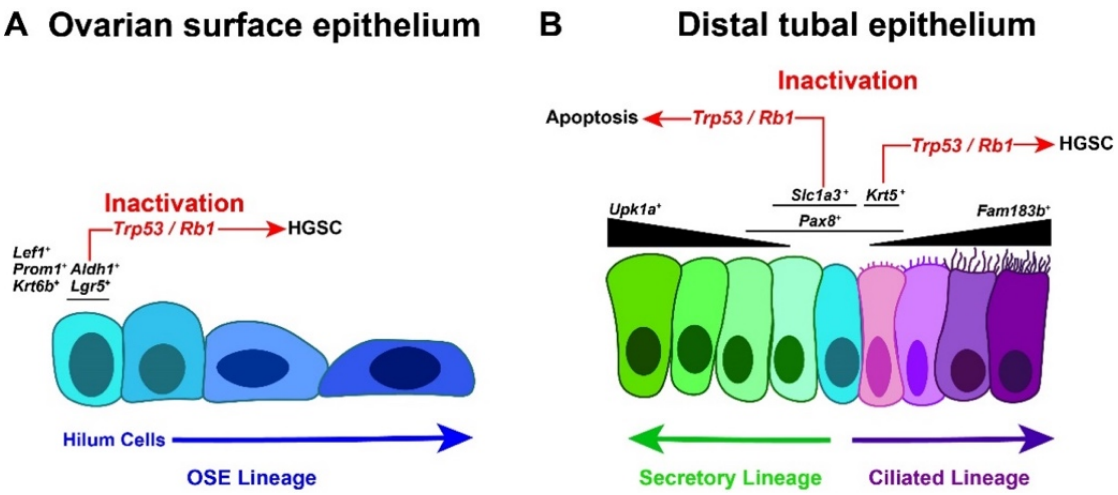

Figure 1. Cancer-prone cell states of the mouse ovarian surface epithelium (OSE) and distal tubal epithelium (DTE). (A) The differentiation trajectory of *Lgr5*$^{+}$, ALDH1^{+} stem/progenitor cells for the (OSE) begins in the hilum and encompasses the whole OSE. Inactivation of *Trp53* and *Rb1* in *Lgr5*$^{+}$ cells lead to high-grade serous carcinoma (HGSC). (B) The DTE has *Slc1a3*$^{+}$ stem/progenitor cells that give rise to secretory (*Upk1a*$^{+}$) and ciliated (*Fam183b*$^{+}$) cell lineages. *Slc1a3*$^{+}$ stem/progenitor cells do not transform and undergo apoptosis, while *Krt5*$^{+}$ pre-ciliated cells do initiate HGSC after inactivation of *Trp53* and *Rb1*. Figure made by Coulter Q. Ralston.

1.3.3 Tubal epithelium

Identifying cells of origin within the TE is exacerbated by its cellular diversity as compared to the OSE, which is composed of simple squamous epithelium. Immunophenotyping, lineage tracing, and single-cell RNA-sequencing (scRNA-seq) experiments suggest that regionally distinct cell lineages contribute to the distal and proximal uterine tube separately (33,34). The distal TE is characterized by its abundance of ciliated cells, whereas the proximal TE consists predominantly of secretory cells. Other cells described within the distal TE are basal cells assumed to be intraepithelial lymphocytes and peg cells that either serve as progenitors or exhausted secretory cells (35).

Genetic cell lineage tracing experiments in mice identified that *Pax8*$^{+}$ cells have the capacity to differentiate into ciliated cells in both the distal and proximal TE (36). Consequently, *Pax8*$^{+}$ progenitor cells have been shown to give rise to STICs and HGSC upon inactivation of *Trp53* with *Rb1* or with *Brca1*, *Brca2*, and *Pten* combinations within mouse models (37,38) (**Figure 1**). Oviductal glycoprotein 1 (OVGP1) is a marker of secretory cells within the TE, and inactivation of *Trp53*, *Brca1*, *Rb1*, and *Nf1* in *Ovgp1*-expressing cells also lead to STIC and HGSC within mouse models (39). Recently, scRNA-seq analysis of mouse uterine tubes revealed that *Pax8* and *Ovgp1* were insufficiently specific markers of epithelial cell states in the distal TE (40). *Slc1a3* was found to be a more distinct marker for stem/progenitors of the distal TE by scRNA-seq, organoid, and mouse lineage tracing studies (40). Furthermore, inactivation of *Trp53* alone or together with *Rb1* in *Slc1a3*$^{+}$ stem/progenitors led to apoptosis rather than HGSC, whereas *Krt5*$^{+}$ pre-ciliated cells expressing *Prom1* and *Trp73* (mouse homologue of *TP73*) did lead to STIC formation and HGSC after inactivation (40). *Prom1*$^{+}$ cells have also been reported

by other lineage tracing studies in mice to be capable of rapid transition into ciliated cells (41).

The characterization of human TE cell states remains incomplete due to a failure to reach a consensus on the cell states present within the TE. Human scRNA-seq analyses have met inconclusive results with discrepancies over lineage dynamics and transitional cell states (42–45). Specifically, *RUNX3*$^{+}$ cells were described as transitional pre-ciliated cells within one study, while another study identified *RUNX3*$^{+}$ cells as basal cells (43,44). Further debate exists among progenitor and lineage dynamics, where some claim that *KRT17*$^{+}$ secretory cells are progenitors, while others believe there are two distinct lineages contributing to ciliated and secretory cells separately (42–44). Among the scRNA-seq analyses, mechanisms involved with ciliogenesis were revealed to share expression with ovarian cancer risk genes, suggesting that ciliated cells are implicated in the origin of HGSC in humans as well (45). Consistent with mouse data, there is further evidence that the ciliated cell lineage is involved with HGSC as ciliogenesis-related *TP73* is upregulated in epithelial ovarian cancers (46). However, more research is needed to identify cellular origins of HGSC in the human TE. Mouse models point to a pre-ciliated cell state as a cell of origin, and a conclusive cell state hierarchy within humans can enable direct comparison of mouse studies to the discovery of a cell of origin in humans.

1.4 Genetic drivers

Genomic sequencing of HGSC and SEC tumor samples has been instrumental in identifying genetic drivers of theses cancers (47,48). Genetic alterations induce transformation and malignant characteristics such as a loss of cell cycle control (RB1

pathways), increased cellular proliferation (RAS and PI3K pathways), and DNA repair deficiencies (HRD pathways).

The tumor suppressor gene *TP53* is mutated in most HGSC and SEC (**Figure 2**). p53 has a critical role in cell cycle progression, apoptosis, genomic stability and senescence. Supporting the critical role of p53 alterations in the early stages of carcinogenesis, almost all STIC and SEIC lesions carry *TP53* mutations (3,47–49). Other mutations in p53 pathway, such as the amplification of *MDM2* (a negative regulator of p53) (50) or dysregulation of *mir-34* (a microRNA regulated by p53), also promote ovarian, prostate, and breast cancers (51–53). However, previous studies have demonstrated that *Trp53* loss in mice and organoid models is necessary but insufficient for initiating HGSC (14,25,26,29,50).

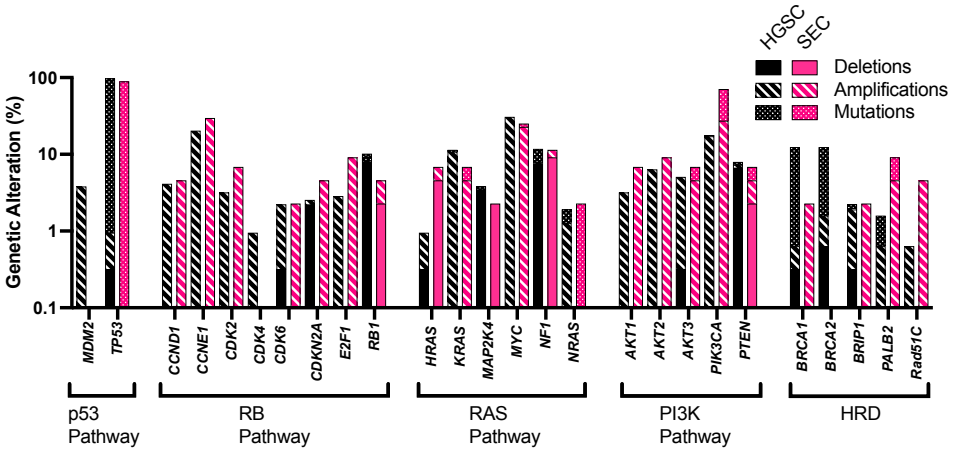

Figure 2. Comparison of genetically altered gene frequency between high-grade serous carcinoma (HGSC) and serous endometrial carcinoma (SEC). Genetic alterations are defined as gene mutations, amplifications and deep deletion events. 316 HGSC (47) samples and 44 SEC (48) samples were analyzed (TCGA datasets extracted via the cBioPortal interface) and plotted on a logarithmic scale. Note lack of *MDM2*, *CDK4*, *BRCA1*, and *BRCA2* alterations in SEC.

The RB1 pathway is also commonly dysfunctional in HGSC and SEC (54–56) (**Figure 2**). This pathway includes the tumor suppressor genes *RB1* and *CDKN2A* and the oncogenes *CCND1, CCNE1, CDK2, CDK4, CDK6* and *E2F1*. Together they control cell cycle progression, chromatin remodeling and senescence (57,58). Genetically altered *RB1* is observed in 10.13% of HGSC (47) and 4.55% of SEC (48,59), respectively. *CDKN2A* is also genetically altered at a frequency of 2.53% in HGSC and 4.55% in SEC. Overall the RB1 pathway gene alterations are observed in 35.76% of HGSC and 45.45% of SEC. Concurrent loss of *Trp53* and RB1 pathway-related genes in genetically modified mice result in HGSC (14,28) and SEC (37,60). These data suggest that loss of *TP53* and alterations in RB1-related pathway are essential for both HGSC and SEC.

In addition to alterations in *Trp53* and RB1 pathway-related genes, HGSC and SEC contain a number of other concurrent alterations that may further facilitate carcinogenesis (29). By using CRISPR-Cas9 mutagenesis in TE and OSE, the combinations of key gene drivers for HGSC development have been identified (25,29,61).

Disruption of the RTK-RAS-MEK pathway allows transformed cells to undergo rapid and uncontrolled proliferation and is common across many cancers, including HGSC and SEC (**Figure 2**). *Nf1* mutations have been shown to drive HGSC and other cancers (25,59,61). However, *KRAS* mutations have been associated with low-grade serous ovarian carcinomas (62,63). Both HGSC and SEC have similar rates of genetic perturbations of RAS pathway related genes (47). MYC, a downstream factor of this pathway, is often overexpressed in HGSC and SEC. Overexpression of MYC in combination with other mutations have been validated in mouse models as drivers of HGSC (14). Loss of *Nf1* in *Trp53* deficient TE cells also results in HGSC-like phenotype

(61,64). The impact of MYC and NF1 alterations on SEC formation in mice remains to be clarified.

Both HGSC and SEC also have alterations in the PI3K pathway regulating cell proliferation and survival (**Figure 2**). However, their contributions significantly differ for some genes. For example, amplified *PIK3CA* is detected in 17.08% of HGSC and 27.27% of SEC. *PTEN* mutations are more common in endometrioid types of ovarian and endometrial carcinomas, but also observed in advanced stages HGSC (47) and SEC (65). *PTEN* deletion is observed in 6.65% HGSC and 2.27% of SEC. *PTEN* loss also causes PARP inhibitor sensitivity reversion (25). PTEN mutations have been validated as a driver of transformation in mouse models. However, secondary mutations are necessary for the most efficient transformation in such models (61).

Mutations causing homologous recombination deficiency (HRD) occur in over 50% of epithelial ovarian and 22% of endometrial carcinomas manifesting HRD respectively (56). HRD supports the accumulation of mutations aiding cell survival in an everchanging tumor microenvironment and in response to common therapeutics. Pan cancer studies have identified *Brca1, Brca2, Brip1, Rad51C,* and *Palb2* as the most commonly mutated genes related to HRD (66–68) (**Figure 2**). Additionally, patients with *BRCA1* mutations are more likely to be long-term survivors and have a higher mutational burden compared to patients lacking *BRCA1* mutations (56,69). Surprisingly, loss of *BRCA1/2* in a *Trp53* deficient background in mouse OSE and TE cells were insufficient to transform both cell types and did not have tumorigenic potential, suggesting that further mutations are necessary for tumorigenic potential (25,29,61). There is some evidence that *BRCA1/BRCA2* mutations play a role in endometrial cancers (70,71).

Patients subjected to salpingo-oophorectomy due to germline *Brca1/Brca2* mutations have an increased risk for the development of SEC (72). However, the causative role of *Brca1/Brca2* mutations in SEC remains to be clarified.

In summary, a loss of cell cycle control, increased cellular proliferation, and DNA repair deficiencies aid in the initiation and progression of HGSC and SEC. Various mutational combinations yield similarities and differences among the requirements for a transformation within TE and OSE. Many of the genes identified in HGSC have been well studied and characterized. However, their combinations driving SEC remain to be elucidated. Further work is necessary to determine whether LE and GE in the endometrium share the same combinations of drivers as TE and/or OSE.

1.5 Future directions

Discovering cancer-prone cell states is limited by the model systems necessary to approach this area of research. Identification of new cell state-specific promoters and cell fate tracing systems should facilitate advancements in studying what cell states can initiate the disease (73). Another important experimental aspect is the development of animal models that better accommodate the differences between human and mouse reproductive systems. Such improvements may involve using aged and oophorectomized mice to better model the postmenopausal age of most HGSC and SEC patients. Another promising approach is to use menstruating spiny mice, which better mimic the native mechanisms of cell turnover in the human reproductive tract (74).

Organoids serve as *ex vivo* models that better recapitulate the architecture and cellular diversity of native human tissue than 2D cultures. However, organoid models may lack

the complexity necessary to study additional factors contributing to carcinogenesis. Assembloid models incorporate multiple cell types to more accurately model human tissue, and these models could provide sufficient complexity to evaluate how additional cell types interact with transformed cell states (73,75).

Additionally, rapidly advancing research efforts in computational approaches are at the forefront of tissue characterization and biomarker identification (76–78). The increased resolution, approaching sub-micrometer, within spatial transcriptomic platforms can allow for direct comparison among the epithelial layers of the reproductive tract (79,80). Combinatorial approaches with genomic, transcriptomic, and epigenomic data applied to a subcellular spatial context at early stages of disease development will be pivotal for the discovery of diagnostic and therapeutic targets. Further development of new computational approaches to compare data among mouse and human tissues should facilitate direct translation of findings from mouse models to humans, while leveraging the flexibility of early disease detection only possible in model systems. Current examples of this include analysis tools such as self-assembling manifold (SAM) algorithm, which uses BLAST to map homology between datasets of distinct species to identify shared expression programs (81). New methods combining lineage tracing and single-cell and spatial RNA sequencing data could provide insight into cell lineage trajectories, susceptible cell states, and tumor evolution by actively tracking differentiation patterns and accumulated mutations (82). Higher-resolution of spatial transcriptomics applied to STIC/SEIC lesions could inform the cell states implicated in both the formation and progression of early HGSC and SEC. The identification of new markers and epigenetic modifications associated with developing tumors could be

leveraged with early detection technologies that analyze methylation patterns of circulating DNA (83), such as the GRAIL's Galleri test (84). The continued advancement in biomedical research technology could allow for the identification of early markers within cancer-prone cell states necessary for disease prevention and early intervention of serous carcinomas.

Unbiased CRISPR combinatorial screens have revealed genetic perturbations that are critical for biological processes (85). Much effort has been made to understand how combinations of genes result in the transformation of healthy cells into malignant cells in HGSC (29). Such screening approaches have yet to be performed in SEC. These studies will show whether the same combinations of genetic drivers in HGSC are also shared in SEC. Additionally, they would determine whether unique sets of combinations specific to SEC suggest differences in cell of origin. This may explain why the development of SEC in women with *BRCA1/2* mutations are only seen following salpingectomy. Many combinatorial screening approaches have been performed in mouse models; therefore, the use of human cells for similar screens may better reflect the minimum transformation requirements of these cell types.

Transformation of healthy cells is driven not only by loss of gene functions, but also by amplification/and gene overexpression or gain of function mutations events. Using CRISPR-based activation (CRISPRa) (86), gene overexpression can be studied to identify the combinations of amplified genes required for transformation. Additionally, screens to test the minimum transformation requirement have only been performed, however utilizing such strategies to identify the most chemotherapy-resistant combinations may help to improve patient outcomes. Development of new approaches

combining genetic perturbation approaches with computational analysis (77,87) will further facilitate our understanding of tumor suppressor and oncogene networks, thereby improving our understanding of both serous carcinoma biology and patient survivability. Taken together, it is increasingly clear that not only cell type but also state of cell differentiation in conjunction with specific genetic alterations define resulting cancer types, their biological behavior, and their response to treatment. Further work in this direction should greatly benefit the progress towards the curing aggressive serous carcinomas of the female reproductive system.

1.6 References

1. Siegel RL, Kratzer TB, Giaquinto AN, Sung H, Jemal A. Cancer statistics, 2025. CA Cancer J Clin. 2025 Jan 16;75(1):10–45.

2. Ferriss JS, Erickson BK, Shih I-M, Fader AN. Uterine serous carcinoma: key advances and novel treatment approaches. Int J Gynecol Cancer. 2021 Aug;31(8):1165–74.

3. Cheng Z, Mirza H, Ennis DP, Smith P, Morrill Gavarró L, Sokota C, et al. The Genomic Landscape of Early-Stage Ovarian High-Grade Serous Carcinoma. Clin Cancer Res. 2022 Jul 1;28(13):2911–22.

4. Kim J, Park EY, Kim O, Schilder JM, Coffey DM, Cho C-H, et al. Cell Origins of High-Grade Serous Ovarian Cancer. Cancers (Basel). 2018 Nov 12;10(11).

5. Gatius S, Matias-Guiu X. Practical issues in the diagnosis of serous carcinoma of the endometrium. Mod Pathol. 2016 Jan;29 Suppl 1:S45-58.

6. Forjaz G, Ries L, Devasia TP, Flynn G, Ruhl J, Mariotto AB. Long-term Cancer Survival Trends by Updated Summary Stage. Cancer Epidemiol Biomarkers Prev. 2023 Nov 1;32(11):1508–17.

7. Giaquinto AN, Broaddus RR, Jemal A, Siegel RL. The changing landscape of gynecologic cancer mortality in the united states. Obstet Gynecol. 2022 Mar 1;139(3):440–2.

8. Datta A, Thomas V, Sebastian A, George R, Thomas A, Ram TS, et al. The clinico pathological features and survival in serous endometrial cancers. Gynecol Oncol Rep. 2023 Jun;47:101194.

9. Hamilton CA, Cheung MK, Osann K, Chen L, Teng NN, Longacre TA, et al. Uterine papillary serous and clear cell carcinomas predict for poorer survival compared to grade 3 endometrioid corpus cancers. Br J Cancer. 2006 Mar 13;94(5):642–6.

10. Wang Y, Yu M, Yang J-X, Cao D-Y, Shen K, Lang J-H. Clinicopathological and survival analysis of uterine papillary serous carcinoma: a single institutional review of 106 cases. Cancer Manag Res. 2018 Oct 25;10:4915–28.

11. del Carmen MG, Birrer M, Schorge JO. Uterine papillary serous cancer: a review of the literature. Gynecol Oncol. 2012 Dec;127(3):651–61.

12. Bogani G, Ray-Coquard I, Concin N, Ngoi NYL, Morice P, Enomoto T, et al. Uterine serous carcinoma. Gynecol Oncol. 2021 Jul;162(1):226–34.

13. Benito V, Lubrano A, Arencibia O, Alvarez EE, León L, Medina N, et al. Pure papillary serous tumors of the endometrium: a clinicopathological analysis of 61 cases from a single institution. Int J Gynecol Cancer. 2009 Nov;19(8):1364–9.

14. Zhang S, Dolgalev I, Zhang T, Ran H, Levine DA, Neel BG. Both fallopian tube and ovarian surface epithelium are cells-of-origin for high-grade serous ovarian carcinoma. Nat Commun. 2019 Nov 26;10(1):5367.

15. Lawrenson K, Fonseca MAS, Liu AY, Segato Dezem F, Lee JM, Lin X, et al. A Study of High-Grade Serous Ovarian Cancer Origins Implicates the SOX18 Transcription Factor in Tumor Development. Cell Rep. 2019 Dec 10;29(11):3726-3735.e4.

16. Hao D, Li J, Jia S, Meng Y, Zhang C, Wang L, et al. Integrated Analysis Reveals Tubal- and Ovarian-Originated Serous Ovarian Cancer and Predicts Differential Therapeutic Responses. Clin Cancer Res. 2017 Dec 1;23(23):7400–11.

17. Medeiros F, Muto MG, Lee Y, Elvin JA, Callahan MJ, Feltmate C, et al. The tubal fimbria is a preferred site for early adenocarcinoma in women with familial ovarian cancer syndrome. Am J Surg Pathol. 2006 Feb;30(2):230–6.

18. Park KJ, Patel P, Linkov I, Jotwani A, Kauff N, Pike MC. Observations on the origin of ovarian cortical inclusion cysts in women undergoing risk-reducing salpingo-oophorectomy. Histopathology. 2018 Apr;72(5):766–76.

19. Kurman RJ, Shih I-M. The origin and pathogenesis of epithelial ovarian cancer: a proposed unifying theory. Am J Surg Pathol. 2010 Mar;34(3):433–43.

20. Schmoeckel E, Odai-Afotey AA, Schleißheimer M, Rottmann M, Flesken-Nikitin A, Ellenson LH, et al. LEF1 is preferentially expressed in the tubal-peritoneal junctions and is a reliable marker of tubal intraepithelial lesions. Mod Pathol. 2017 Sep;30(9):1241–50.

21. Seidman JD. Serous tubal intraepithelial carcinoma localizes to the tubal-peritoneal junction: a pivotal clue to the site of origin of extrauterine high-grade serous carcinoma (ovarian cancer). Int J Gynecol Pathol. 2015 Mar;34(2):112–20.

22. Lee Y, Miron A, Drapkin R, Nucci MR, Medeiros F, Saleemuddin A, et al. A candidate precursor to serous carcinoma that originates in the distal fallopian tube. J Pathol. 2007 Jan;211(1):26–35.

23. Chien Y-W, Wang Y, Huang P, Lawson BC, Kolin DL, Chui MH, et al. Morphologic and Molecular Heterogeneity of High-grade Serous Carcinoma Precursor Lesions. Am J Surg Pathol. 2024 Apr 1;48(4):475–86.

24. Nicosia SV, Saunders BO, Acevedo-Duncan ME, Setrakian S, Degregorio R. Biopathology of ovarian mesothelium. In: Familiari G, Makabe S, Motta PM, editors. Ultrastructure of the ovary. Boston, MA: Springer US; 1991. p. 287–310.

25. Lõhmussaar K, Kopper O, Korving J, Begthel H, Vreuls CPH, van Es JH, et al. Assessing the origin of high-grade serous ovarian cancer using CRISPR-modification of mouse organoids. Nat Commun. 2020 May 27;11(1):2660.

26. Flesken-Nikitin A, Choi K-C, Eng JP, Shmidt EN, Nikitin AY. Induction of carcinogenesis by concurrent inactivation of p53 and Rb1 in the mouse ovarian surface epithelium. Cancer Res. 2003 Jul 1;63(13):3459–63.

27. McCool KW, Freeman ZT, Zhai Y, Wu R, Hu K, Liu C-J, et al. Murine Oviductal High-Grade Serous Carcinomas Mirror the Genomic Alterations, Gene Expression Profiles, and Immune Microenvironment of Their Human Counterparts. Cancer Res. 2020 Feb 15;80(4):877–89.

28. Flesken-Nikitin A, Hwang C-I, Cheng C-Y, Michurina TV, Enikolopov G, Nikitin AY. Ovarian surface epithelium at the junction area contains a cancer-prone stem cell niche. Nature. 2013 Mar 14;495(7440):241–5.

29. Yamulla RJ, Nalubola S, Flesken-Nikitin A, Nikitin AY, Schimenti JC. Most Commonly Mutated Genes in High-Grade Serous Ovarian Carcinoma Are Nonessential for Ovarian Surface Epithelial Stem Cell Transformation. Cell Rep. 2020 Sep 1;32(9):108086.

30. Fu D-J, Wang L, Chouairi FK, Rose IM, Abetov DA, Miller AD, et al. Gastric squamous-columnar junction contains a large pool of cancer-prone immature osteopontin responsive Lgr5-CD44+ cells. Nat Commun. 2020 Jan 3;11(1):84.

31. Bajaj J, Diaz E, Reya T. Stem cells in cancer initiation and progression. J Cell Biol. 2020 Jan 6;219(1).

32. Fu D-J, Miller AD, Southard TL, Flesken-Nikitin A, Ellenson LH, Nikitin AY. Stem Cell Pathology. Annu Rev Pathol. 2018 Jan 24;13:71–92.

33. Ford MJ, Harwalkar K, Pacis AS, Maunsell H, Wang YC, Badescu D, et al. Oviduct epithelial cells constitute two developmentally distinct lineages that are spatially separated along the distal-proximal axis. Cell Rep. 2021 Sep 7;36(10):109677.

34. Harwalkar K, Ford MJ, Teng K, Yamanaka N, Yang B, Burtscher I, et al. Anatomical and cellular heterogeneity in the mouse oviduct-its potential roles in reproduction and preimplantation development†. Biol Reprod. 2021 Jun 4;104(6):1249–61.

35. Paik DY, Janzen DM, Schafenacker AM, Velasco VS, Shung MS, Cheng D, et al. Stem-like epithelial cells are concentrated in the distal end of the fallopian tube: a site for injury and serous cancer initiation. Stem Cells. 2012 Nov;30(11):2487–97.

36. Ghosh A, Syed SM, Tanwar PS. In vivo genetic cell lineage tracing reveals that oviductal secretory cells self-renew and give rise to ciliated cells. Development. 2017 Sep 1;144(17):3031–41.

37. Fu D-J, De Micheli AJ, Bidarimath M, Ellenson LH, Cosgrove BD, Flesken-Nikitin A, et al. Cells expressing PAX8 are the main source of homeostatic regeneration of adult mouse endometrial epithelium and give rise to serous endometrial carcinoma. Dis Model Mech. 2020 Oct 30;13(10).

38. Perets R, Wyant GA, Muto KW, Bijron JG, Poole BB, Chin KT, et al. Transformation of the fallopian tube secretory epithelium leads to high-grade serous ovarian cancer in Brca;Tp53;Pten models. Cancer Cell. 2013 Dec 9;24(6):751–65.

39. Zhai Y, Wu R, Kuick R, Sessine MS, Schulman S, Green M, et al. High-grade serous carcinomas arise in the mouse oviduct via defects linked to the human disease. J Pathol. 2017 Sep;243(1):16–25.

40. Flesken-Nikitin A, Ralston CQ, Fu D-J, De Micheli AJ, Phuong DJ, Harlan BA, et al. Pre-ciliated tubal epithelial cells are prone to initiation of high-grade serous ovarian carcinoma. Nat Commun. 2024 Oct 5;15(1):8641.

41. Ford MJ, Harwalkar K, Kazemdarvish H, Yamanaka N, Yamanaka Y. CD133/Prom1 marks proximal mouse oviduct epithelial progenitors and adult epithelial cells with a low generative capacity. Biol Open. 2023 Sep 15;12(9).

42. Hu Z, Artibani M, Alsaadi A, Wietek N, Morotti M, Shi T, et al. The Repertoire of Serous Ovarian Cancer Non-genetic Heterogeneity Revealed by Single-Cell Sequencing of Normal Fallopian Tube Epithelial Cells. Cancer Cell. 2020 Feb 10;37(2):226-242.e7.

43. Dinh HQ, Lin X, Abbasi F, Nameki R, Haro M, Olingy CE, et al. Single-cell transcriptomics identifies gene expression networks driving differentiation and tumorigenesis in the human fallopian tube. Cell Rep. 2021 Apr 13;35(2):108978.

44. Ulrich ND, Shen Y-C, Ma Q, Yang K, Hannum DF, Jones A, et al. Cellular heterogeneity of human fallopian tubes in normal and hydrosalpinx disease states identified using scRNA-seq. Dev Cell. 2022 Apr 11;57(7):914-929.e7.

45. Lengyel E, Li Y, Weigert M, Zhu L, Eckart H, Javellana M, et al. A molecular atlas of the human postmenopausal fallopian tube and ovary from single-cell RNA and ATAC sequencing. Cell Rep. 2022 Dec 20;41(12):111838.

46. Rohozinski J, Diaz-Arrastia C, Edwards CL. Do some epithelial ovarian cancers originate from a fallopian tube ciliate cell lineage? Med Hypotheses. 2017 Sep;107:16–21.

47. Cancer Genome Atlas Research Network. Integrated genomic analyses of ovarian carcinoma. Nature. 2011 Jun 29;474(7353):609–15.

48. Kandoth C, McLellan MD, Vandin F, Ye K, Niu B, Lu C, et al. Mutational landscape and significance across 12 major cancer types. Nature. 2013 Oct 17;502(7471):333–9.

49. Kurman RJ, Hedrick Ellenson L, Ronnett BM, editors. Blaustein's pathology of the female genital tract. Cham: Springer International Publishing; 2019.

50. Chui MH, Momeni Boroujeni A, Mandelker D, Ladanyi M, Soslow RA. Characterization of TP53-wildtype tubo-ovarian high-grade serous carcinomas: rare exceptions to the binary classification of ovarian serous carcinoma. Mod Pathol. 2021 Feb;34(2):490–501.

51. Cheng C-Y, Hwang C-I, Corney DC, Flesken-Nikitin A, Jiang L, Öner GM, et al. miR-34 cooperates with p53 in suppression of prostate cancer by joint regulation of stem cell compartment. Cell Rep. 2014 Mar 27;6(6):1000–7.

52. Corney DC, Hwang C-I, Matoso A, Vogt M, Flesken-Nikitin A, Godwin AK, et al. Frequent downregulation of miR-34 family in human ovarian cancers. Clin Cancer Res. 2010 Feb 15;16(4):1119–28.

53. Chuang C-H, Yang D, Bai G, Freeland A, Pruitt SC, Schimenti JC. Post-transcriptional homeostasis and regulation of MCM2-7 in mammalian cells. Nucleic Acids Res. 2012 Jun;40(11):4914–24.

54. Burkhart DL, Sage J. Cellular mechanisms of tumour suppression by the retinoblastoma gene. Nat Rev Cancer. 2008 Sep 1;8(9):671–82.

55. Corney DC, Flesken-Nikitin A, Choi J, Nikitin AY. Role of p53 and Rb in ovarian cancer. Adv Exp Med Biol. 2008;622:99–117.

56. Kotnik EN, Mullen MM, Spies NC, Li T, Inkman M, Zhang J, et al. Genetic characterization of primary and metastatic high-grade serous ovarian cancer tumors reveals distinct features associated with survival. Commun Biol. 2023 Jul 3;6(1):688.

57. Knudsen ES, Nambiar R, Rosario SR, Smiraglia DJ, Goodrich DW, Witkiewicz AK. Pan-cancer molecular analysis of the RB tumor suppressor pathway. Commun Biol. 2020 Apr 2;3(1):158.

58. Sherr CJ, Beach D, Shapiro GI. Targeting CDK4 and CDK6: from discovery to therapy. Cancer Discov. 2016 Apr;6(4):353–67.

59. Albitar L, Carter MB, Davies S, Leslie KK. Consequences of the loss of p53, RB1, and PTEN: relationship to gefitinib resistance in endometrial cancer. Gynecol Oncol. 2007 Jul;106(1):94–104.

60. Flesken-Nikitin A, Pirtz MG, Ashe CS, Ellenson LH, Cosgrove BD, Nikitin AY. Dysregulation of cell state dynamics during early stages of serous endometrial carcinogenesis. BioRxiv. 2024 Mar 19;

61. Zhang S, Iyer S, Ran H, Dolgalev I, Gu S, Wei W, et al. Genetically defined, syngeneic organoid platform for developing combination therapies for ovarian cancer. Cancer Discov. 2021 Feb;11(2):362–83.

62. Singer G, Oldt R, Cohen Y, Wang BG, Sidransky D, Kurman RJ, et al. Mutations in BRAF and KRAS characterize the development of low-grade ovarian serous carcinoma. J Natl Cancer Inst. 2003 Mar 19;95(6):484–6.

63. Manning-Geist B, Gordhandas S, Liu YL, Zhou Q, Iasonos A, Da Cruz Paula A, et al. MAPK Pathway Genetic Alterations Are Associated with Prolonged Overall Survival in Low-Grade Serous Ovarian Carcinoma. Clin Cancer Res. 2022 Oct 14;28(20):4456–65.

64. Walton JB, Farquharson M, Mason S, Port J, Kruspig B, Dowson S, et al. CRISPR/Cas9-derived models of ovarian high grade serous carcinoma targeting Brca1, Pten and Nf1, and correlation with platinum sensitivity. Sci Rep. 2017 Dec 4;7(1):16827.

65. Risinger JI, Hayes K, Maxwell GL, Carney ME, Dodge RK, Barrett JC, et al. PTEN mutation in endometrial cancers is associated with favorable clinical and pathologic characteristics. Clin Cancer Res. 1998 Dec;4(12):3005–10.

66. Nguyen L, W M Martens J, Van Hoeck A, Cuppen E. Pan-cancer landscape of homologous recombination deficiency. Nat Commun. 2020 Nov 4;11(1):5584.

67. Peng G, Mills GB. Surviving Ovarian Cancer: An Affair between Defective DNA Repair and RB1. Clin Cancer Res. 2018 Feb 1;24(3):508–10.

68. Song H, Dicks EM, Tyrer J, Intermaggio M, Chenevix-Trench G, Bowtell DD, et al. Population-based targeted sequencing of 54 candidate genes identifies PALB2 as a susceptibility gene for high-grade serous ovarian cancer. J Med Genet. 2021 May;58(5):305–13.

69. Yang Q, Yang Y, Zhou N, Tang K, Lau WB, Lau B, et al. Epigenetics in ovarian cancer: premise, properties, and perspectives. Mol Cancer. 2018 Jul 31;17(1):109.

70. Beiner ME, Finch A, Rosen B, Lubinski J, Moller P, Ghadirian P, et al. The risk of endometrial cancer in women with BRCA1 and BRCA2 mutations. A prospective study. Gynecol Oncol. 2007 Jan;104(1):7–10.

71. Segev Y, Iqbal J, Lubinski J, Gronwald J, Lynch HT, Moller P, et al. The incidence of endometrial cancer in women with BRCA1 and BRCA2 mutations: an international prospective cohort study. Gynecol Oncol. 2013 Jul;130(1):127–31.

72. Saule C, Mouret-Fourme E, Briaux A, Becette V, Rouzier R, Houdayer C, et al. Risk of Serous Endometrial Carcinoma in Women With Pathogenic BRCA1/2 Variant After Risk-Reducing Salpingo-Oophorectomy. J Natl Cancer Inst. 2018 Feb 1;110(2).

73. Liberali P, Schier AF. The evolution of developmental biology through conceptual and technological revolutions. Cell. 2024 Jul 11;187(14):3461–95.

74. Bellofiore N, McKenna J, Ellery S, Temple-Smith P. The Spiny Mouse-A Menstruating Rodent to Build a Bridge From Bench to Bedside. Front Reprod Health. 2021 Nov 26;3:784578.

75. Crawford AJ, Forjaz A, Bons J, Bhorkar I, Roy T, Schell D, et al. Combined assembloid modeling and 3D whole-organ mapping captures the microanatomy and function of the human fallopian tube. Sci Adv. 2024 Sep 27;10(39):eadp6285.

76. Patel AS, Yanai I. A developmental constraint model of cancer cell states and tumor heterogeneity. Cell. 2024 Jun 6;187(12):2907–18.

77. Rood JE, Hupalowska A, Regev A. Toward a foundation model of causal cell and tissue biology with a Perturbation Cell and Tissue Atlas. Cell. 2024 Aug 22;187(17):4520–45.

78. Deshpande D, Chhugani K, Ramesh T, Pellegrini M, Shiffman S, Abedalthagafi MS, et al. The evolution of computational research in a data-centric world. Cell. 2024 Aug 22;187(17):4449–57.

79. Liu L, Chen A, Li Y, Mulder J, Heyn H, Xu X. Spatiotemporal omics for biology and medicine. Cell. 2024 Aug 22;187(17):4488–519.

80. You Y, Fu Y, Li L, Zhang Z, Jia S, Lu S, et al. Systematic comparison of sequencing-based spatial transcriptomic methods. Nat Methods. 2024 Sep;21(9):1743–54.

81. Tarashansky AJ, Musser JM, Khariton M, Li P, Arendt D, Quake SR, et al. Mapping single-cell atlases throughout Metazoa unravels cell type evolution. eLife. 2021 May 4;10.

82. Yang D, Jones MG, Naranjo S, Rideout WM, Min KHJ, Ho R, et al. Lineage tracing reveals the phylodynamics, plasticity, and paths of tumor evolution. Cell. 2022 May 26;185(11):1905-1923.e25.

83. Liu MC, Oxnard GR, Klein EA, Swanton C, Seiden MV, CCGA Consortium. Sensitive and specific multi-cancer detection and localization using methylation signatures in cell-free DNA. Ann Oncol. 2020 Jun;31(6):745–59.

84. Klein EA, Richards D, Cohn A, Tummala M, Lapham R, Cosgrove D, et al. Clinical validation of a targeted methylation-based multi-cancer early detection test using an independent validation set. Ann Oncol. 2021 Sep;32(9):1167–77.

85. Bock C, Datlinger P, Chardon F, Coelho MA, Dong MB, Lawson KA, et al. High-content CRISPR screening. Nat Rev Methods Primers. 2022 Feb 10;2(1):8.

86. Gilbert LA, Horlbeck MA, Adamson B, Villalta JE, Chen Y, Whitehead EH, et al. Genome-scale CRISPR-mediated control of gene repression and activation. Cell. 2014 Oct 23;159(3):647–61.

87. Belli O, Karava K, Farouni R, Platt RJ. Multimodal scanning of genetic variants with base and prime editing. Nat Biotechnol. 2024 Nov 12;

Chapter 2: Gene combinations driving transformation of tubal epithelial organoids and differential sensitivity to high-grade serous ovarian carcinoma drugs

The following chapter is adapted from a manuscript submitted to *biorxiv* (https://doi.org/10.1101/2025.03.10.642422)

DJP, JCS and AYN designed experiments; DJP, CQR, TME, CSA and APA performed experiments and performed pathological evaluations; AFN and RJY provided resources; DJP wrote the paper; DJP, JCS, AYN revised and edited the paper.

Authors: Daryl J. Phuong, Coulter Q. Ralston, Tony M. Ezzat, Christopher S. Ashe, Amanda P. Armstrong, Andrea Flesken-Nikitin, Robert J. Yamulla, Alexander Yu. Nikitin, John C. Schimenti

2.1 Abstract

High-grade serous ovarian carcinoma (HGSC) is the sixth leading cause of female death from cancer. The majority of HGSC cases are likely to arise from the Fallopian tubal epithelium (TE), while some carcinomas may originate from the ovarian surface epithelium (OSE). Individual tumors bear numerous mutations with uncertain roles in carcinogenesis. To identify mutation combinations that drive transformation and pathological phenotypes, we used a TE-derived organoid platform to screen, *en masse*, 20 candidate HGSC driver genes via combinatorial CRISPR mutagenesis (>7 per clonal organoid). In addition to known drivers (*Brca1*, *Brca2, Nf1, Rb1, Trp53*, and *Pten*), mutations of *Cdkn2a* and *Map2k4* were identified as being critical for TE transformation. *Brca2* and *Map2k4* mutations were not identified in previous OSE screens. Despite both *Map2k4* and *Nf1* being part of the MAPK pathway, they led to distinct tumor types: *Map2k4* mutations gave rise to papillary carcinomas that more closely resemble typical HGSC, while *Nf1* mutations resulted in poorly differentiated mesenchymal-like neoplasms. Additionally, different combinations of mutations affected the sensitivity or resistance of transformed organoid cells to drugs commonly used to treat HGSC, with varying responses depending on the presence or absence of the Rho kinase inhibitor, ROCKi. Our findings support the notion that specific HGSC gene disruptions reflect the cell of origin, drive pathological subtypes, and influence differential cancer drug responsiveness.

2.2 Introduction

The transformation of normal cells into cancer cells is driven by multiple genetic events. However, pinpointing the exact combination of mutations that fuel cancer progression and which influence treatment responses is challenging. High-grade serous carcinoma (HGSC) accounts for over 70% of ovarian cancer deaths (1), and TCGA data (available at cBioportal.org) reveal an average of 46 mutations per HGSC sample. Chromosomal rearrangements that disrupt key tumor suppressors like *RB1, NF1, RAD51B*, and *PTEN* have been valuable for identifying key drivers of HGSC (1–8). Furthermore, combinations of somatic and germline mutations play a critical role in determining patient outcomes, tumor characteristics, and immune responses, highlighting why sequencing individual tumors is key to personalized treatment (1,5). Although *TP53* mutations are present in >90% of HGSCs, *Trp53* ablation alone is insufficient for HGSC induction in mice; alterations of 1-3 additional genes are necessary (8–11).

HGSC originates from both ovarian surface epithelium (OSE) and tubal epithelium (TE) cells (7,12–15), but whether they share the same genetic drivers for malignant transformation is unclear. Studies show up to 60% of HGSCs are linked to serous tubal intraepithelial carcinoma (STIC) lesions (16–20), with STICs found in 8% of patients with *BRCA1/2* mutations undergoing risk-reducing salpingo-oophorectomy (18,21–25). Although HGSC was originally believed to only be of OSE origin, mounting evidence suggests that the preponderance of cases arise from the TE (2,20,26).

Arguably, organoids are a more biologically relevant model than traditional 2-D cell cultures for studying cancer biology. Mouse OSE and TE organoids have been used to

identify HGSC cell origins and to validate key genetic drivers like *Trp53* and *Rb1* (10,11,27). For example, TE organoids with *Trp53*, *Brca1*, and *Nf1* mutations showed higher tumorigenic potential than OSE organoids with the same mutations (10), supporting the notion that tumors arising from different cell types are driven by distinct mutational landscapes and cell interactions (3,28). The complexity of mutational load in different HGSCs challenges the practical use of predefined gene combinations, especially in genetically engineered mouse models that acquire secondary mutations similar to those in humans (29). Organoids offer a platform to explore additional genes, mutation combinations, and drug sensitivities in HGSC.

HGSC is classified into four molecular subtypes associated with tumor progression - immunoreactive, proliferative, mesenchymal, and differentiated - though their prognostic value for patient survival remains unclear (30–35). Pathologically, HGSC can present in various patterns the most common of which are papillary, glandular, solid, or SET (solid, pseudoendometrioid, transitional) (31,36,37). *Brca1* mutations are often associated with SET tumors and the immunoreactive subtype (38–40). However, over 70% of HGSC cases are diagnosed at advanced stages, complicating the identification of early genetic drivers and their impact on subtypes and histology (41–43).

To identify genetic drivers of TE transformation, we coupled an organoid platform with random combinatorial mutagenesis. This approach allowed us to induce mutations in seven or more HGSC-associated genes simultaneously. Remarkably, different mutational combinations led to phenotypic variation at the organoid level and resulted in diverse cancer pathologies when transplanted into mice. For example, *Map2k4* mutations drove papillary carcinoma phenotypes that closely resemble the growth patterns of HGSC - a

hitherto unreported feature in mouse organoid derived tumor models. Additionally, *Map2k4*-mutated cells were sensitive to paclitaxel but resistant to trametinib, which is surprising given that most studies link *Map2k4* mutations to trametinib sensitivity (44,45). Our findings, which reveal a preferential mesenchymal phenotype associated with *Nf1* mutations and a papillary-glandular phenotype driven by *Map2k4* mutations, underscore the importance of studying specific mutation combinations to unravel the mechanisms of carcinogenesis and to evaluate targeted therapeutic strategies.

2.3 Results

2.3.1 Approach for screening candidate HGSC suppressors in a TE organoid model

We leveraged a combinatorial CRISPR/Cas9 mutagenesis screen in TE organoids as a high-throughput platform for identifying mutation combinations that drive HGSC. TE organoids have several important properties for the task: they can form from single cells (Sup. Fig. 1A, B), express key differentiation markers (acetylated alpha-tubulin/FOXJ1 for ciliated cells, OVGP1 for secretory cells, and PAX8 for immature cells) (Sup. Fig. 1C) (10,11,15,46), and if genetically transformed they exhibit morphological changes linked to increased tumorigenic potential in mice (10,11,46). The mutagenesis screen involved infecting individual TE organoid-derived cells (derived from the uterine tube) with a lentiviral library at high multiplicity of infection (MOI), then allowing them to form new organoids. Those with abnormal morphologies were selected, and the gRNAs borne by each were detected (Fig. 1). Prior to screening, the gRNA distribution of the library was determined as a baseline for identification of enriched targeting vectors in aberrant organoid clones (Sup. Fig. 1D, E). We confirmed that secondary organoids were clonal, since cells independently infected with GFP or mCherry reporters, then mixed, formed organoids without dual reporter expression (Sup. Fig. 1B).

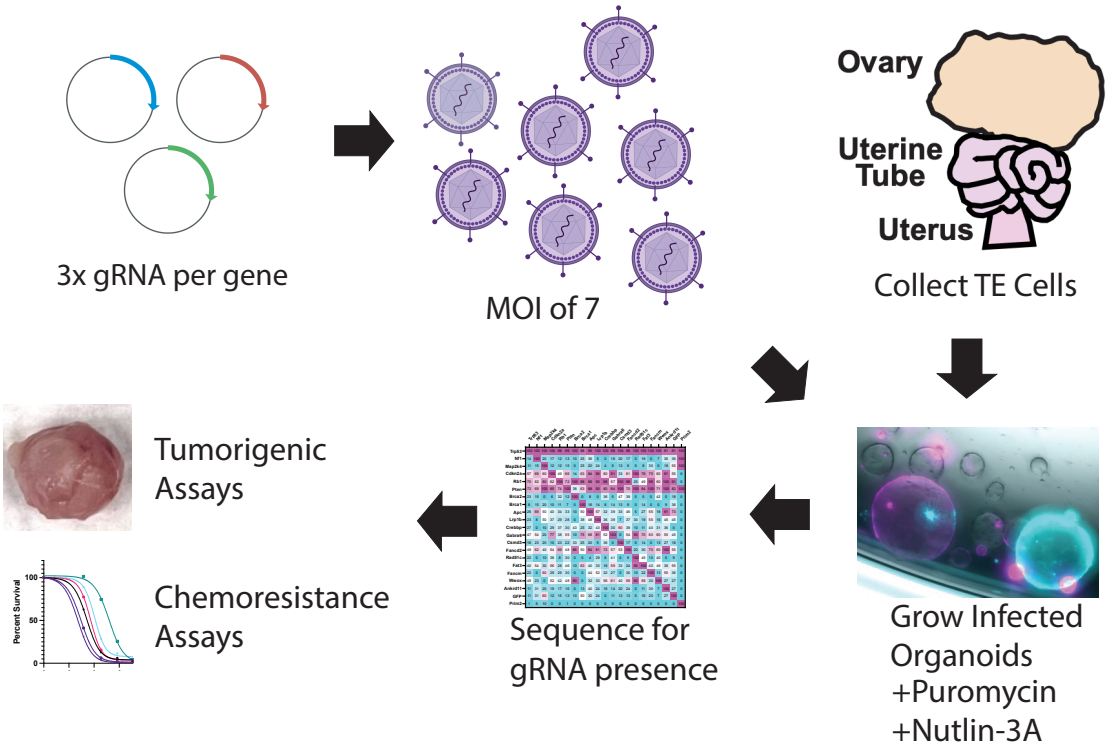

Figure 1. Schematic of screening strategy. Tubal epithelial cells (TE) are from the uterine tube. Created with help from biorender.com.

2.3.2 Identification of target genes enriched in aberrant organoids

We designed the screen to target 20 genes, 18 of which are commonly mutated in HGSC (based on TCGA data) and two others, *Fancm* and *Apc*, that are also cancer-related (33,47). A lentiviral library consisted of three gRNAs per gene was cloned into a plasmid vector (lentiCRISPRv2) designed to express both the gRNA and Cas9, packaged as lentiviruses, and used to infect TE organoid-forming cells at an estimated multiplicity of infection (MOI) of 7 (Fig. 1). Given that *TP53* mutations are found in over 90% of HGSC cases, the organoids were grown in Nutlin-3a to select for *Trp53*-deficient cells (Fig. 1) (47). After 14 days, we visually screened for abnormal organoids - those with folds, grapelike structures, protrusions, solid formations, or larger sizes compared to controls lacking only *Trp53* (Fig. 2A). The fraction of aberrant organoids was 0.28% ± SD = 0.0311 (n=5 independent library infections). We then picked and expanded these organoids, extracted DNA to sequence vector amplicons, and found that individual organoids had an average of 8 gRNAs (Fig. 2B). Although we expected that all the clones would contain a gRNA targeting *Trp53* due to Nutlin-3A selection, 11 of 95 did not; it is possible that the lentivirus did not stably integrate in these clones (yet they survived short term puromycin selection), or that *Trp53* was poorly expressed or inactivated by other means in these organoids.

After adjusting for vector representation in the plasmid library used to package lentivirus, the most dramatically enriched gRNAs corresponded to *Map2k4* and *Brca1* (Fig. 2C), whereas several were highly underrepresented, notably *Brca2*. The underrepresentation of other vectors may reflect either a compromise to viability or a

dependency of co-mutation with certain other genes in order to confer abnormal organoid phenotypes. For example, *Nf1* and *Cdkn2a*, which were not enriched when considering their overall normalized representation (Fig. 2C), were amongst the most statistically enriched in pairwise combinations (Fig. 2D). The most enriched triple mutant combinations (all including *Trp53,* abbreviated "T") involved *Nf1* (N)*, Map2k4* (M), *Cdkn2a* (C)*, Rb1* (R)*, Pten* (P)*, Brca2* (B2) and *Brca1* (B1) and will henceforth be abbreviated as indicated when in combinations (Fig. 2D, E).

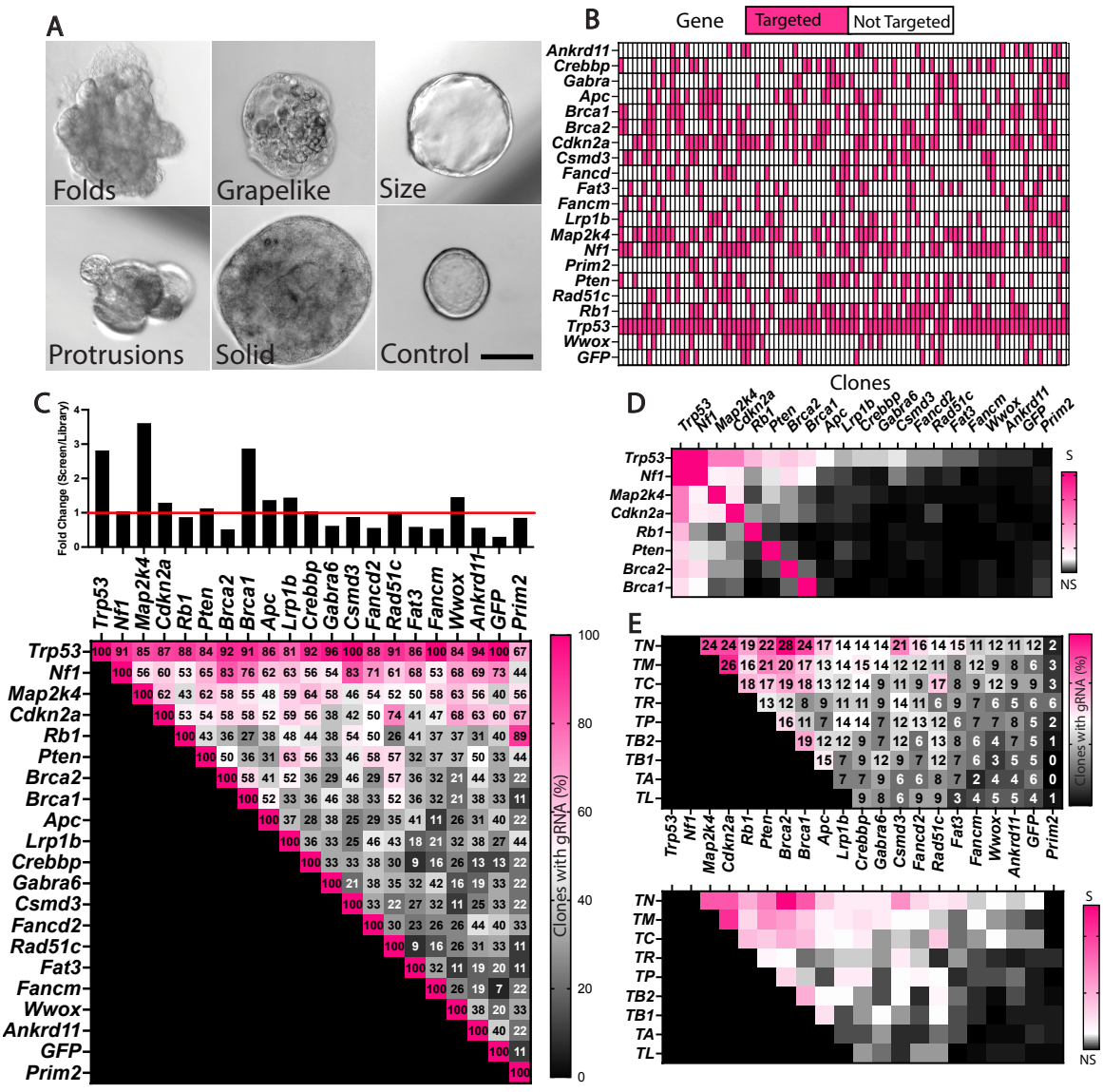

Figure 2. **Mutation combinations in transformed TE organoids**. A) Phenotypes of mutant organoids. Scale bar = 100µm. B) gRNA vectors identified in each aberrant organoid clone. C) Enrichment of targeting vectors in aberrant clones. The fold change was calculated based on % representation in clonal organoids over % representation in library. The red horizontal line represents no representation difference between gRNA frequency found in library and screen. (Bottom) Frequency of co-mutations in organoids. Numbers are percentages. D) c2 analysis of significant TE double mutations, DF, 19, P<0.05%, S=

Significant, NS= not significant. E) Number of clones that contain gRNA's targeting genes in triple mutations containing the top 9 overrepresented genes in the screen. (Bottom) c2 analysis of significant TE triple mutations, DF, 19, P<0.05%. S= Significant, NS= Not Significant.

2.3.3 Key mutation combinations driving TE transformation

To validate the combinatorial contribution of gene disruptions to transformation, we infected organoid-forming TE cells with specific pairs or trios of lentiviral vectors. Co-mutations of *Nf1* or *Pten* with *Trp53* increased the fraction of aberrant organoids (Fig. 3A, B), consistent with previous findings that loss of *Nf1* and *Pten* drives HGSC (46). *Nf1* mutations resulted in larger organoids with fold structures and intact lumens, while *Pten* mutations caused blob-like protrusions with denser cores (Fig. 3E). In contrast, other double mutations reduced organoid diameter and formation rate (Fig. 3A-D). The TB1 combination, showing poor organoid growth, aligns with previous data suggesting homozygous *Brca1* loss is rare in rapidly growing organoid systems (10).

Trp53 mutations with homozygous *Nf1* and *Pten* deletions are present in 1.26% of human HGSCs (Firehose legacy data in cBioPortal), and TE organoids with these mutations form HGSC-like tumors upon transplantation (46). We generated specific triple mutant organoid combinations to validate the bulk (Fig. 2E) screen results. Disruption of genes besides *Pten* enhanced transformation with TN deficiency, particularly mutations in *Map2k4*, *Cdkn2a*, *Rb1*, or *Brca2*, which increased transformation compared to *Trp53* alone. However, only *Pten* or *Brca2* mutation markedly enhanced transformation in TN-deficient organoids (Fig. 3A, B). The TNB1 combination resulted in poor growth *ex vivo* (10) (Fig. 3C). Our data (Fig. 3A, B) supports previous findings showing that TNP disruption increased aberrant organoid formation rate (46). Interestingly, the phenotype of these organoids was a hybrid of those with TN and TP mutation combinations, exhibiting less overall folding but more ruffled edges and smaller blob-like protrusions (Fig. 3E).

The most overrepresented targeted gene in the screen was *Map2k4*, which acts in the JNK pathway and is considered a potential HGSC tumor suppressor (48,49) but hasn't been functionally studied in mice or organoids for involvement in ovarian cancer. In TCGA data, *MAP2K4* mutations and homozygous deletions are found in 0.32% and 4.2% of HGSC cases, respectively (50). Mutation of the RAS suppressor *Nf1* enhanced TE organoid transformation as described previously (Fig. 3A) in triple mutation combinations compared to double mutants (Fig. 3B, E). *Map2k4* mutations also increased transformation with additional mutations except for *Brca2* but had less impact on organoid diameter than *Nf1* (Fig. 3C, F). Interestingly, TMB1 mutants showed increased transformation, while TMB2 did not - opposite to the patterns seen in TNB1 and TNB2 (Fig. 3A, B). This aligns with the screen's overrepresentation of *Map2k4* and *Brca1* (Fig. 2C).

We next investigated the role of *Cdkn2a*, as it was the third most co-mutated gene in triple mutation combinations with *Trp53* in the screen (Fig. 3E). *Cdkn2a* encodes p14 and p16 proteins, which are involved in the RB pathway and often used to distinguish HGSC from other ovarian cancers (51). Co-mutating *Cdkn2a* with *Trp53* reduced transformation potential, organoid size, and formation rate compared to *Trp53* alone (Fig. 3A-D). Adding *Rb1* to TC only slightly improved these parameters, while *Brca1/2* additions restored them to levels similar to *Trp53* alone. Only *Nf1*, *Map2k4*, or *Pten* co-mutations further improved transformation (Fig. 3A-D). TCP organoids resembled TMP in phenotype (Fig. 3E).

We analyzed HGSC samples with *TP53* mutations and identified the most significant triple mutations as *Map2k4/Cdkn2a* and *Nf1/Pten* (Sup. Fig. 4A, B). For transformed organoids, additional overrepresented mutations included [*Nf1, Pten, Brca2,*

Crebbp, Rad51, Wwox] and [*Map2k4, Cdkn2a, Brca1, Lrp1b, Crebbp*] (Sup. Fig. 4A, B). Quadruple mutant combinations TNP*Rad51C* and TMCP enhanced transformation (Sup. Fig. 4C, D). Organoid formation frequency increased with co-mutation of *Map2k4, Cdkn2a, Brca1, Lrp1b*, or *Csmd3* in a TNP deficient background, and *Rb1* or *Csmd3* increased formation with TMC (Sup. Fig. 4C, D). Our findings suggest that while a fourth mutation does not significantly enhance transformation in most cases, it does not rule out roles in cell growth, survival, metastasis, and chemoresistance, warranting further exploration of novel triple combinations.

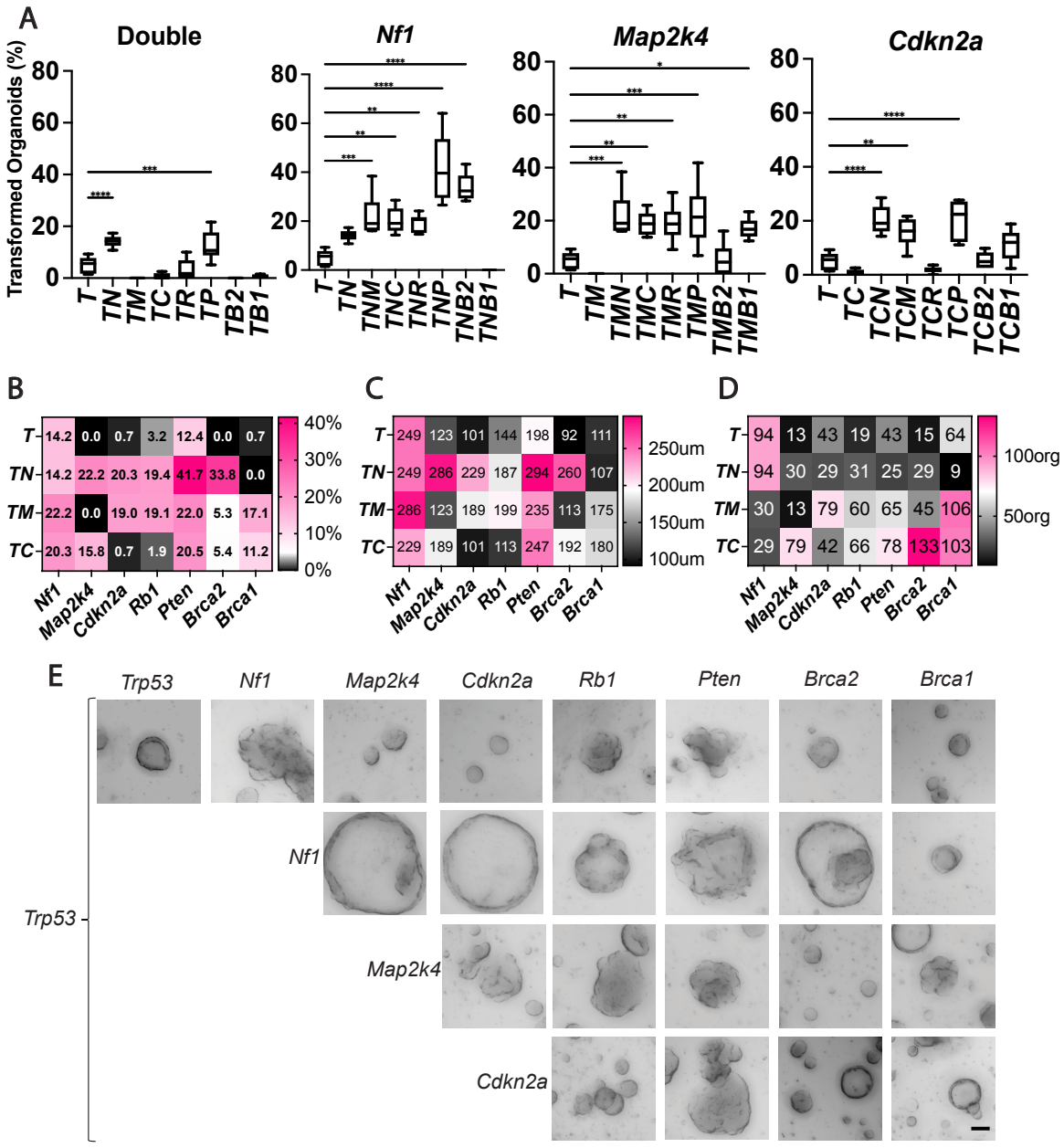

Figure 3. **Validation of mutation combinations driving TE organoid transformation.** Percent transformation of A) Double mutant combinations, Triple mutant combinations with *Nf1*^{mut}, *Map2k4*^{mut} or *Cdkn2a* ^{mut} background. B) Organoid transformation percentage of combinations compared to *Trp53*$^{-/-}$ alone. C) Average organoid diameters vs *Trp53*$^{-/-}$ alone D) Average organoid (org) formation vs *Trp53*$^{-/-}$ alone. E) Representative images of organoids for each combination tested. Scale bar = 100µm. One-way anova was used to

assess significance, n=6 per condition. P-value < * = 0.05, <** = 0.01, <*** = 0.001, <****= 0.0001.

2.3.4 Mutation combinations influence responses to common HGSC therapeutics

Modern precision cancer treatment has been revolutionized by considering the key genes involved in a person's cancer. When cancer cells survive and gain mutations that promote resistance following first-line treatments, patient survival is often poor. For example, platinum-based therapeutics are initially highly effective but become less successful with each round of treatment (52). Therefore, integrating genetics with treatment modalities is integral for improving patient outcomes. The organoid platform enables facile screening of anticancer agents that are most effective against transformed cells bearing various mutant combinations. To test how TE organoids bearing different genetic combinations respond to common HGSC treatments, we performed dose-response survivability assays with carboplatin (a cisplatin analog causing DNA crosslinks), gemcitabine (a base analog that inhibits DNA replication), niraparib (PARP inhibitor), paclitaxel (a microtubule inhibitor that blocks mitosis), and trametinib (MEK inhibitor), with or without ROCK (Rho-associated protein kinase) inhibitor (ROCKi; a disruptor of cytoskeletal function).

Removing ROCKi from the culture media increased resistance (increased in the inhibitory concentration) of transformed organoids to carboplatin (180%), gemcitabine (122%), and niraparib (133%), while paclitaxel sensitivity remained unchanged and trametinib became more effective (64%) (Sup. Fig. 5A). In the presence of ROCKi, *Nf1*-deficient organoids were 24% more resistant to carboplatin than other combinations (Fig. 4A), likely due to rapid proliferation allowing platinum-resistant organoids to regrow. Without ROCKi, *Rb1/Cdkn2a* mutant organoids showed no change in gemcitabine

response, but ROCKi increased resistance of mutants by 28% (Fig. 4B). *Map2k4* mutants were generally more sensitive to paclitaxel (Fig. 4C). Trametinib, a treatment for neurofibromatosis, had a similar impact on cells regardless of *Nf1* status when ROCKi was absent, but ROCKi conferred resistance in *Nf1* mutants (Fig. 4E). Interestingly, TNM cells were unaffected by trametinib, contrary to expectations, as we expected *Map2k4* mutations to act similarly to *Nf1* mutations (Fig. 4E), and that inhibition of both the RAS/ERK and JNK arms of the MAPK signaling pathways are effective in inhibiting cancer cell growth (44,45,53). These differences could be due to differences in p53 status or the culture conditions that prevent apoptosis. Removal of ROCKi increased resistance in *Map2k4* mutants, while no correlation between *Map2k4* mutations and trametinib sensitivity was seen with ROCKi (Fig. 4E), suggesting that ROCKi may play a role in promoting cell survival. There were differences between treatments with and without ROCKi, with some mutations becoming more sensitive while others becoming more resistant (Fig. 4F). These results, particularly the high resistance in TNM combinations, demonstrate the need to study specific mutational perturbations.

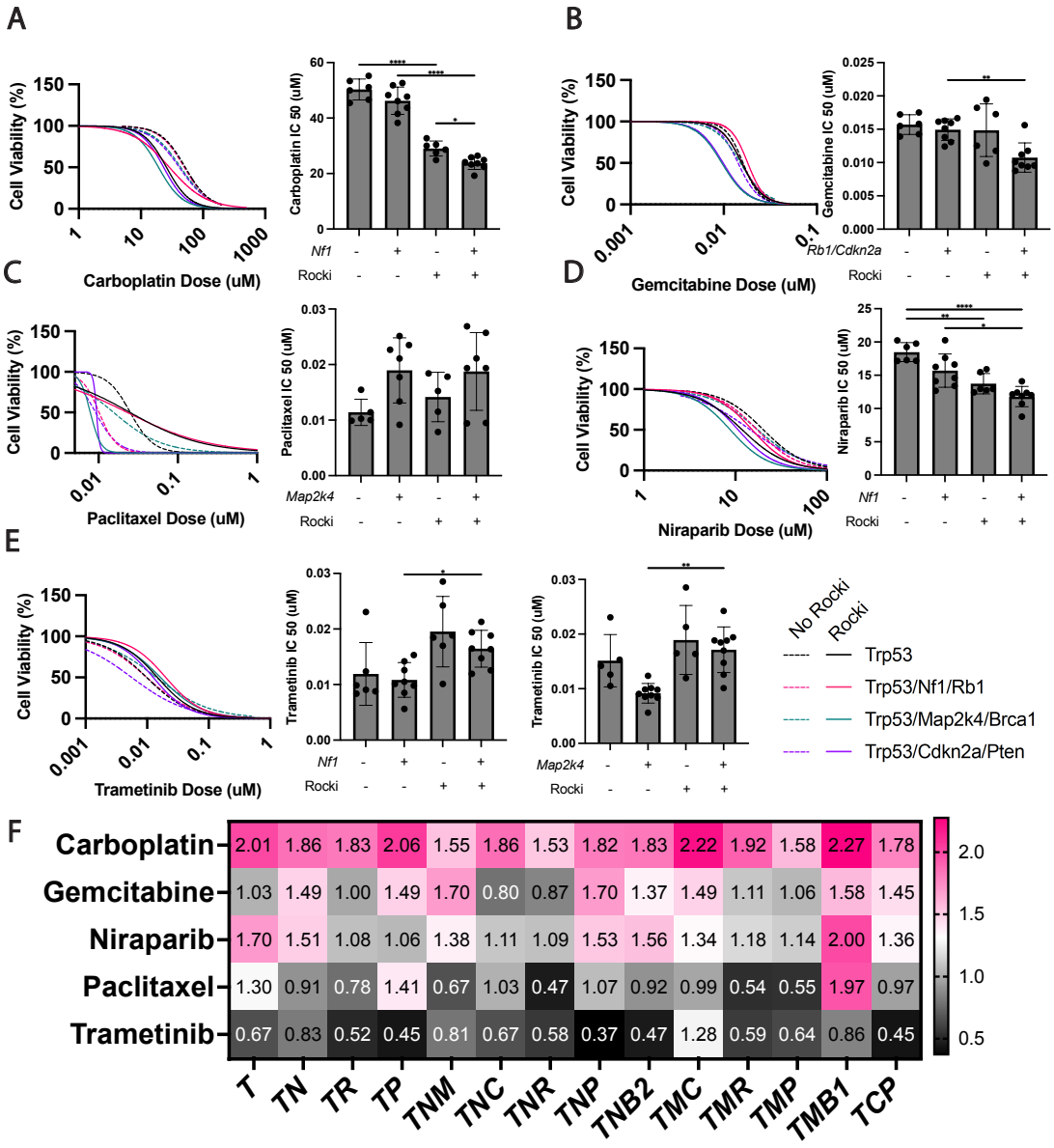

Figure 4. **Impacts of mutations on drug responses.** Dose response curves were performed and combinations representing most of the genes were graphed. A) Carboplatin, *Nf1*^{mut} are 22% more resistant to carboplatin B) Gemcitabine, *Rb1*^{mut}*Cdkn2a*^{mut} are 38% more resistant to gemcitabine C) Paclitaxel, *Map2k4*^{mut} are 25% (with ROCKi) or 40% (without ROCKi) more sensitive to paclitaxel D) Niraparib, *Nf1*^{mut} containing mutants are ~16% more resistant to niraparib. E) Trametinib, *Map2k4*^{mut} are 65% more resistant to trametinib. F) IC50 fold change Rocki- /Rocki+.

One-way anova, Brown-Forsythe and Welch Tests were performed to assess differences in sensitivity and resistance. Two independent experiments were conducted per mutation combination in triplicate. One-way anova was used to assess significance. P-value < * = 0.05, <** = 0.01, <*** = 0.001, <****= 0.0001.

2.3.5 Mutation combinations drive differences in tumorigenic potential, gene expression and tumor pathology

To assess whether mutation combinations linked to aberrant organoid formation and morphology reflect *in vivo* tumorigenic potential, we performed subcutaneous flank injections of organoid derived cells into immunodeficient (NSG) female mice and monitored them for up to 200 days. Loss of *Trp53* alone did not result in tumor formation, consistent with prior studies (2,5,7). Among the combinations tested, TNP led to the shortest survival, with tumors reaching 1 cm within an average of 70 days post-injection (Fig. 5A). In contrast, survival times were longer for TN (138 days) and TP (172 days) combinations (Fig. 5A). Adding *Brca2* (136 days) or *Map2k4* (124 days) to the TN background had minimal impact on survival (Fig. 5A).

In the context of TP deficiency, additional mutations in *Map2k4* or *Cdkn2a* reduced survival by 46 and 28 days, respectively, but tumor size doubling times increased to 62 and 48 days compared to 27 days for TP alone (Fig. 5A). Tumor latency mirrored these findings, with TPM and TPC averaging 96 and 95 days, respectively, compared to 138 days for TP (though this lacked statistical significance due to small sample size; Fig. 5B). Notably, organoids with TM co-mutations and additional losses in *Cdkn2a, Rb1,* or *Brca1* failed to efficiently form tumors within 200 days. Collectively, these results suggest that *Trp53* loss combined with either *Nf1* or *Pten* constitutes a minimal requirement for tumor formation, and additional losses of *Map2k4, Cdkn2a*, or *Brca2* enhance tumor growth and formation rates.

We next assessed whether organoid metrics - formation, transformation, and diameter (Figs. 3E–G) - predicted mouse survival after tumor induction via organoid-

derived cell injections. In general, larger organoid diameter and faster transformation rate, but not formation efficiency, correlated with reduced survival (Fig 5A, C-E). Only the TNP mutations had a significantly higher tumor formation rate and growth than TN or TP, leaving open the possibility that certain mutation combinations might impact tumor presentation.

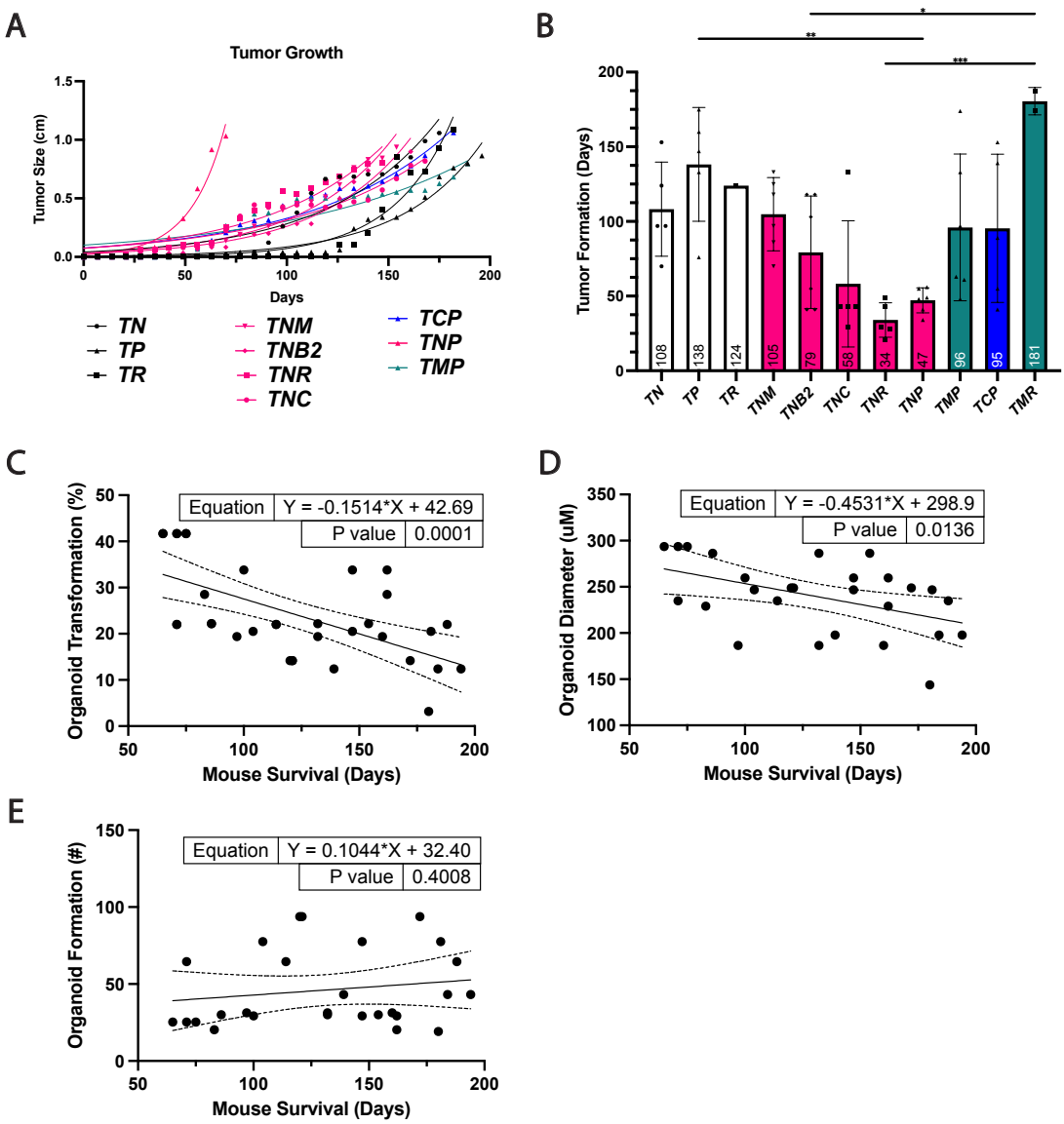

Figure 5. TE organoid transformation reflects tumorigenic potential. A) Tumor growth as measured on a weekly basis. B) Initial tumor formation, when a palpable mass was first observed. One-way anova was used to assess significance. P-value < * = 0.05, <** = 0.01, <*** = 0.001, <****= 0.0001. C-E) Organoid metrics mapped against mouse survivability.

After subcutaneous transplantation, neoplasms arising from genetically altered TE organoids could be stratified into 3 groups (Figure 6., Sup. Table 1). Organoids containing *Nf1* mutations, such as TN, commonly resulted in poorly differentiated mesenchymal-like neoplasms (Figure 6A). Such neoplasms were largely composed of tightly arranged spindle cells, contained low to moderate of amount of cytoplasmic KRT8 and nuclear PAX8, and were marked by a medium to high proliferation index according to nuclear Ki67 immunostaining, and a high number of mitotic figures. Organoids with *Map2k4* mutations predominantly formed carcinomas with slit-like spaces forming labyrinthine patterns typical for HGSC (7/16 vs 3/37 for other mutations Fisher's P=0.0078). Cells of such neoplasms consistently expressed KRT8 and PAX8, and they had regionally variable proliferative indices and high-grade nuclear atypia. Mixed neoplasms contained mesenchymal and glandular-papillary patterns of growth. All neoplasms invited underlying striated muscles and upper levels of dermis at the place of organoid transplantation. Additionally, we noticed that *Nf1* mutation-containing tumors exhibiting spindle cells were derived from organoids with well-defined lumens, while tumors with glandular patterns arose from organoids with more blob-like structures (Fig. 3H). These findings relate specific genetic alterations to distinct features of HGSC.

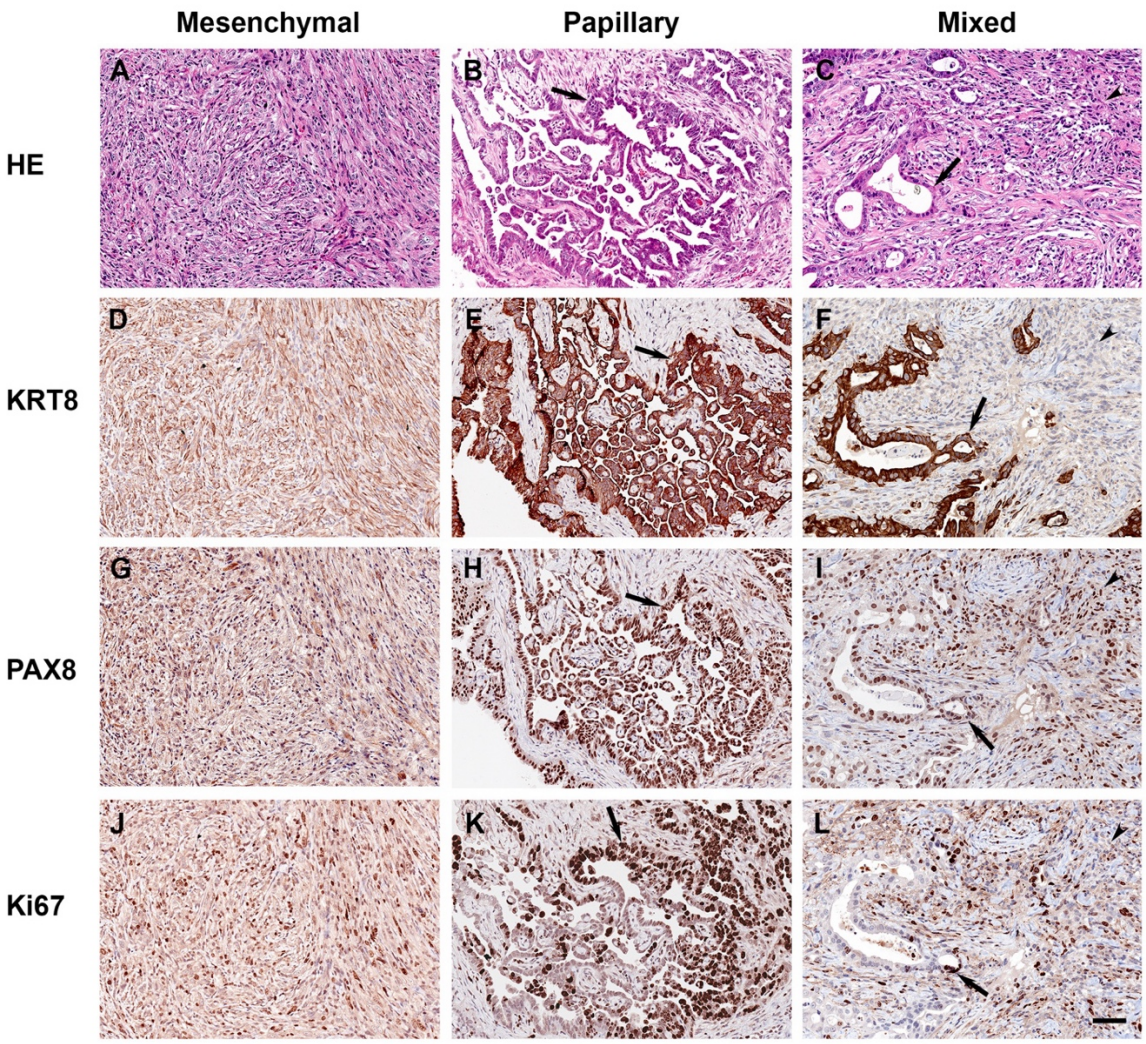

Figure 6. Characterization of neoplasms arising from genetically altered TE organoid cells transplanted subcutaneously. A) Spindle-cell (Mesenchymal) neoplasm with monotonous tight growth pattern, TN. B) Papillary carcinoma (Papillary) with slit-like spaces forming complex labyrinthine pattern (arrow), TP. C) Neoplasm with mixed spindle-cell (arrowhead) and glandular (arrow) patterns of growth (Mixed), TMP. Hematoxylin and eosin (HE; A-C). D-L) Expression (brown color) of KRT8 (D-F), PAX8

(G-I), and Ki67 (J-L) in neoplastic cells. Counterstaining with hematoxylin (D-L). Scale bar, all panels 60 μm.

2.4 Discussion

High-grade serous ovarian carcinoma presents as a heterogeneous solid tumor that is genetically unstable with multiple clonal lineages (54,55). These aspects have made treating HGSC especially challenging in stage III-IV HGSC, where 70% of patients relapse within 3 years (56). Early evidence suggests that HGSC does not follow a typical tumor growth trajectory; instead, dissemination occurs as a single rapid wave late in the tumor's evolutionary trajectory (57). Therefore, affect tumor initiation, progress, and presentation will be pivotal for developing diagnostic tools at earlier stages and improving patient outcomes. Our finding that tumors containing *Map2k4* genetic alterations have more differentiated papillary phenotypes typical for HGSC, provides a potentially useful target for intervention. It also opens a possibility for designing more accurate mouse models of HGSC involving inactivation of *Map2k4.*

Whereas HGSC can originate from both OSE and TE cells it is unknown if they utilize the same driver combinations. In our TE organoid screen, we used the same CRISPR KO mini library and infection conditions as we used in a prior screen of OSE (47). The transformation rates were similar: 0.28% for TE and 0.21% for OSE (47). Both OSE and TE transformation involved key HGSC drivers (*Trp53*, *Cdkn2a*, *Rb1*, *Pten*) (Sup. Fig. 7A) (8,9,11,12,15,47), but TE transformation was further enhanced by *Nf1*, *Map2k4*, *Brca2*, and *Brca1* ablation, while OSE transformation was enhanced by *Fancd2*, *Wwox*, *Gabra6*, and *Fat3* mutations (Sup. Fig. 7B). Notably, combinations like *TNP+Fancd2* or *TMC+Wwox* did not increase TE organoid transformation beyond their core triple mutant counterparts (Sup. Fig. 4C, D). Pathway analysis suggests that genes like *Wwox, Gabra6*, and *Fat3* may regulate the MAPK and AKT pathways, while *Fancd2* is involved in DNA

repair and interacts with BRCA1/2 (Fig. 7) (58–68). Despite some gene-specific differences, there may be shared altered pathways during malignant transformation. Other studies have compared the transformation potential of OSE and TE cells in organoid models and found differential results with respect to tumorigenic potential (10,11). However, OSE cells are flat cuboidal cells that exist as a single monolayer surrounding the ovary whereas TE cells exist in a pseudo-stratified structure that requires a 3D space. To this extent, our screening methods to assess transformation potential by adherence-independent growth (OSE) and aberrant morphology (TE) are more suitable approaches for maintaining cells in their native state. In summary, *Fancd2, Wwox, Gabra6,* and *Fat3* appear OSE-specific, while *Nf1, Map2k4, Brca2*, and *Brca1* are TE-specific, though these findings need further validation in direct comparisons.

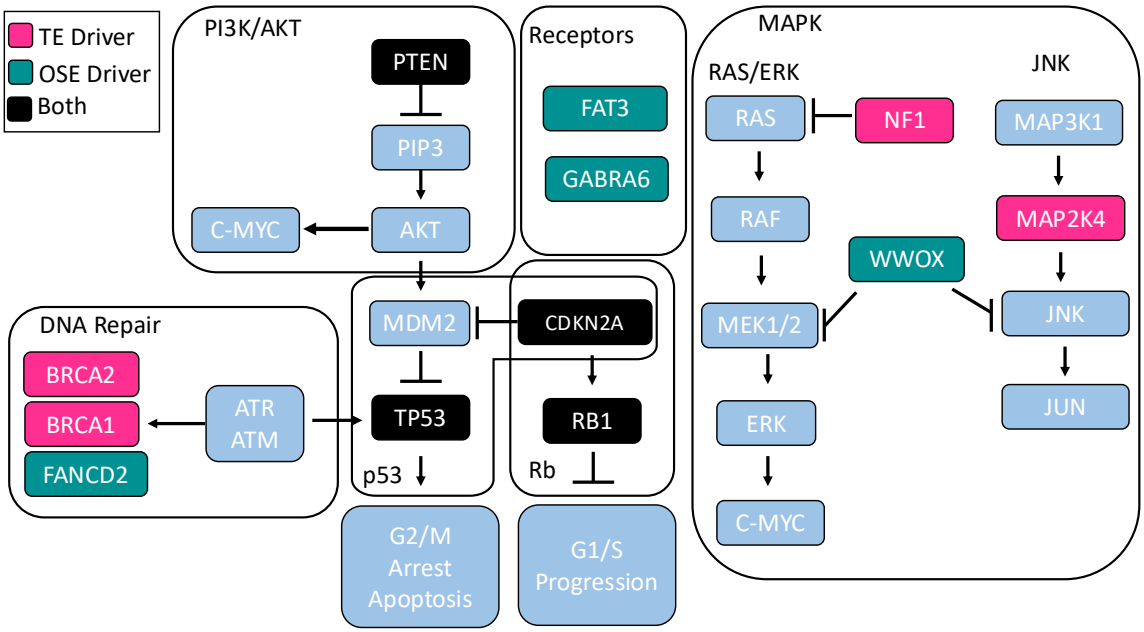

Figure 7. Summary of pathways of gene drivers identified in OSE and TE screens.

Of the seven transformation driver genes identified in our screen, *Map2k4* was the most intriguing. Encoding MKK4 in the JNK pathway, *Map2k4* phosphorylates JNK or p38 in a context-dependent manner (44,45,48,69). Evolutionary analyses of human HGSC suggest that aberrant MAPK signaling is associated with an early evolutionary state, marked by fewer subclones, diploid cancers, and better therapy response (70). Further tumor trajectory analysis implicates *MAP2K4* mutations in metastasis, particularly in the dissemination from the ovary to the omentum and ascites (57). While *Map2k4* overexpression can reduce tumor metastasis (71,72), our data show enhanced organoid transformation when co-mutated with *Nf1, Cdkn2a, Rb1, Pten*, or *Brca1*, though not all combinations formed tumors within 200 days (Sup. Table 1). This suggests that aberrant organoid formation may reflect metastatic potential or tumor subtype presentation, rather than just carcinogenesis (72).

Recent research on HGSC treatment has focused on how genetic perturbations influence responses to common therapies (carboplatin, gemcitabine, niraparib, paclitaxel, trametinib). Other studies have shown that differences in cell of origin and chemoresponse exist (10,11). For instance, WT OSE and TE organoids exhibited differential responses to HGSC treatments, highlighting the impact of culture conditions on drug efficacy. One group has shown that genes regulating similar pathways, such as RAS, have differences in response to common therapeutics that are gene context-dependent, such as MYC^{OE}, $KRAS^{OE}$, or $NF1^{-/-}$ (46). We observed that *Rb1/Cdkn2a* mutant cells responded similarly to gemcitabine regardless of ROCKi addition, though there were two subgroups: one more sensitive in the presence of ROCKi, the other less so. Generally, *Pten* and *Map2k4* mutations increased sensitivity, while *Nf1* mutations contributed to resistance in the

presence of ROCKi. Previous studies have shown that overexpression of *Ccne1* enhances gemcitabine sensitivity (46), and we found *Trp53/Rb1* mutants to be among the most resistant, with *Nf1* mutations maintaining resistance and *Map2k4* mutations increasing sensitivity.

We found that in general there was no difference between paclitaxel treated samples with ROCKi or not. We made the novel finding that *Map2k4* mutants were particularly sensitive to paclitaxel treatment, providing a potentially new avenue of treatment when considering JNK pathway altered cancers, primarily those implicating *Map2k4* and its downstream targets. Other groups have also shown that *Pten* mutations tend to drive resistances when compared to *Nf1* (46), but we found the opposite in our system. Altogether this may be due to differences in culture conditions or assay design. Nonetheless this implores the need to consider the whole tumor and identifying dominant mutations that are important for diagnosis and treatment of patients.

ROCKi (e.g., Fasudil) is emerging as a promising tool in combination therapy due to its roles in cytoskeletal regulation, cell migration, proliferation, survival, and metastasis (73,74). Previous studies have shown its potential to enhance chemo-sensitivity in resistant cancers, such as pancreatic cancer when combined with gemcitabine (75). Our data support this, showing that ROCKi treatment with gemcitabine significantly reduced transformed organoid survival compared to untreated controls (Sup. Fig. 6A). ROCKi also increased sensitivity to carboplatin and niraparib but conferred resistance to trametinib (Sup. Fig. 6A). Notably, transformed TE cells with *Nf1* mutations showed more resistance to paclitaxel than those with *Map2k4* mutations, with no significant difference between ROCKi -treated and untreated conditions. However, *Map2k4* mutations were more resistant

to trametinib without ROCKi. While other groups have shown that RAS-driven cancers containing *Map2k4* mutations are more sensitive to trametinib treatment, our data shows the opposite and our most resistant combination was TNM (44,45,53). These findings suggest that ROCKi could enhance treatment efficacy for specific mutations, offering new therapeutic possibilities.

Here, we present a comprehensive study demonstrating the tumorigenic potential of transformed TE organoids, confirming their utility as a model for studying tumor growth. While previous groups have shown that *TNP* mutations readily form tumors (46), our study goes further by detailing the specific impact of these mutations on tumor progression (Fig. 5). We also show that organoid metrics of transformation and diameter correlate with patient survival, a previously unreported correlation. Additionally, we report that *Nf1* mutations preferentially form mesenchymal tumors while *Map2k4* mutations preferentially form papillary tumors (Fig. 6). This observation drives the need to develop new mouse models focused on *Map2k4* mutations.

HGSC is characterized by numerous mutations, which makes identifying driver genes challenging. Our studies highlight the potential of rapidly screening genetic manipulations to explore the cell of origin and genetic drivers in HGSC. For example, our previous OSE screen showed that stem cells are more prone to transformation than non-stem cells (47). Recently we described TE cell lineage hierarchy and reported that inactivation of *Trp53* and *Rb1* in pre-ciliated cells leads to HGSC formation in the mouse (15). Future organoid studies should facilitate pinpointing cells most vulnerable to cancer cell states and their genetic drivers. Our KO screen also confirmed *Map2k4* as a key driver of TE cell transformation, revealing its sensitivity to paclitaxel and resistance to trametinib.

Additionally, our platform is amenable to modeling of amplification/overexpression events using CRISPRa (76) and assessing how gene combinations respond to therapies. The high throughput and speed of our platform allowed us to identify novel genetic drivers and optimal treatment strategies and can be further translated into human models to quickly assess patients for the most beneficial treatment outcomes.

2.5 Methods

Experimental animals. NOD.Cg-*Prkdc*^{scid} *Il2rg*$^{tm1wjl/}$SzJ (NSG) mice (Stock number 005557 were obtained from The Jackson Laboratory (Bar Harbor, ME, USA). The number of animals used in every experiment is indicated as biological replicates in Fig. legends and supplementary tables. Animals were euthanized if they became moribund or developed tumors over 1 cm in diameter. All the experiments and maintenance of the mice were conducted under protocols approved by the Cornell University Institutional Laboratory Animal Use and Care Committee (protocols numbers 2000-0116, 2001-0072 and 2004-0038). Mice were housed within a 10/14 light cycle. The lights came on at 5 a.m. and went off at 7 p.m., the humidity ranged from 30 – 70 %, and the ambient temperature was kept at 72°F +/- 2°F.

TE organoid derivation and culture. TE Organoids were cultured and derived as previously described (15). TE cells were isolated and cultured into organoids from 2-3 month old *Gt(ROSA)26Sor*$^{tm9(CAG-tdTomato)Hze}$ (*Rosa-loxp-stop-loxp*-tdTomato/Ai9, Stock number 007909 Jackson Laboratory) were sacrificed, oviducts isolated and dispersed into single cells with collagenase/dispase. Cells were rescued with 20% FBS containing media and plated as rims with matrigel (Corning #356231) at a density of 10kcells/100uL of matrigel per well in a 24w plate. Organoids were then expanded and cultured for at least 5 passages before experiments were performed. Organoids were passaged on day 7 unless otherwise specified. To passage organoids, media was aspirated from the wells, 300uL of cultrex organoid harvesting solution (R&D 3700-100-01) was added to each well and vigorously pipeted to disrupt matrigel. Dissolved matrigel was then transferred to a 15mL

conical and allowed to rest on ice for 1hour. Organoids were then spun down at 600xg for 5 minutes at 4C. If matrigel is still present, more cultrex organoid harvesting media was added and incubated for 30 minutes followed by centrifugation as described above. Once all matrigel is gone, supernatant was removed and 1mL of Trypsin EDTA 0.25% (Gibco 25200072) was added and incubated at 37C. Every 5 minutes organoids were disrupted into single cells with a P1000 pipet (vigorous pipetting at least 50 times up and down). This step was repeated 3 times for a total of 15 minutes. 20% FBS containing media was then added and cells were pelleted as described above. Cells were then resuspended in TE media and counted to be passaged as described above.

Lentiviral production and transduction. Lentivirus were produced in 293T cells and titer determined via limiting dilutions of virus in TE organoid cells as previously described (47). Briefly, 293T cells were seeded into 10cm dishes before LentiCRISPRv2 (Addgene #52961), PMD.2G (Addgene #12259) and PSPAX2 (Addgene #12260) were transfected using Transit-LT1 transfection reagent (Mirus bio, MIR2306) via manufacturer instructions. Virus was collected at 48 and 72 hours post transfection. Lenti-X Concentrator (Takara, 631231) was used as instructed to concentrate virus. Virus was then resuspended in TE organoid media with polybrene (Sigma, TR-1003-G) and frozen at -80C until use. LentiCRISPRv2-GFP (Addgene #82416) reporter plasmid was used to evaluate the quality of virus produced. To titer the virus, 5K TE organoid cells were subjected to limiting dilutions of virus in a 96 well plate and spinoculated at 600xg for 1hour at 37C as previously described (46). Lentiviral transduction continued for 6 hours at 37C in a cell incubator before cells were collected, mixed with matrigel and plated. After 48 hours

2ug/mL of puromycin was used to select for properly infected cells. Infection percent was evaluated by determining the number of surviving cells in treated versus non treated samples. The multiplicity of infection was calculated by using a survival percent below 30% to exclude double infection events. These values were then multiplied and averaged to determine an MOI of 7 (47).

Screen and validation. Day 7 TE organoids were broken into single cell suspensions as described above and infected with the minilibrary at an MOI of 7 and plated at a density of 5K cells per 25uL Matrigel droplet. 48 hours post infection, cells were treated with puromycin (2ug/mL, Sigma, A1113803) and at 96 hours media was changed to contain 10uM Nutlin-3A (SelleckChem, S8059). Media was changed every 2-3 days containing 10uM Nutlin-3A until day 14 where organoid transformation was assessed. Mutant organoids were then released from Matrigel with a P1000 wide bore tip in cultrex organoid harvesting media and allowed to settle by gravity. Supernatent was aspirated and replaced with more cultrex organoid harvesting media and allowed to settle by gravity. Organoids were then released onto a poly-hema (Sigma, P3932) coated tissue culture plate, picked as whole organoids, expanded in 2D culture, genomic DNA harvested with GeneJET Genomic DNA Purification Kit (Thermo Fisher, K0722), and PCR amplification with the following primers: CTTGGCTTTATATATCTTGTGGAAAGG and CGACTCGGTGCCACTTT was performed with Illumina overhangs also added to each primer. Indexing reactions were performed to barcode each individual colony and pooled. 300bp paired end sequencing was performed using Illumina Miseq to detect gRNA presence in a particular clone at a read depth of 4 million. Each sequenced clone was

aligned with a custom built library containing each of the gRNA's in the screen to identify "hits," where genome integration had taken place as described previously (47,75).

After identification of key combinations that result in TE organoid transformation, targeted lentiviral libraries were prepared and single cell suspensions from TE organoids were infected with the libraries at a minimum MOI of 7. Cells were then plated, treated with both puromycin and Nutlin-3A as described above. Organoid transformation rate was determined by counting the total number of aberrant organoids and dividing that by the total number of organoids formed after 14 days of culture. Images were acquired on a Zeiss Axiovert microscope.

Organoid preparation for histological evaluation. Organoids were released with organoid harvesting solution as described above. Organoids were placed on ice for 1 hour to release and allowed to settle to the tube bottom before aspirating the media without disturbing the pellet. Organoids were then washed with 10mL of ice cold 1X PBS to remove any residual Matrigel. Organoids were allowed to settle by gravity, the PBS was aspirated, then fixed in 4% PFA (diluted in PBS) on ice for 1 hour. Organoids were then washed twice with ice cold 1X PBS, then mixed with an equal volume of HistoGel (Epredia, HG4000012) preheated to 65°C and dispensed into dome-shaped molds for embedding. HistoGel molds set for 10 minutes prior to standard tissue processing, paraffin embedding, and preparation of 4-μm-thick tissue sections followed by immunohistochemistry (15,76).

Mouse tumorigenic studies. According to previous results (10), frequency of tumor formation by mutant TE organoids was not impacted by site (s.c. vs, orthotopic) of organoid

transplantation. Targeted library preparation and TE organoid infections were performed as described above. After passaging to expand cells, day 14 organoids were then disrupted into single cells and $5x10^5$ cells were mixed with 100uL of 1X PBS (Gibco 10010023) and Matrigel (Corning #356231) at a 1:1 ratio and injected subcutaneously in the flanks of NSG mice. All mice received bilateral injections and were monitored weekly for tumor formation, and growth of tumors. Mice were sacrificed when tumors reached 1 cm in diameter.

Drug Assays. Organoids were grown and dispersed into single cells as described above. Cells were diluted to a concentration of 100 cells per uL of Matrigel. 10uL of Matrigel containing cells were then seeded per well into the bottom of a black walled clear bottom 96 well plate (Corning #3603) and 100uL of media was added. 1 day after plating, cells were treated with the concentrations of drugs, media was changed on day 3 and on day 5 media was removed and 100uL of 3D Cell titer glo (Promega # G9683) was added for 1hr at room temperature and read on a biotek plate reader (10). Prism 10 was used to fit graphs and interpret IC50 values with the "[inhibitor] vs. response- variable slope (normalized)" option.

Immunohistochemistry and image analysis. For paraffin embedding, organoids and tissues were fixed in 4% paraformaldehyde overnight at 4°C followed by standard tissue processing, paraffin embedding and preparation of 4 μm-thick tissue sections. For immunohistochemistry, antigen retrieval was performed by incubation of deparaffinized and rehydrated tissue sections in boiling 10 mM sodium citrate buffer (pH 6.0) for 10

minutes. The primary antibodies were incubated either at 4°C for overnight or at room temperature for 2 hours, followed by incubation with secondary biotinylated antibodies (dilution 1:200, 45 minutes, at room temperature, RT). Modified Elite avidin-biotin peroxidase (ABC) technique (Vector Laboratories, Burlingame, CA, USA; pk-6100) was performed at room temperature for 30 minutes. Hematoxylin was used as the counterstain. All primary and secondary antibodies used for immunostaining are listed in Supplementary Table 2. For quantitative studies, sections were scanned by ScanScope CS2 or FL (Leica Biosystems, Vista, CA) with a 40× objective, followed by the analysis with the ImageJ software (National Institutes of Health, Bethesda, MD, USA).

Statistical analyses

Statistical comparisons were performed using a two-tailed Fisher's exact test with InStat 3 and Prism 6 software (GraphPad Software Inc., La Jolla, CA, USA). Prism 10 software was used to perform one-way anova, IC50 calculations, welch's two tailed t-test. Cbioportal was used to perform analysis of human data. c^2 analysis was performed in excel.

2.6 References

1. Patch A-M, Christie EL, Etemadmoghadam D, Garsed DW, George J, Fereday S, et al. Whole-genome characterization of chemoresistant ovarian cancer. Nature. 2015 May 28;521(7553):489–94.

2. Labidi-Galy SI, Papp E, Hallberg D, Niknafs N, Adleff V, Noe M, et al. High grade serous ovarian carcinomas originate in the fallopian tube. Nat Commun. 2017 Oct 23;8(1):1093.

3. Polak P, Karlić R, Koren A, Thurman R, Sandstrom R, Lawrence M, et al. Cell-of-origin chromatin organization shapes the mutational landscape of cancer. Nature. 2015 Feb 19;518(7539):360–4.

4. Sinkala M. Mutational landscape of cancer-driver genes across human cancers. Sci Rep. 2023 Aug 7;13(1):12742.

5. Garsed DW, Pandey A, Fereday S, Kennedy CJ, Takahashi K, Alsop K, et al. The genomic and immune landscape of long-term survivors of high-grade serous ovarian cancer. Nat Genet. 2022 Dec 1;54(12):1853–64.

6. Yang SYC, Lheureux S, Karakasis K, Burnier JV, Bruce JP, Clouthier DL, et al. Landscape of genomic alterations in high-grade serous ovarian cancer from exceptional long- and short-term survivors. Genome Med. 2018 Oct 31;10(1):81.

7. Zhai Y, Wu R, Kuick R, Sessine MS, Schulman S, Green M, et al. High-grade serous carcinomas arise in the mouse oviduct via defects linked to the human disease. J Pathol. 2017 Sep;243(1):16–25.

8. Flesken-Nikitin A, Hwang C-I, Cheng C-Y, Michurina TV, Enikolopov G, Nikitin AY. Ovarian surface epithelium at the junction area contains a cancer-prone stem cell niche. Nature. 2013 Mar 14;495(7440):241–5.

9. Flesken-Nikitin A, Choi K-C, Eng JP, Shmidt EN, Nikitin AY. Induction of carcinogenesis by concurrent inactivation of p53 and Rb1 in the mouse ovarian surface epithelium. Cancer Res. 2003 Jul 1;63(13):3459–63.

10. Lõhmussaar K, Kopper O, Korving J, Begthel H, Vreuls CPH, van Es JH, et al. Assessing the origin of high-grade serous ovarian cancer using CRISPR-modification of mouse organoids. Nat Commun. 2020 May 27;11(1):2660.

11. Zhang S, Dolgalev I, Zhang T, Ran H, Levine DA, Neel BG. Both fallopian tube and ovarian surface epithelium are cells-of-origin for high-grade serous ovarian carcinoma. Nat Commun. 2019 Nov 26;10(1):5367.

12. Perets R, Wyant GA, Muto KW, Bijron JG, Poole BB, Chin KT, et al. Transformation of the fallopian tube secretory epithelium leads to high-grade serous ovarian cancer in Brca;Tp53;Pten models. Cancer Cell. 2013 Dec 9;24(6):751–65.

13. Kim J, Coffey DM, Creighton CJ, Yu Z, Hawkins SM, Matzuk MM. High-grade serous ovarian cancer arises from fallopian tube in a mouse model. Proc Natl Acad Sci USA. 2012 Mar 6;109(10):3921–6.

14. Maniati E, Berlato C, Gopinathan G, Heath O, Kotantaki P, Lakhani A, et al. Mouse ovarian cancer models recapitulate the human tumor microenvironment and patient response to treatment. Cell Rep. 2020 Jan 14;30(2):525-540.e7.

15. Flesken-Nikitin A, Ralston CQ, Fu D-J, De Micheli AJ, Phuong DJ, Harlan BA, et al. Pre-ciliated tubal epithelial cells are prone to initiation of high-grade serous ovarian carcinoma. Nat Commun. 2024 Oct 5;15(1):8641.

16. Chong GO, Park JY, Lee HJ. Incidental Serous Tubal Intraepithelial Carcinoma that Developed into Primary Peritoneal Serous Carcinoma in a Patient without BRCA Mutation. Am J Case Rep. 2020 Feb 8;21:e921146.

17. Patrono MG, Iniesta MD, Malpica A, Lu KH, Fernandez RO, Salvo G, et al. Clinical outcomes in patients with isolated serous tubal intraepithelial carcinoma (STIC): A comprehensive review. Gynecol Oncol. 2015 Dec;139(3):568–72.

18. Saccardi C, Zovato S, Spagnol G, Bonaldo G, Marchetti M, Alessandrini L, et al. Efficacy of risk-reducing salpingo-oophorectomy in BRCA1-2 variants and clinical outcomes of follow-up in patients with isolated serous tubal intraepithelial carcinoma (STIC). Gynecol Oncol. 2021 Nov;163(2):364–70.

19. Weinberger V, Bednarikova M, Cibula D, Zikan M. Serous tubal intraepithelial carcinoma (STIC) - clinical impact and management. Expert Rev Anticancer Ther. 2016 Dec;16(12):1311–21.

20. Ducie J, Dao F, Considine M, Olvera N, Shaw PA, Kurman RJ, et al. Molecular analysis of high-grade serous ovarian carcinoma with and without associated serous tubal intra-epithelial carcinoma. Nat Commun. 2017 Oct 17;8(1):990.

21. Powell CB, Swisher EM, Cass I, McLennan J, Norquist B, Garcia RL, et al. Long term follow up of BRCA1 and BRCA2 mutation carriers with unsuspected neoplasia identified at risk reducing salpingo-oophorectomy. Gynecol Oncol. 2013 May;129(2):364–71.

22. Kauff ND, Satagopan JM, Robson ME, Scheuer L, Hensley M, Hudis CA, et al. Risk-reducing salpingo-oophorectomy in women with a BRCA1 or BRCA2 mutation. N Engl J Med. 2002 May 23;346(21):1609–15.

23. Rhiem K, Foth D, Wappenschmidt B, Gevensleben H, Büttner R, Ulrich U, et al. Risk-reducing salpingo-oophorectomy in BRCA1 and BRCA2 mutation carriers. Arch Gynecol Obstet. 2011 Mar;283(3):623–7.

24. Smith MJ, Gerber D, Olsen A, Khouri OR, Wang Y, Liu M, et al. Uptake and timing of risk-reducing salpingo-oophorectomy among patients with BRCA1 and BRCA2 mutations. Am J Obstet Gynecol. 2021 Nov;225(5):508.e1-508.e10.

25. Kauff ND, Barakat RR. Risk-reducing salpingo-oophorectomy in patients with germline mutations in BRCA1 or BRCA2. J Clin Oncol. 2007 Jul 10;25(20):2921–7.

26. Shih I-M, Wang Y, Wang T-L. The origin of ovarian cancer species and precancerous landscape. Am J Pathol. 2021 Jan;191(1):26–39.

27. Kopper O, de Witte CJ, Lõhmussaar K, Valle-Inclan JE, Hami N, Kester L, et al. An organoid platform for ovarian cancer captures intra- and interpatient heterogeneity. Nat Med. 2019 May;25(5):838–49.

28. Fiorini E, Veghini L, Corbo V. Modeling cell communication in cancer with organoids: making the complex simple. Front Cell Dev Biol. 2020 Mar 18;8:166.

29. McCool KW, Freeman ZT, Zhai Y, Wu R, Hu K, Liu C-J, et al. Murine Oviductal High-Grade Serous Carcinomas Mirror the Genomic Alterations, Gene Expression Profiles, and Immune Microenvironment of Their Human Counterparts. Cancer Res. 2020 Feb 15;80(4):877–89.

30. Khashaba M, Fawzy M, Abdel-Aziz A, Eladawei G, Nagib R. Subtyping of high grade serous ovarian carcinoma: histopathological and immunohistochemical approach. J Egypt Natl Canc Inst. 2022 Feb 9;34(1):6.

31. Murakami R, Matsumura N, Mandai M, Yoshihara K, Tanabe H, Nakai H, et al. Establishment of a Novel Histopathological Classification of High-Grade Serous Ovarian Carcinoma Correlated with Prognostically Distinct Gene Expression Subtypes. Am J Pathol. 2016 May;186(5):1103–13.

32. Chen GM, Kannan L, Geistlinger L, Kofia V, Safikhani Z, Gendoo DMA, et al. Consensus on Molecular Subtypes of High-Grade Serous Ovarian Carcinoma. Clin Cancer Res. 2018 Oct 15;24(20):5037–47.

33. Cancer Genome Atlas Research Network. Integrated genomic analyses of ovarian carcinoma. Nature. 2011 Jun 29;474(7353):609–15.

34. Chen J, Shi X, Xiao L, Li Z, Li Z, Sun L. Better or worse? The prognostic role of the mesenchymal subtype in patients with high-grade serous ovarian carcinoma: A systematic review and meta-analysis. Cancer Med. 2022 Oct;11(20):3761–70.

35. Hu Y, Taylor-Harding B, Raz Y, Haro M, Recouvreux MS, Taylan E, et al. Are epithelial ovarian cancers of the mesenchymal subtype actually intraperitoneal metastases to the ovary? Front Cell Dev Biol. 2020 Jul 17;8:647.

36. Hatano Y, Tamada M, Asano N, Hayasaki Y, Tomita H, Morishige K-I, et al. High-grade serous ovarian carcinoma with mucinous differentiation: report of a rare and unique case suggesting transition from the "SET" feature of high-grade serous carcinoma to the "STEM" feature. Diagn Pathol. 2019 Jan 12;14(1):4.

37. Uner H, Demir M, Goksuluk D, Kars A, Uner M, Usubutun A. Evidence for Diverse Prognosis in High-Grade Serous Ovarian Carcinoma: Solid, Pseudoendometrioid, and Transitional-Like; So-Called "SET Morphology" and Progesterone Receptor Status. Turk Patoloji Derg. 2022;38(3):240–50.

38. Press JZ, De Luca A, Boyd N, Young S, Troussard A, Ridge Y, et al. Ovarian carcinomas with genetic and epigenetic BRCA1 loss have distinct molecular abnormalities. BMC Cancer. 2008 Jan 22;8:17.

39. Zheng M, Hu Y, Gou R, Liu O, Nie X, Li X, et al. Identification of immune-enhanced molecular subtype associated with BRCA1 mutations, immune checkpoints and clinical outcome in ovarian carcinoma. J Cell Mol Med. 2020 Mar;24(5):2819–31.

40. Wei Y, Ou T, Lu Y, Wu G, Long Y, Pan X, et al. Classification of ovarian cancer associated with BRCA1 mutations, immune checkpoints, and tumor microenvironment based on immunogenomic profiling. PeerJ. 2020 Nov 24;8:e10414.

41. González-Martín A, Pothuri B, Vergote I, DePont Christensen R, Graybill W, Mirza MR, et al. Niraparib in Patients with Newly Diagnosed Advanced Ovarian Cancer. N Engl J Med. 2019 Dec 19;381(25):2391–402.

42. Ditzel HM, Strickland KC, Meserve EE, Stover E, Konstantinopoulos PA, Matulonis UA, et al. Assessment of a Chemotherapy Response Score (CRS) System for Tubo-Ovarian High-Grade Serous Carcinoma (HGSC). Int J Gynecol Pathol. 2019 May;38(3):230–40.

43. Moore K, Colombo N, Scambia G, Kim B-G, Oaknin A, Friedlander M, et al. Maintenance Olaparib in Patients with Newly Diagnosed Advanced Ovarian Cancer. N Engl J Med. 2018 Dec 27;379(26):2495–505.

44. Xue Z, Vis DJ, Bruna A, Sustic T, van Wageningen S, Batra AS, et al. MAP3K1 and MAP2K4 mutations are associated with sensitivity to MEK inhibitors in multiple cancer models. Cell Res. 2018 Jul;28(7):719–29.

45. Jansen RA, Mainardi S, Dias MH, Bosma A, van Dijk E, Selig R, et al. Small-molecule inhibition of MAP2K4 is synergistic with RAS inhibitors in KRAS-mutant cancers. Proc Natl Acad Sci USA. 2024 Feb 27;121(9):e2319492121.

46. Zhang S, Iyer S, Ran H, Dolgalev I, Gu S, Wei W, et al. Genetically defined, syngeneic organoid platform for developing combination therapies for ovarian cancer. Cancer Discov. 2021 Feb;11(2):362–83.

47. Yamulla RJ, Nalubola S, Flesken-Nikitin A, Nikitin AY, Schimenti JC. Most Commonly Mutated Genes in High-Grade Serous Ovarian Carcinoma Are Nonessential for Ovarian Surface Epithelial Stem Cell Transformation. Cell Rep. 2020 Sep 1;32(9):108086.

48. Davis SJ, Choong DYH, Ramakrishna M, Ryland GL, Campbell IG, Gorringe KL. Analysis of the mitogen-activated protein kinase kinase 4 (MAP2K4) tumor suppressor gene in ovarian cancer. BMC Cancer. 2011 May 17;11:173.

49. Yang H, Mao W, Rodriguez-Aguayo C, Mangala LS, Bartholomeusz G, Iles LR, et al. Paclitaxel Sensitivity of Ovarian Cancer Can be Enhanced by Knocking Down Pairs of Kinases that Regulate MAP4 Phosphorylation and Microtubule Stability. Clin Cancer Res. 2018 Oct 15;24(20):5072–84.

50. Phuong DJ, Pirtz MG, Ralston CQ, Cosgrove BD, Schimenti JC, Flesken-Nikitin A, et al. Aggressive Serous Carcinomas of the Female Reproductive Tract: Cancer-Prone Cell States and Genetic Drivers. Cancers (Basel). 2025 Feb 11;17(4):604.

51. Sallum LF, Andrade L, Ramalho S, Ferracini AC, de Andrade Natal R, Brito ABC, et al. WT1, p53 and p16 expression in the diagnosis of low- and high-grade serous ovarian carcinomas and their relation to prognosis. Oncotarget. 2018 Mar 23;9(22):15818–27.

52. Uno K, Yoshikawa N, Tazaki A, Ohnuma S, Kitami K, Iyoshi S, et al. Significance of platinum distribution to predict platinum resistance in ovarian cancer after platinum treatment in neoadjuvant chemotherapy. Sci Rep. 2022 Mar 16;12(1):4513.

53. Geistlinger L, Oh S, Ramos M, Schiffer L, LaRue RS, Henzler CM, et al. Multiomic Analysis of Subtype Evolution and Heterogeneity in High-Grade Serous Ovarian Carcinoma. Cancer Res. 2020 Oct 15;80(20):4335–45.

54. Denisenko E, de Kock L, Tan A, Beasley AB, Beilin M, Jones ME, et al. Spatial transcriptomics reveals discrete tumour microenvironments and autocrine loops within ovarian cancer subclones. Nat Commun. 2024 Apr 3;15(1):2860.

55. González-Martín A, Harter P, Leary A, Lorusso D, Miller RE, Pothuri B, et al. Newly diagnosed and relapsed epithelial ovarian cancer: ESMO Clinical Practice Guideline for diagnosis, treatment and follow-up. Ann Oncol. 2023 Oct;34(10):833–48.

56. Sveen A, Johannessen B, Klokkerud SMK, Kraggerud SM, Meza-Zepeda LA, Bjørnslett M, et al. Evolutionary mode and timing of dissemination of high-grade serous carcinomas. JCI Insight. 2024 Feb 8;

57. Liu S, Huang J, Zhang Y, Liu Y, Zuo S, Li R. MAP2K4 interacts with Vimentin to activate the PI3K/AKT pathway and promotes breast cancer pathogenesis. Aging (Albany NY). 2019 Nov 25;11(22):10697–710.

58. Liu C-C, Ho P-C, Lee I-T, Chen Y-A, Chu C-H, Teng C-C, et al. WWOX phosphorylation, signaling, and role in neurodegeneration. Front Neurosci. 2018 Aug 15;12:563.

59. Lo J-Y, Chou Y-T, Lai F-J, Hsu L-J. Regulation of cell signaling and apoptosis by tumor suppressor WWOX. Exp Biol Med (Maywood). 2015 Mar;240(3):383–91.

60. Pavese JM, Ogden IM, Voll EA, Huang X, Xu L, Jovanovic B, et al. Mitogen-activated protein kinase kinase 4 (MAP2K4) promotes human prostate cancer metastasis. PLoS ONE. 2014 Jul 14;9(7):e102289.

61. Baroja I, Kyriakidis NC, Halder G, Moya IM. Expected and unexpected effects after systemic inhibition of Hippo transcriptional output in cancer. Nat Commun. 2024 Mar 27;15(1):2700.

62. Seo S, Kim YA, Lee J, Lee S, Kim J, Lee S. Fat3 regulates neural progenitor cells by promoting Yap activity during spinal cord development. Sci Rep. 2022 Aug 30;12(1):14726.

63. Guo Z, Yan X, Song C, Wang Q, Wang Y, Liu X-P, et al. FAT3 mutation is associated with tumor mutation burden and poor prognosis in esophageal cancer. Front Oncol. 2021 Mar 19;11:603660.

64. Gumireddy K, Li A, Kossenkov AV, Sakurai M, Yan J, Li Y, et al. The mRNA-edited form of GABRA3 suppresses GABRA3-mediated Akt activation and breast cancer metastasis. Nat Commun. 2016 Feb 12;7:10715.

65. Li T-J, Jiang J, Tang Y-L, Liang X-H. Insights into the leveraging of GABAergic signaling in cancer therapy. Cancer Med. 2023 Jul;12(13):14498–510.

66. Bell-Horner CL, Dohi A, Nguyen Q, Dillon GH, Singh M. ERK/MAPK pathway regulates GABAA receptors. J Neurobiol. 2006 Nov;66(13):1467–74.

67. Han B, Shen Y, Zhang P, Jayabal P, Che R, Zhang J, et al. Overlooked FANCD2 variant encodes a promising, portent tumor suppressor, and alternative polyadenylation contributes to its expression. Oncotarget. 2017 Apr 4;8(14):22490–500.

68. Canovas B, Nebreda AR. Diversity and versatility of p38 kinase signalling in health and disease. Nat Rev Mol Cell Biol. 2021 May;22(5):346–66.

69. Lahtinen A, Lavikka K, Virtanen A, Li Y, Jamalzadeh S, Skorda A, et al. Evolutionary states and trajectories characterized by distinct pathways stratify patients with ovarian high grade serous carcinoma. Cancer Cell. 2023 Jun 12;41(6):1103-1117.e12.

70. Spillman MA, Lacy J, Murphy SK, Whitaker RS, Grace L, Teaberry V, et al. Regulation of the metastasis suppressor gene MKK4 in ovarian cancer. Gynecol Oncol. 2007 May;105(2):312–20.

71. Yamada SD, Hickson JA, Hrobowski Y, Vander Griend DJ, Benson D, Montag A, et al. Mitogen-activated protein kinase kinase 4 (MKK4) acts as a metastasis suppressor gene in human ovarian carcinoma. Cancer Res. 2002 Nov 15;62(22):6717–23.

72. McLeod R, Kumar R, Papadatos-Pastos D, Mateo J, Brown JS, Garces AHI, et al. First-in-Human Study of AT13148, a Dual ROCK-AKT Inhibitor in Patients with Solid Tumors. Clin Cancer Res. 2020 Sep 15;26(18):4777–84.

73. Barcelo J, Samain R, Sanz-Moreno V. Preclinical to clinical utility of ROCK inhibitors in cancer. Trends Cancer. 2023 Mar;9(3):250–63.

74. Kim S, Kim SA, Han J, Kim I-S. Rho-Kinase as a Target for Cancer Therapy and Its Immunotherapeutic Potential. Int J Mol Sci. 2021 Nov 29;22(23).

75. Gilbert LA, Horlbeck MA, Adamson B, Villalta JE, Chen Y, Whitehead EH, et al. Genome-scale CRISPR-mediated control of gene repression and activation. Cell. 2014 Oct 23;159(3):647–61.

76. Flesken-Nikitin A, Harlan BA, Nikitin AY. Transplantation into the mouse ovarian fat pad. J Vis Exp. 2016 Sep 7;(115).

Acknowledgements

This work was supported by NIH grants (CA182413, CA260115 and CA248524) to AYN, Ovarian Cancer Research Fund grant (327516) to AYN, Sandra Atlas Bass Endowment for Cancer Research to AYN and JCS, and the NSF Graduate Research Fellowship Program (GRFP) awarded to CQR (DGE-2139899).

2.7 Supplementary Information

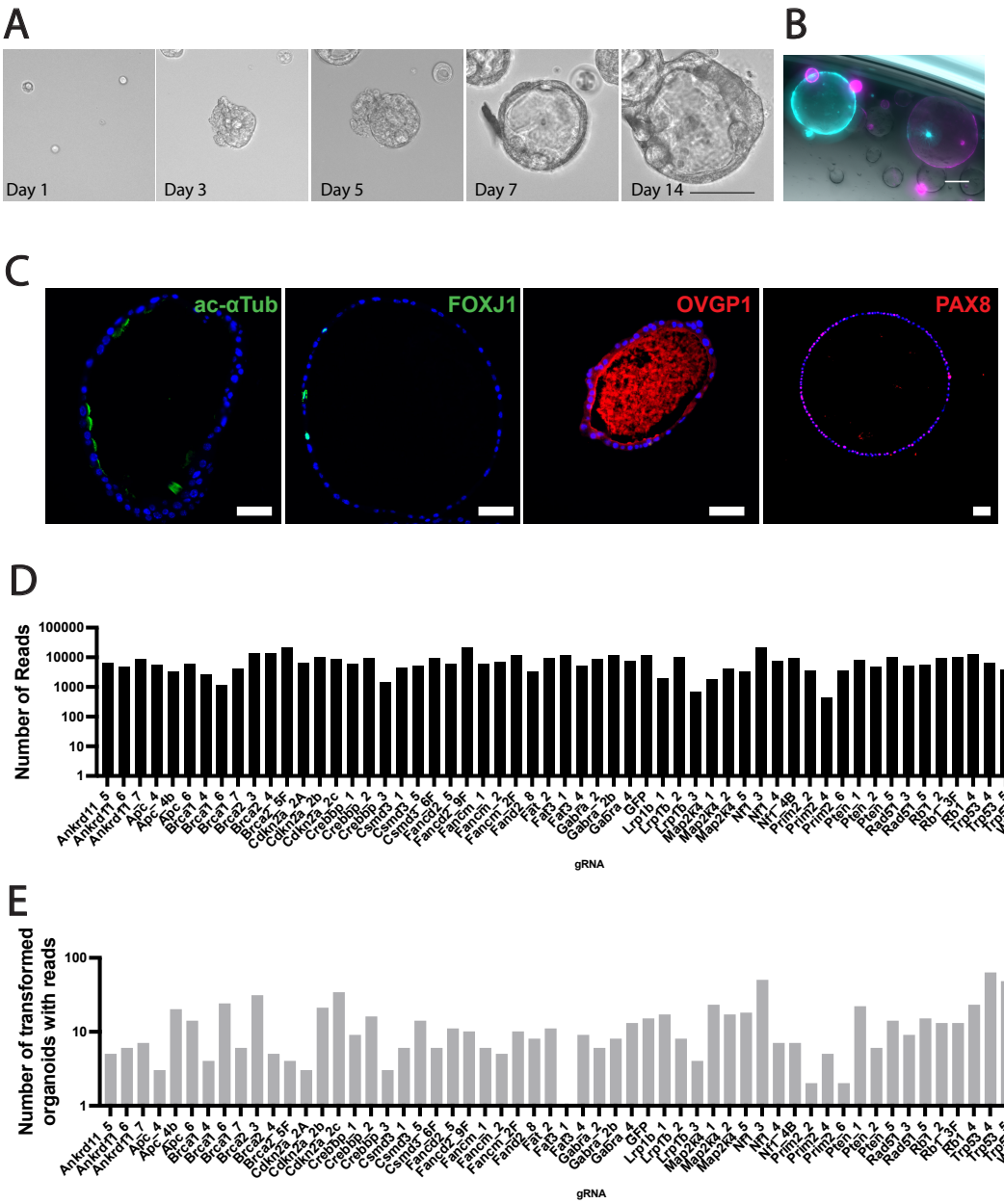

Supplementary Figure 1. Validation of TE organoids and minilibrary for CRISPR screening. A) TE Organoids grow and self organize. Scale bar = 100µm B) TE Organoids express either mCherry (magenta) or GFP (teal) after lentiviral infection with a lack of signal co-localization. Scale bar = 100µm C) TE Organoids express canonical mature markers in both traditional organoids and mouse oviduct. Scale bar = 50µm. D) LentiCRISPR mini-library distribution post infection in 293T cells. E) gRNA presence in clones of organoids.

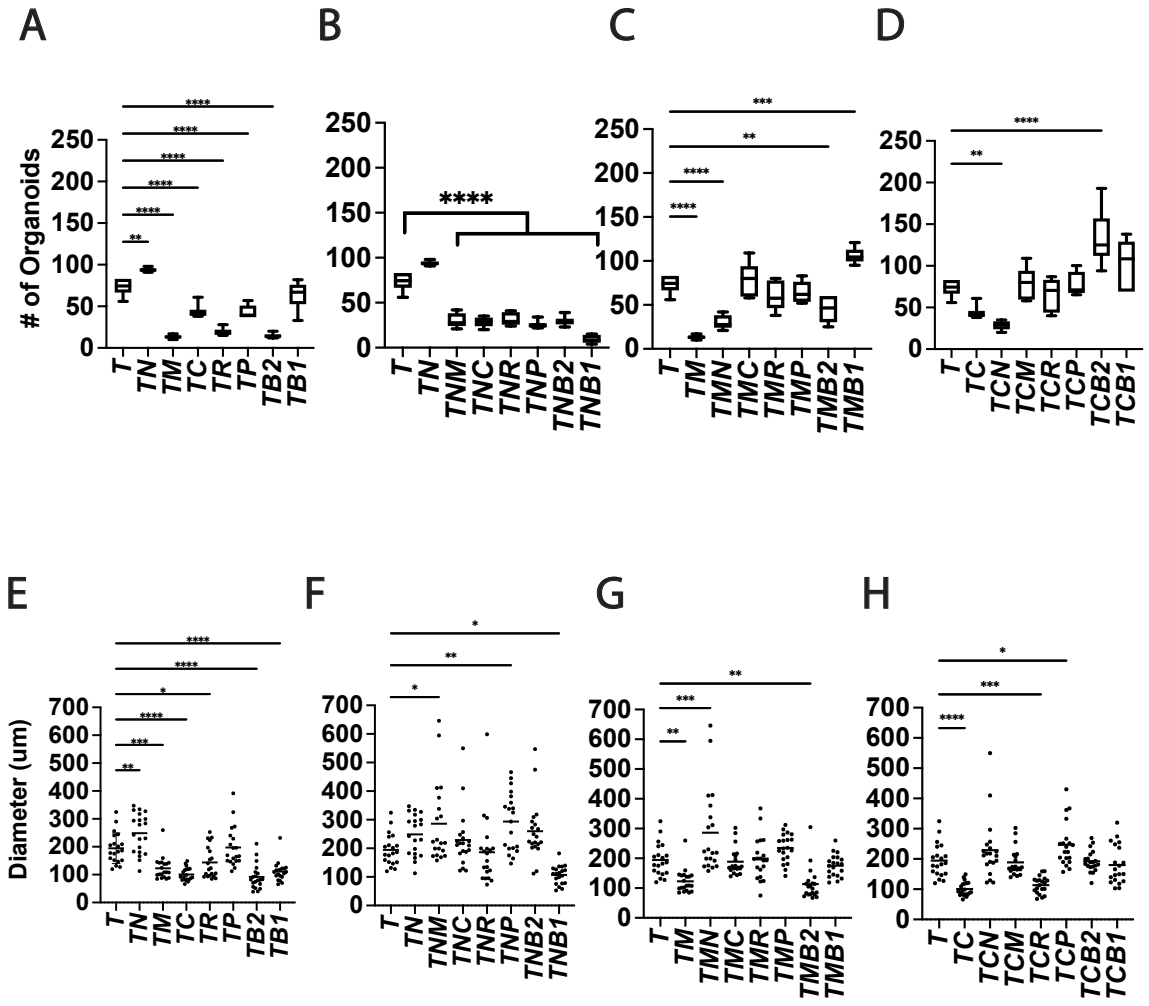

Supplementary Figure 2. **Validation of organoid formation and diameter from combinations identified in screen.** ABCD) Formation of organoids with different combinations. N = 6. EFGH) Organoid diameter was measured, n= 20 organoids. One-way anova was performed to assess significance. P-value < * = 0.05, <** = 0.01, <*** = 0.001, <****= 0.0001.

A

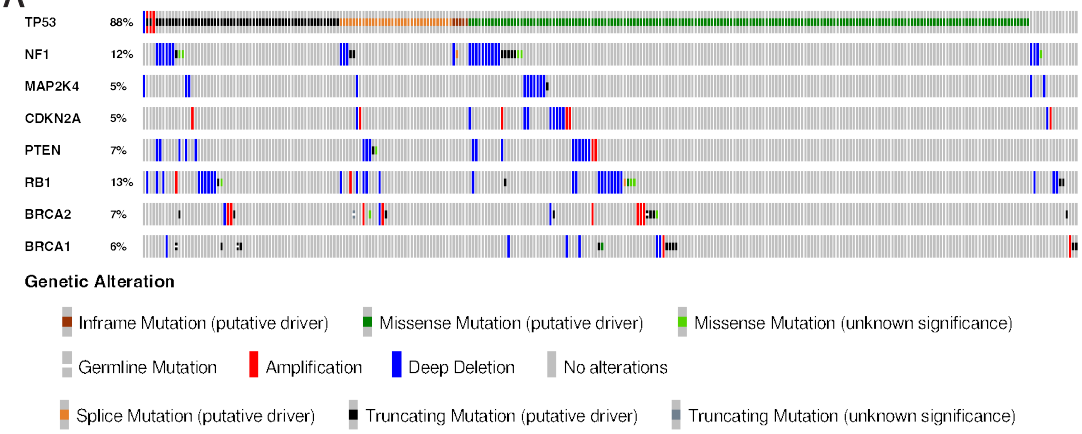

B

Gene A	Gene B	Samples with neither	Samples with Gene	Samples with Gene	Samples with both	p-Value	q-Value	Tendency
MAP2K4	*CDKN2A*	251	8	11	3	0.014	0.226	CO
NF1	*PTEN*	225	27	15	6	0.028	0.226	CO
RB1	*PTEN*	224	28	15	6	0.032	0.226	CO
PTEN	*BRCA2*	235	17	17	4	0.065	0.342	CO
NF1	*RB1*	213	26	27	7	0.153	0.644	CO
RB1	*BRCA1*	226	30	13	4	0.243	0.851	CO
CDKN2A	*BRCA2*	240	12	19	2	0.293	0.88	CO
NF1	*MAP2K4*	229	33	11	0	0.371	0.973	ME
NF1	*BRCA1*	226	30	14	3	0.442	1	CO
MAP2K4	*PTEN*	242	10	20	1	0.593	1	CO
CDKN2A	*BRCA1*	243	13	16	1	0.603	1	CO
NF1	*CDKN2A*	228	31	12	2	0.68	1	CO
RB1	*BRCA2*	220	32	19	2	1	1	ME
MAP2K4	*BRCA2*	241	11	21	0	1	1	ME
PTEN	*BRCA1*	236	20	16	1	1	1	ME
BRCA2	*BRCA1*	236	20	16	1	1	1	ME
CDKN2A	*PTEN*	239	13	20	1	1	1	ME
CDKN2A	*RB1*	226	13	33	1	1	1	ME
MAP2K4	*RB1*	229	10	33	1	1	1	ME
NF1	*BRCA2*	221	31	19	2	1	1	ME
MAP2K4	*BRCA1*	245	11	17	0	1	1	ME

Supplementary Figure 3. Analysis of genetic alterations in human HGSC. A) OncoPrint (from cBio Portal; Firehose legacy) of human HGSC genetic alterations of selected tumor suppressor genes. B) Co-occurrence of gene drivers identified in screen as seen in human HGSC (only samples containing a *TP53* mutation were assessed). CO = Co-occurrence, ME = Mutual Exclusivity.

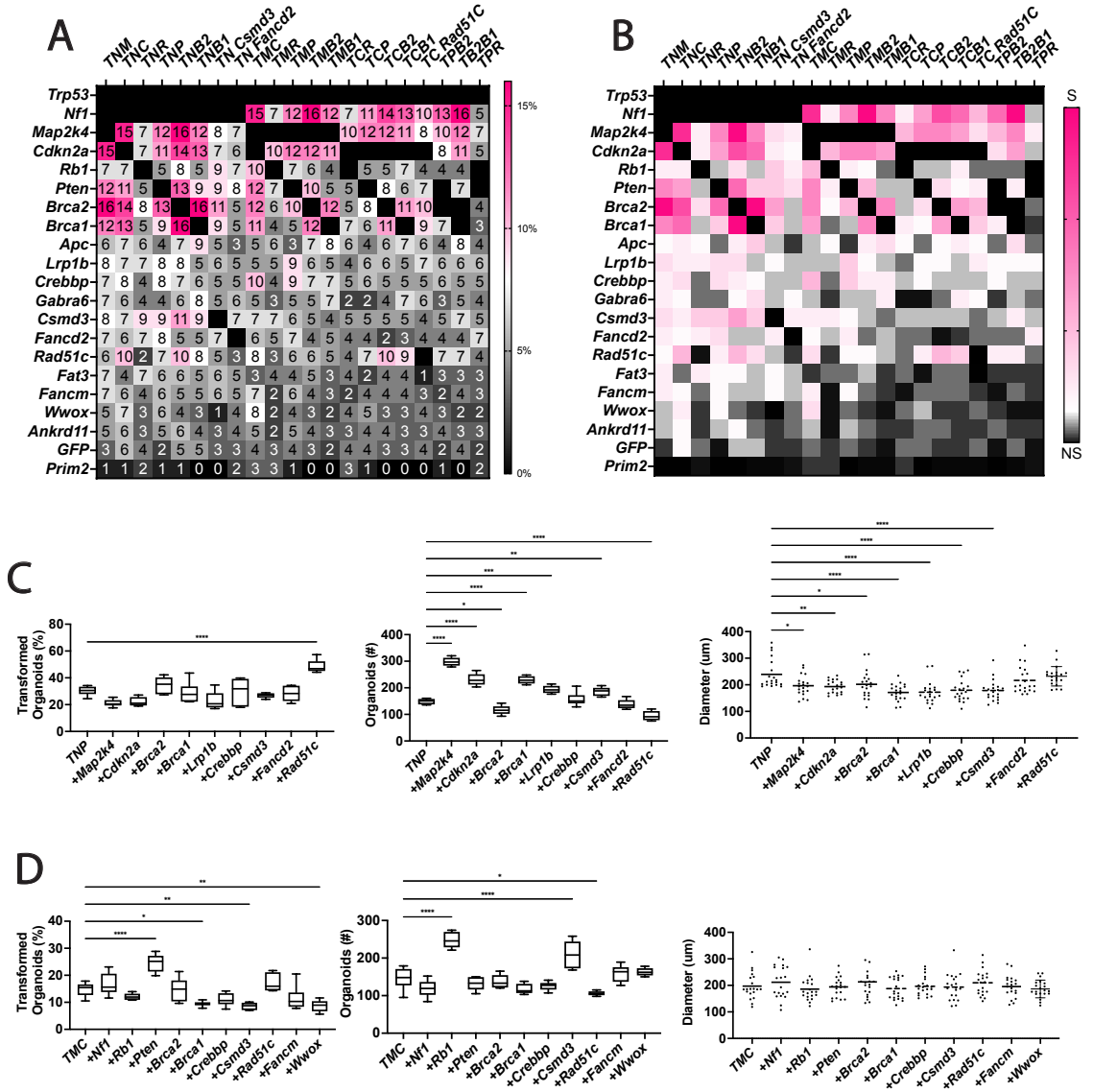

Supplementary Figure 4. **Analysis and validation of quadruple mutant combinations.** A) Starting with the most overrepresented triple combinations, the most significant quadruple mutations are plotted. B) c^2 analysis of significant TE triple quadruple mutants, DF, 19, P<0.05%. S = Significant, NS = Not Significant C) Transformed organoids in a *Trp53*$^{-/-}$*Nf1*^{mut}*Pten*^{mut} deficient background, D) Organoid formation, E) Organoid size. F) Transformed organoids in a *Trp53*$^{-/-}$*Map2k4*^{mut}*Cdkn2a*^{mut} deficient background G)

Organoid formation H) Organoid size. n=6 was analyzed per condition, with organoid size measuring n=20 organoids per condition. One-way anova was performed to assess significance. P-value < * = 0.05, <** = 0.01, <*** = 0.001, <****= 0.0001.

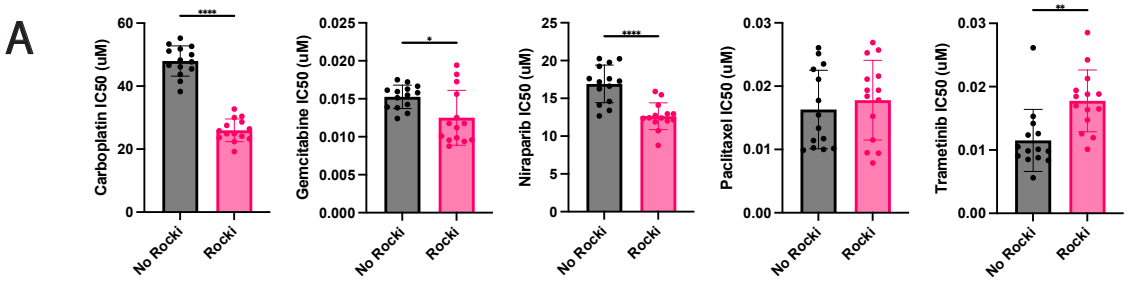

Supplementary Figure 5. IC50 calculations and dose response curves to common HGSC therapeutics. A) IC50 for all gene combinations with and without ROCKi. Welch's two tailed t-test P-value < * = 0.05, <** = 0.01, <*** = 0.001, <****= 0.0001.

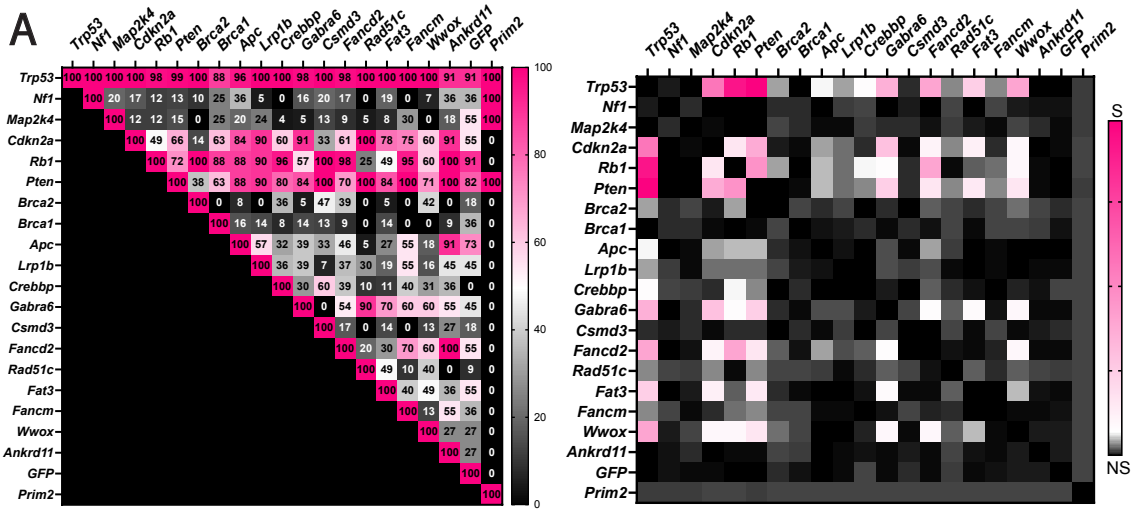

Supplementary Figure 6. Unique and shared drivers of transformation in OSE cells

A) Frequency of co-mutations in OSE colonies, (Right) c^2 analysis of significant OSE double mutations, DF, 19, P<0.05%. S = Significant, NS = Not Significant

Supplementary Table 1 Organoid combinations tested in mouse models and histological analysis

Combination	Tumors formed (#)	Mesenchymal	Papillary	Mixed
Trp53	0/6			
Trp53/Nf1	5/6	4		1
Trp53/Pten	4/6			4
Trp53/Rb1	1/6			1
Trp53/Nf1/Map2k4	6/6	3		3
Trp53/Nf1/Cdkn2a	5/6	4	1	
Trp53/Nf1/Rb1	5/6			5
Trp53/Nf1/Pten	6/6	3		3
Trp53/Nf1/Brca2	6/6	5		1
Trp53/Map2k4/Cdkn2a	0/6			
Trp53/Map2k4/Rb1	4/6	1	3	
Trp53/Map2k4/Pten	6/6	2	4	
Trp53/Map2k4/Brca1	0/6			
Trp53/Cdkn2a/Pten	5/6		2	3

Supplementary Table 2. Antibodies used for immunostaining.

Antigen, conjugation	Antibody source, catalogue number	Clone	Host	Retrieval, Dilution
Acetylated α-Tubulin	Sigma-Aldrich, T7451	6-11B-1	Mouse	Citrate, 1:200 ([&]IF)
FOXJ1	Novus Biologicals, AF3619-SP	*PC	Goat	Citrate, 1:600 (IF)
Ki67	Invitrogen, 14-5698-82	SolA15	Rat	Citrate, 1:4000 ([#]IHC)
Cytokeratin 8, CK8	Developmental Studies Hybridoma Bank, AB_531826 (20μg mL^{-1})	TROMA-I	Rat	Citrate, 1:50 (IHC)
OVGP1	Abcam, ab118590	PC	Rabbit	Citrate, 1:600 (IF)
P16	Abcam, ab241543	PABLO33B	Rat	Citrate, 1:500 (IHC)
Pax8	Proteintech, 10336-1-AP	PC	Rabbit	Citrate, 1:4000 (IHC), 1:200 (IF)
Wilm's Tumor Antigen, WT1	Abcam, ab267377	EPR23963-116	Rabbit	Citrate, 1:500 (IHC)
tdTomato/RFP	Rockland Immunochemicals Inc., 600-401-379S	PC	Rabbit	No retrieval, 1:4000 (IHC)
Anti-rabbit IgG, biotinylated	Vector Labs, BA-1000-1.5	PC	Goat	1:200
Anti-rat IgG, biotinylated	Vector Labs, BA-4000-1.5	PC	Rabbit	1:200

*PC, polyclonal
[&]IF, immunofluorescence
[#]IHC, immunoperoxidase-ABC Elite method

Chapter 3: Organoid validation of SLC1A3 expression as a stem/progenitor cell marker

This chapter was adapted from a manuscript published in *Nature Communications* (PMID: 39366996 PMCID: PMC11452611 DOI: 10.1038/s41467-024-52984-1)

A.F.N. and A.Y.N. designed experiments; C.Q.R., D.J.F., D.J.P., B.A.H., C.S.A., A.P.A., and S.G. performed experiments; C.Q.R., A.J.D.M., D.W.M., and B.D.C. carried our bioinformatics analyses; D.J.F., L.H.E., and A.Y.N. performed pathological evaluations; J.C.S., and B.D.C. provided resources; A.F.N., C.Q.R. and A.Y.N. wrote the paper.

Authors: Andrea Flesken-Nikitin, Coulter Q. Ralston, Dah-Jiun Fu, Andrea J. De Micheli, Daryl J. Phuong, Blaine A. Harlan, Christopher S. Ashe, Amanda P. Armstrong, David W. McKellar, Sangeeta Ghuwalewala, Lora H. Ellenson, John C. Schimenti, Benjamin D. Cosgrove & Alexander Yu. Nikitin.

3.1 Abstract:

The distal region of the uterine (Fallopian) tube is commonly associated with high-grade serous carcinoma (HGSC), the predominant and most aggressive form of ovarian or extra-uterine cancer. Specific cell states and lineage dynamics of the adult tubal epithelium (TE) remain insufficiently understood, hindering efforts to determine the cell of origin for HGSC. Here, we report a comprehensive census of cell types and states of the mouse uterine tube. We show that distal TE cells expressing the stem/progenitor cell marker *Slc1a3* can differentiate into both secretory (*Ovgp1*+) and ciliated (acetyl α-tubulin+) cells. These findings identify transitional pre-ciliated cells as a cancer-prone cell state and point to pre-ciliation mechanisms as diagnostic and therapeutic targets.

3.2 Introduction

Ovarian cancer is the sixth leading cause of death for women in the United States (1). High-grade serous carcinoma (HGSC) is the most common and aggressive type of ovarian cancer (2,3). Over 80% of HGSC are detected at advanced stage and have limited treatment options(2,4,5). This is attributed to latent progression of the disease with lack of early symptoms and detection methods (2). Detection and treatment of HGSC at earlier stages could be crucial to improving the prognosis of patients with this malignancy. However, identification of new diagnostic markers and therapeutic targets is hindered by our inadequate knowledge about the cells in which HGSC originates and the mechanisms underlying disease initiation.

The location of HGSC initiation has long been debated, but the emerging consensus is that both the ovarian surface epithelium (OSE) and the tubal epithelium (TE) of the uterine tube, also known as the oviduct or Fallopian tube, have potential to progress into HGSC(6–11). While cancer-prone stem/progenitor cells have been described for the OSE(12,13), the cell of origin of HGSC arising from TE remains unclear. It has been shown that the majority of familial HGSC cases may begin with the appearance of early dysplastic lesions, *TP53* signatures, and serous tubal intraepithelial carcinomas (STICs)(6,14). These lesions are found exclusively in the distal region of the uterine tube(2,14,15). Both *TP53* signatures and STICs lack ciliation, express the transcriptional factor PAX8, and harbor mutations in the *TP53* gene (also known as *Trp53* in the mouse), which encodes for p53. *TP53* mutations are the most frequent genetic alterations in HGSC, being present in over 96% of cases(16,17). Consistent with these observations, early dysplastic lesions can be induced by inactivation of tumor

suppressor genes commonly associated with human HGSC, such as *Trp53*, *Brca1*, *Brca2, Pten*, and *Rb1* in *Pax8*-expressing tubal epithelial cells of the mouse uterine tube(18,19). In both humans and rodents, uterine tubes consist of distal (infundibulum, ampulla, and ampullary-isthmic junction) and proximal regions (isthmus and intramuscular utero-tubal junction). The uterine tube is formed by the simple pseudostratified TE surrounded by a thin stromal layer, two circular smooth muscle layers, and the mesothelium. Two main cellular components of the TE are ciliated cells (also known as multi-ciliated cells), predominantly located in the distal regions of the tube, and secretory cells, which are more abundant in the proximal regions. Additionally, there are basal cells, representing intraepithelial T-lymphocytes and peg cells. Peg cells have been described as either exhausted secretory cells or CD44+ progenitor cells (20–22).

Previous mouse lineage-tracing studies have reported that cells expressing *Pax8* have the capacity to self-renew and differentiate into ciliated cells in both distal and proximal regions after labeling during embryonic or prepubertal development (23). However, recent studies based on immunophenotyping, lineage tracing, and limited single cell RNA-sequencing (scRNA-seq) suggest presence of distinct cell lineages in the distal (*Pax8*+) and the proximal (*Pax2*+) regions of the adult mouse uterine tube(24).

It is well established that many types of cancer arise from stem cell niches(25–27). Previously, using a genetically defined mouse model, we have shown that OSE stem/progenitor cells can be efficiently transformed after inactivation of tumor suppressor genes *Trp53* and *Rb1* and lead to HGSC formation (12,13,28). Notably, tumors arising from non-stem OSE cells were slow-growing and non-metastatic. However, in other

cancer types, neoplasms may originate from differentiated or transitional state cells that have acquired some stem cell properties (28–30). It has been hypothesized that some ovarian carcinomas may arise from the ciliated cell lineage (31). However, no direct experimental data has been offered to support this idea.

Here, we conduct scRNA-seq to establish a comprehensive census of cell types found in the mouse uterine tube. Proximal and distal sections are sequenced separately to investigate characteristics underscoring the distal region's predisposition towards cancer initiation. By using a combination of computational lineage trajectory projections and genetic cell fate, we identify a TE stem/progenitor cell population and interrogate unique epithelial cell states for their propensity for malignant transformation. We found that *Slc1a3*+ epithelial cells are stem/progenitor cells of the distal TE, form ciliated organoids with high efficiency, and are not cancer prone. These studies reveal that pre-ciliated cells may serve as a specific cell state susceptible to malignant transformation.

3.3 Results

3.3.1 *Slc1a3*+ epithelial cells are stem/progenitor cells for the TE

Within this study, scRNA-seq was performed on 62 uterine tubes from 31 mice and divided into both distal and proximal regions. After processing of the data, clusters were identified, and epithelial cells were categorized into subpopulations of secretory, ciliated and stem-like epithelial cells. Further investigation of the distal epithelial clusters via PHATE analysis found that ciliated cells and their precursors were more likely to be found in the distal region while secretory cells were more prevalent in the proximal region. While *Pax8* expression has primarily thought to be secretory related, our data

suggests that *Pax8* expression are detected in stem/progenitor cells and transitional pre-ciliogenic cells.

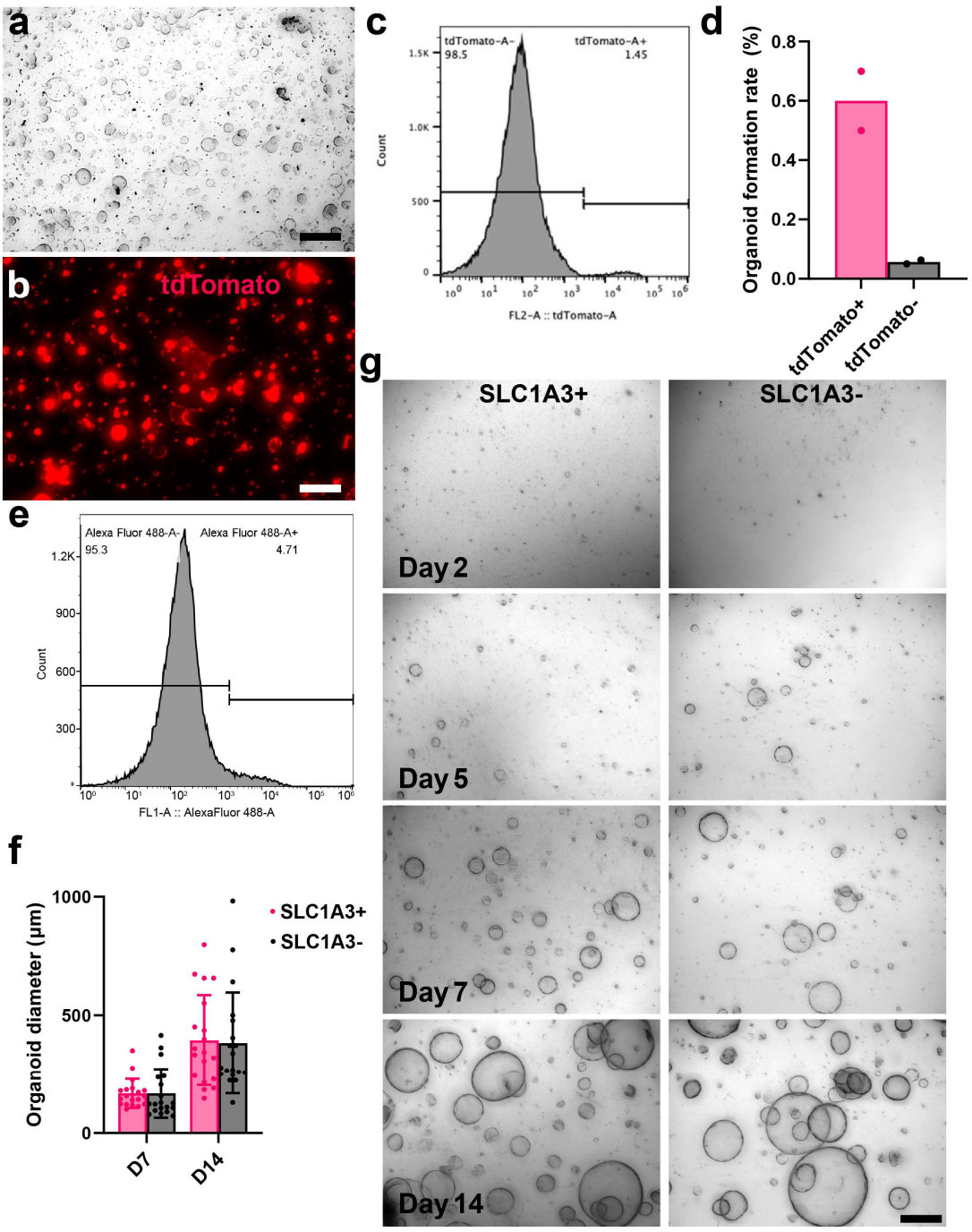

Figure 1. Tubal epithelium (TE) organoid formation. (a-b) Organoid formation by distal TE cells isolated from Slc1a3-CreERT Ai9 mice and treated with tamoxifen. Phase contrast (a) and tdTomato fluorescence (red, b). (c) Representative histogram of tdTomato+ TE cells separated by FACS 36 hours after tamoxifen

administration. (d) Quantification of organoid formation rate of TE cells separated for tdTomato expression by FACS. Biological replicates n=2. (e) Representative histogram of SLC1A3+ TE cells separated by MACS. (f) Organoid size measured 7 days and 14 days between SLC1A3+ and SLC1A3- cells from two MACS experiments (n=19). (g) Representative images of SLC1A3+ and SLC1A3- organoids 2, 5, 7, and 14 days after isolation from a single MACS experiment. Scale bar represents 170 μm (a and b) and 500 μm (g). Source data are provided as a Source Data file.

3.3.2 SLC1A3+ stem/progenitor cells form ciliated organoids with high efficiency

Consistent with previous studies of mouse and human TE (20,32,33), organoids were formed by harvesting the mouse distal TE. The organoid-forming ability of tdTomato+ cells from Slc1a3-CreERT Ai9 mice was confirmed with isolation from the distal region after separation by fluorescence-activated cell sorting (FACS) (Fig. 1a–d). To further distinguish the SLC1A3+ stem/progenitor cells from others within the TE, we completed magnetic-activated cell sorting (MACS) to split pure epithelial cell pools into SLC1A3+ and SLC1A3- groups (Fig. 1e and Table 1). Consistent with previous FACS experiments, organoids derived from SLC1A3+ epithelial cells formed organoids at a significantly higher rate as compared to organoids formed by SLC1A3- cells (Fig. 2a). After 14 days of culture, organoids grew to similar sizes (Fig. 1f, g) and contained OVGP1+ cells in both groups (Fig. 2b). However, organoids formed from SLC1A3+ cells were marked by a significantly larger population of ciliated cells (Fig. 2c–e), thereby supporting bidirectional differentiation potential of SLC1A3+ cells.

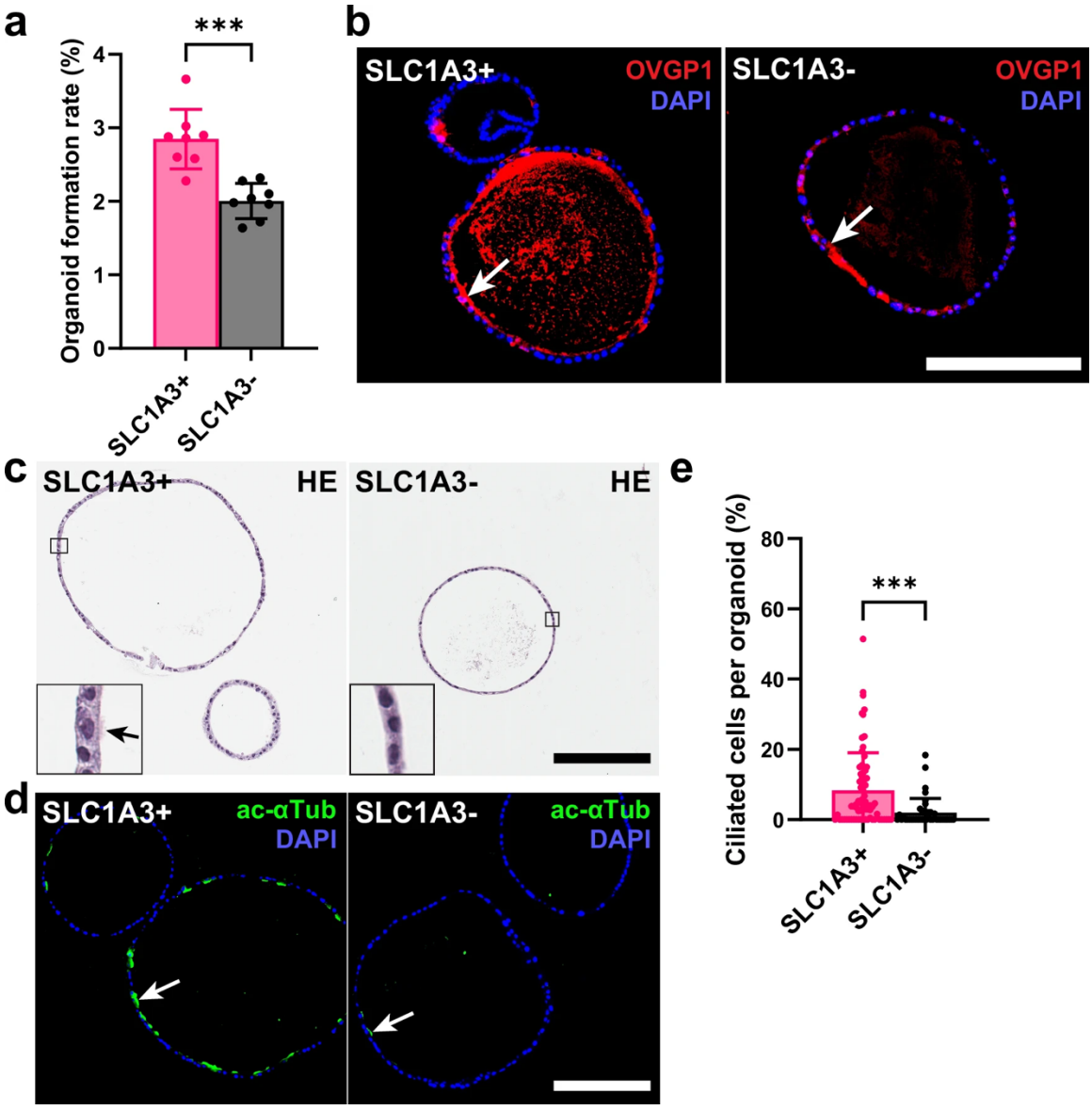

Figure. 2. Organoid formation by SLC1A3+ and SLC1A3- cells. Organoid formation rate of distal tubal epithelial cells isolated for SLC1A3 expression by MACS ($n = 8$). **b** Organoid sections of day 14 SLC1A3+ and SLC1A3- cell derived organoids stained for secretory marker OVGP1 (red, arrows). Counterstaining with DAPI (blue). **c** Hematoxylin and Eosin (HE) staining of SLC1A3+ and SLC1A3- cell derived organoids after 14 days of culture. Arrow denotes cilia. **d** Representative images of ciliation (green, acetylated α-Tubulin) between SLC1A3+ and SLC1A3- cell derived

organoids. Counterstaining with DAPI (blue). **b**–**d** Scale bar all images 200 μm. **e** Quantification of ciliated cells between SLC1A3+ ($n = 71$) and SLC1A3- ($n = 40$) cell derived organoids. **a**, **e** ***$P = 0.0002$, ****$P = 0.0005$, two-tailed unpaired *t*-tests. Data are presented as mean values ± SD.

3.4 Discussion

Our single-cell transcriptomics allowed for unique cell states and cell lineage hierarchy to be identified in the context of healthy adult mouse uterine tubes. Further experimentation has confirmed that *Slc1a3*+ cells are long living and give rise to both secretory and ciliated cells in the distal region of the uterine tube.

We did not observe any significant contribution of *Slc1a3*+ cells to cells of the proximal uterine tube and saw few if any organoids formed from the proximal region. This can be explained by the existence of developmentally distinct cell lineages forming the proximal region (24).

By comparative evaluation of *Pax8*+ cells lacking concomitant *Slc1a3* expression, we identified a cancer-prone cell population along the ciliogenic lineage. This observation is consistent with prevalence of early dysplastic lesions, *TP53* signatures and STICs in the distal, ciliated cell-rich, region of the uterine tube(2,14,15). Furthermore, the majority of HGSC putative driver genes(13,34), either preferentially expressed in stem/progenitor cells with a bias towards pre-ciliogenic trajectory (*Rb1, Nf1* and *Pten)*, or mainly detected in cilia-forming cells (*Brca1*, *Brca2* and *Csmd3*). Thus, aberrations in these genes may have the most transformation potential in the context of pre-ciliogenic cell state, as opposed to secretory differentiation (Figure 3).

There are potential limitations within this study. The use of scRNA-seq may be limited by its low capture efficiency and high level of noise. While scRNA-seq may fail to capture all transcripts in each cell, the technique was sufficient for identifying markers of cell states within the distal TE. Furthermore, organoids were generated from pools of epithelial cells split by their SLC1A3 expression. However, there may be other epithelial

cell states that are less likely to form organoids among the SLC1A3+ and SLC1A3- populations, which may impact the organoid formation rate. Finally, we explore cancer-prone cell states by inactivating *Trp53* and *Rb1*. Inactivation of these genes leads to HGSC arising from pre-ciliated TE cells. However, other combinations of driver mutations may transform other cell states and/or produce different types of ovarian carcinoma.

In summary, our study establishes the cell hierarchy, cell lineage dynamics, and identity of stem/progenitor cells in the distal TE. Furthermore, we show resistance of TE stem/progenitor cells to malignant transformation and provide direct experimental evidence for cancer propensity of cells in the transitional pre-ciliated state. These findings explain the preferential appearance of neoplastic lesions in the distal region of the uterine tube and point to the pre-ciliation state as a diagnostic and therapeutic target.

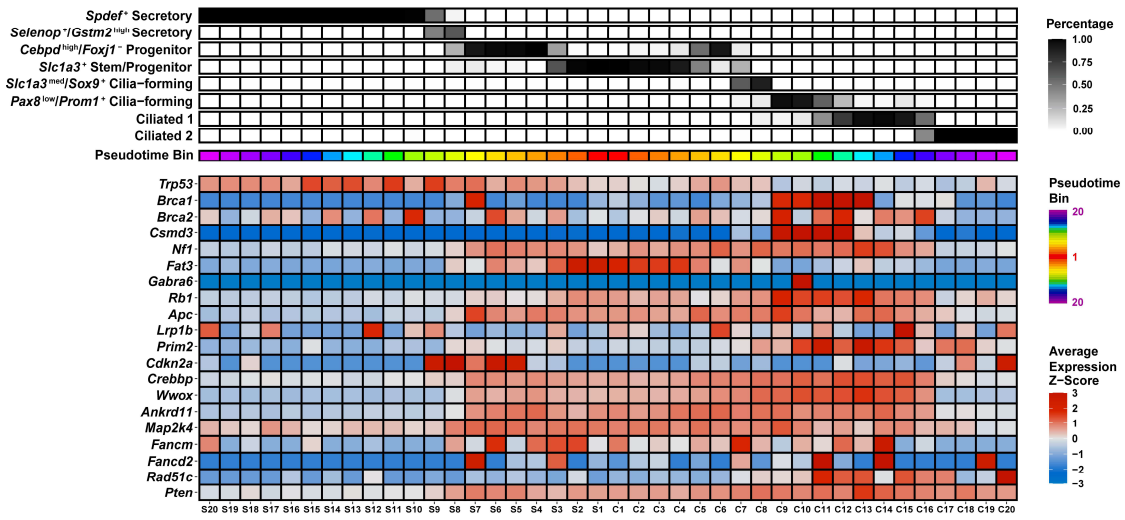

Figure 3. Expression of putative HGSC driver genes along inferred pseudotime trajectories of secretory and ciliated epithelial cell lineages. The average zscored expression was calculated for each gene. Each pseudotime bin is equally sized and consists of about 150 cells. Driver genes were derived from the Cancer Genome Atlas Research Network. Most genes, except for FANCM and APC were found to be significantly mutated or deleted in HGSC tumors by TCGA1, 2. Source data are provided as a Source Data file. Figure created by Coulter Q. Ralston.

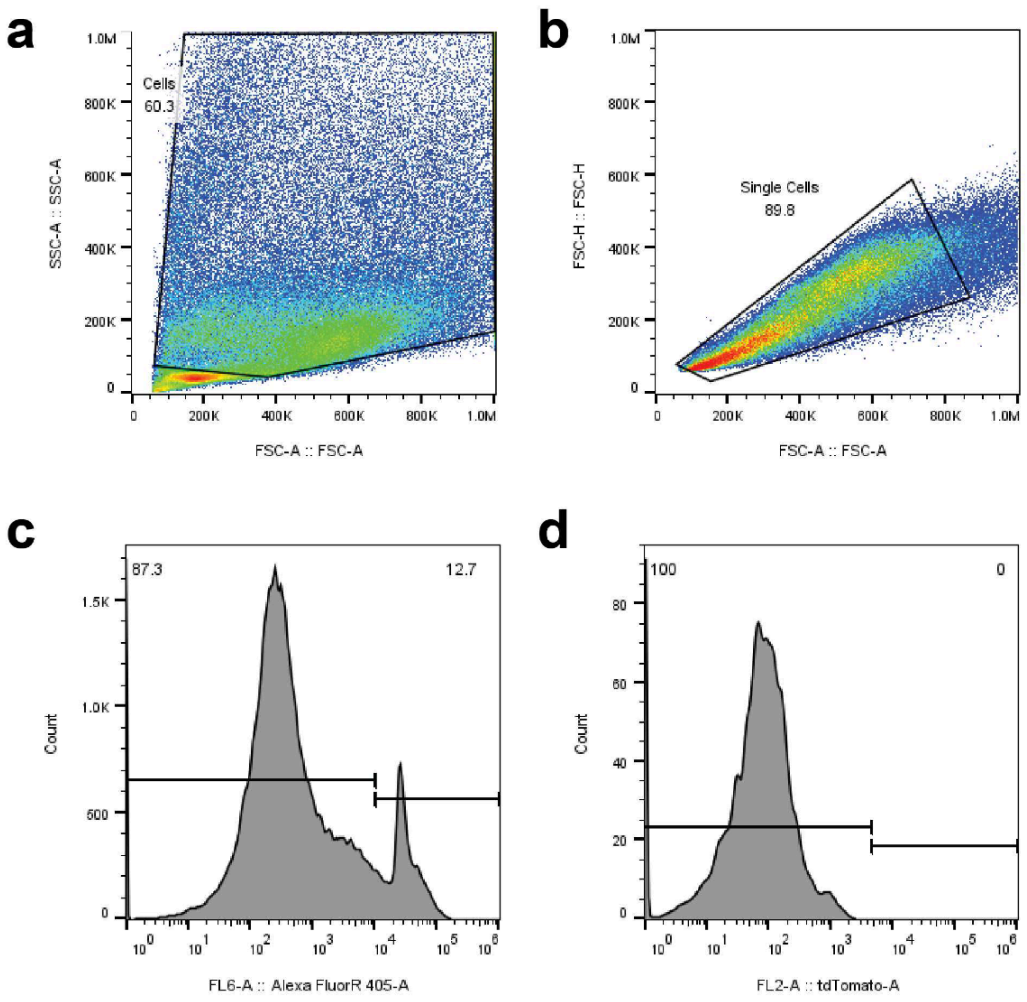

Figure 4. Gating strategy for tdTomato+ TE cells. (a) Forward scatter (FSC) and side scatter (SSC) gating strategy for removal of debris within distal TE cells isolated from Slc1a3-CreERT Ai9 mice after tamoxifen treatment. (b) FSC gating for single cell purification. (c) SYTOX Blue dead cell staining to remove positively stained dead cells. (d) Counts for tdTomato+ distal TE cells isolated from Ai9H mice after tamoxifen treatment as a negative control.

Supplementary Table 1.
Magnetic-activated cell sorting (MACS) for organoid-forming SLC1A3+ and SLC1A3- cells.

Fractions*	Total cells (± s.d.)	Fraction of total cells (%)
After primary isolation	$5.66x10^{5} \pm 1.47x10^{5}$	100
After stromal removal	$2.76x10^{5} \pm 0.65x10^{5}$	48.8
SLC1A3+ cells	$0.20x10^{5} \pm 0.13x10^{5}$	3.5
SLC1A3- cells	$2.55x10^{5} \pm 0.49x10^{5}$	45.1

*Total cells and percentages were determined by cell counts made from cell fractions at different stages of MACS preparation.

3.5 Methods

Experimental animals

The Tg(Slc1a3-cre/ERT)1Nat/J (Slc1a3-CreERT, Stock number 012586), *Gt(ROSA)26Sor*$^{tm9(CAG\text{-}tdTomato)Hze}$ (*Rosa-loxp-stop-loxp*-tdTomato/Ai9, Stock number 007909), and C57BL6 (Stock number 000664) mice were obtained from The Jackson Laboratory (Bar Harbor, ME, USA). Only females were used for our studies of the female reproductive tract. The number of animals used in every experiment is indicated as biological replicates in figure legends and supplementary tables. All the experiments and maintenance of the mice followed ethical regulations for animal testing and research. They were approved by the Cornell University Institutional Laboratory Animal Use and Care Committee (protocols numbers 2000-0116 and 2001-0072). Mice were housed within a 10/14 light cycle. The lights came on at 5 a.m. and went off at 7 p.m., the humidity ranged from 30–70 %, and the ambient temperature was kept at 72 °F ± 2 °F.

Doxycycline and tamoxifen induction

For organoid assays after FACS, 5 Slc1a3-CreERT Ai9 mice 6–12 week-old mice per experiment received a single 36 h tamoxifen pulse (100 μg/g body weight as described above). All mice were euthanized by CO_2 and further analyses were carried out.

Anatomical nomenclature

“Uterine tube”, “Fallopian tube”, and “oviduct” are terms commonly used by different groups of investigators. The term “uterine tube” precisely describes its location and function as a tube leading from the ovary to the uterus. “Fallopian tube,” named after the 16th-century Italian anatomist Gabriele Falloppio, is a more traditional term, but it’s less

descriptive anatomically. “Oviduct” is anatomically descriptive, indicating a duct for the ovum (egg), but it is less specific to human anatomy and is often used in the context of various animals. We use the term “uterine tube” as the most anatomically accurate name for this structure. The “uterine tube” is also the most unifying term allowing to be efficiently used for comparative human/mouse studies common in experimental research.

Immunohistochemistry, apoptosis detection, and image analysis

Immunofluorescent detection of FAM183B (IF, dilution 1:150) and OVGP1 (IF, dilution 1:600, 1:800, IHC, 1:800, 1:2000–8000) was performed in 7 μm-thick frozen sections according to standard protocols. For paraffin embedding, tissues were fixed in 4% paraformaldehyde overnight at 4 °C followed by standard tissue processing, paraffin embedding, and preparation of 4 μm-thick tissue sections. All primary and secondary antibodies used for immunostaining are listed in the paper.

For quantitative studies, sections were scanned with a ScanScope CS2 (Leica Biosystems, Vista, CA), 40x objective, a Zeiss LSM 710 Confocal Microscope for tile scans with a pixel dwell of 1.58 μsec and an averaging of 2 using the ZEN (blue edition, Zeiss) software, or a Leica TCS SP5 Confocal Microscope, 20x and 40x objective, followed by the analysis with Fiji software (National Institutes of Health, Bethesda, MD, USA).

TE organoid preparation

Mouse tubal epithelial cells (TE) were isolated from Slc1a3-CreERT Ai9 positive and negative littermates. Single cell suspensions for organoids were adapted from previously described methods[7,10,56]. Briefly, mouse uterine tubes were collected, washed with wash

buffer (Phosphate buffered saline pH 7.4, Thermo Fisher 10010023, 10,000 U/ml Penicillin-Streptomycin, Thermo Fisher 15140122) and digested with digestion buffer (Gibco DMEM/F12, Fisher 11320033; 4 µg/ml Roche Collagenase/Dispase, Sigma 10269638001; 10 µg/ml DNaseI, Sigma 1128459638001) for two rounds (45 min each) at 37 °C. Between rounds, previous digestion buffer was collected and neutralized with 20% FBS containing media in a new tube. New digestion buffer was added to the tissue and mixed vigorously, and digestion allowed to continue. After neutralization, cells were spun down at 600 × *g* for 5 min at 4 °C and mixed with Matrigel. For every 2 mice (4 uterine tubes), 100 µl of Matrigel would be used and plated along the rim of a 24 well tissue culture plate. Plates were then be incubated in 5% CO_2 cell incubator at 37 °C for 60 min, after which Matrigel would be set and organoid media (Gibco Advanced DMEM/F12, Thermo Fisher 12634010; 25% L-WRN Conditioned Medium, ATCC CRL-3276; 12 mM HEPES, Thermo Fisher 15630080; 1% GlutaMax, Thermo Fisher 35050079; 2% B27, Thermo Fisher 17504044; 1% N2, Thermo Fisher 17502048; 10 ng/ml hEGF, Sigma E9644; 100 ng/ml Human FGF-10, 1 mM Nicotinamide, Sigma N0636; 10 µM Y-27632 (ROCKi), Millipore 688000; 2.5 µM TGF-B RI Kinase Inhibitor VI, Millipore 616464) was added.

For passaging, organoids were released from Matrigel with organoid harvesting media (R&D 3700-100-01) by pipetting around the rim of the plate. Released cells were transferred to a 15 ml falcon tube and allowed to chill on ice for 1 h. Cells were then spun down in a refrigerated centrifuge at 600 × *g* for 5 min at 4 °C. Supernatant was aspirated, and 1 ml of TrypLE (Thermo Fisher 12604013) was added. Cells were then incubated at 37 °C for 10 min and vigorously pipetted. Cells were then recovered with 20% FBS

containing media and spun down at 600xg for 5 min at 4 °C. Supernatant was aspirated, organoid media was added, and cells were counted. Typically, cells were plated at 500 cells/µl of Matrigel for expansion. To induce Slc1a3-Cre-ERT mediated recombination, 1 µM 4-Hydroxytamoxifen (Selleck Chem S7827) was supplemented to the media for 48 h.

FACS preparation and analysis

Organoid cells were prepared as described above in organoid preparation. After rescuing cells from digestion, cells were washed in 1x PBS + 1% BSA three times. After the last wash, cells were suspended in 1x PBS + 1% BSA. FACS was performed on a Sony MA900 in two separate experiments with single replicates. Data was acquired using Sony MA-900 complementary software. Analysis was performed using FlowJo software (BD Biosciences). Post FACS, organoids were visualized under a microscope to check for tdTomato expression. Slc1a3-CreERT negative littermates were used to gate negative controls (Fig. 4). After gating single cells, Sytox Blue was used to gate for live or dead populations (Fig. 4). From the live cell population, tdTomato+ cells were determined by using Slc1a3-CreERT negative litter mates (Fig. 4). Cells were then plated in Matrigel at a density of 1000 cells per 10 µl. 1000 SLC1A3+ cells and 30,000 SLC1A3- cells were plated. Assessment of organoid forming potential was calculated by counting the number of organoids formed against the number of cells sorted. Each replicate contained uterine tubes pooled from at least 5 mice.

MACS preparation and analysis

Single cell suspensions from the distal mouse uterine tube were prepared as described above from 10 C57BL6 adult female mice aged 6–12 weeks. Magnetic activated cell

sorting was performed following the manufacturer protocol (Invitrogen 11533D). Negative selection was first performed to remove stromal cells by incubating cells with biotinylated antibodies against CD45 (Biolegend, 103103, 0.5 µg per million cells), TER-119 (Biolegend, 116203, 0.5 µg per million cells), CD140a (Biolegend, 135910, 0.5 µg per million cells), CD31 (Biolegend, 102503, 0.5 µg per million cells). Positive selection was then performed on the unbound fraction of cells by incubating with a biotinylated antibody against SLC1A3 (Novus biologicals, NB100-1869B, 0.5 µg per million cells). After removal of the unbound fraction, bound cells were released with 200U of DNase I (Sigma, 1128459638001). Cells were counted and equal numbers of cells were plated for both the SLC1A3+ and SLC1A3- populations (100 cells/µl Matrigel). 5000 cells were plated per Matrigel droplet in a 24 well plate. Representative images were taken every few days from plating to day 14. Day 14 organoids were counted for organoid formation rate, organoid size, and sections prepared to assess for expression of organoid markers.

Organoid histological preparation and analysis

Organoids were released from Matrigel with Cultrex Organoid Harvesting Solution and chilled on ice for 1 h as per the passaging protocol. Organoids were then centrifuged in a refrigerated centrifuge at 100 × *g* for 30 s at 4 °C. Organoids were fixed on ice in 5 ml of 4% PBS-buffered paraformaldehyde while avoiding exposure to light. Organoids were spun down at 100 × *g* for 30 s and replaced with 1x PBS to rinse. Organoids were spun down once more at 100 × *g* for 30 s to aspirate the remaining PBS. Organoids were then mixed in 200 µl of HistoGel (Epredia, HG4000012) preheated to 65 °C and dispensed into dome-shaped molds for embedding. HistoGel molds set for 10 min prior to standard

tissue processing, paraffin embedding, and preparation of 4-μm-thick tissue sections followed by immunohistochemistry (37).

3.6 References

1. Siegel RL, Giaquinto AN, Jemal A. Cancer statistics, 2024. CA Cancer J Clin. 2024 Jan 17;74(1):12–49.

2. Seidman JD, Ronnett BM, Shie Ie M, Cho KR, Kurman RJ. Blaustein's Pathology of the Female Genital Tract. Kurman RJ, Ellenson LH, Ronnett BM, editors. Springer; 2019.

3. Carlson JW, Gilks CB, Soslow RA. Tumors of the Ovary and Fallopian Tube. American Registry of Pathology; 2023.

4. Kurman RJ, Shih I-M. The origin and pathogenesis of epithelial ovarian cancer: a proposed unifying theory. Am J Surg Pathol. 2010 Mar;34(3):433–43.

5. Landen CN, Birrer MJ, Sood AK. Early events in the pathogenesis of epithelial ovarian cancer. J Clin Oncol. 2008 Feb 20;26(6):995–1005.

6. Kim J, Park EY, Kim O, Schilder JM, Coffey DM, Cho C-H, et al. Cell Origins of High-Grade Serous Ovarian Cancer. Cancers (Basel). 2018 Nov 12;10(11).

7. Zhang S, Dolgalev I, Zhang T, Ran H, Levine DA, Neel BG. Both fallopian tube and ovarian surface epithelium are cells-of-origin for high-grade serous ovarian carcinoma. Nat Commun. 2019 Nov 26;10(1):5367.

8. Lawrenson K, Fonseca MAS, Liu AY, Segato Dezem F, Lee JM, Lin X, et al. A Study of High-Grade Serous Ovarian Cancer Origins Implicates the SOX18 Transcription Factor in Tumor Development. Cell Rep. 2019 Dec 10;29(11):3726-3735.e4.

9. Hao D, Li J, Jia S, Meng Y, Zhang C, Wang L, et al. Integrated Analysis Reveals Tubal- and Ovarian-Originated Serous Ovarian Cancer and Predicts Differential Therapeutic Responses. Clin Cancer Res. 2017 Dec 1;23(23):7400–11.

10. Lõhmussaar K, Kopper O, Korving J, Begthel H, Vreuls CPH, van Es JH, et al. Assessing the origin of high-grade serous ovarian cancer using CRISPR-modification of mouse organoids. Nat Commun. 2020 May 27;11(1):2660.

11. Maniati E, Berlato C, Gopinathan G, Heath O, Kotantaki P, Lakhani A, et al. Mouse ovarian cancer models recapitulate the human tumor microenvironment and patient response to treatment. Cell Rep. 2020 Jan 14;30(2):525-540.e7.

12. Flesken-Nikitin A, Hwang C-I, Cheng C-Y, Michurina TV, Enikolopov G, Nikitin AY. Ovarian surface epithelium at the junction area contains a cancer-prone stem cell niche. Nature. 2013 Mar 14;495(7440):241–5.

13. Yamulla RJ, Nalubola S, Flesken-Nikitin A, Nikitin AY, Schimenti JC. Most Commonly Mutated Genes in High-Grade Serous Ovarian Carcinoma Are Nonessential for Ovarian Surface Epithelial Stem Cell Transformation. Cell Rep. 2020 Sep 1;32(9):108086.

14. Schmoeckel E, Odai-Afotey AA, Schleißheimer M, Rottmann M, Flesken-Nikitin A, Ellenson LH, et al. LEF1 is preferentially expressed in the tubal-peritoneal junctions and is a reliable marker of tubal intraepithelial lesions. Mod Pathol. 2017 Sep;30(9):1241–50.

15. Seidman JD. Serous tubal intraepithelial carcinoma localizes to the tubal-peritoneal junction: a pivotal clue to the site of origin of extrauterine high-grade serous carcinoma (ovarian cancer). Int J Gynecol Pathol. 2015 Mar;34(2):112–20.

16. Kuhn E, Kurman RJ, Vang R, Sehdev AS, Han G, Soslow R, et al. TP53 mutations in serous tubal intraepithelial carcinoma and concurrent pelvic high-grade serous carcinoma--evidence supporting the clonal relationship of the two lesions. J Pathol. 2012 Feb;226(3):421–6.

17. Lee Y, Miron A, Drapkin R, Nucci MR, Medeiros F, Saleemuddin A, et al. A candidate precursor to serous carcinoma that originates in the distal fallopian tube. J Pathol. 2007 Jan;211(1):26–35.

18. Perets R, Wyant GA, Muto KW, Bijron JG, Poole BB, Chin KT, et al. Transformation of the fallopian tube secretory epithelium leads to high-grade serous ovarian cancer in Brca;Tp53;Pten models. Cancer Cell. 2013 Dec 9;24(6):751–65.

19. Fu D-J, De Micheli AJ, Bidarimath M, Ellenson LH, Cosgrove BD, Flesken-Nikitin A, et al. Cells expressing PAX8 are the main source of homeostatic regeneration of adult mouse endometrial epithelium and give rise to serous endometrial carcinoma. Dis Model Mech. 2020 Oct 30;13(10).

20. Paik DY, Janzen DM, Schafenacker AM, Velasco VS, Shung MS, Cheng D, et al. Stem-like epithelial cells are concentrated in the distal end of the fallopian tube: a site for injury and serous cancer initiation. Stem Cells. 2012 Nov;30(11):2487–97.

21. Stewart CA, Behringer RR. Mouse oviduct development. Results Probl Cell Differ. 2012;55:247–62.

22. Avilés M, Coy P, Rizos D. The oviduct: A key organ for the success of early reproductive events. Animal Frontiers. 2015 Jan 1;5(1):25–31.

23. Ghosh A, Syed SM, Tanwar PS. In vivo genetic cell lineage tracing reveals that oviductal secretory cells self-renew and give rise to ciliated cells. Development. 2017 Sep 1;144(17):3031–41.

24. Ford MJ, Harwalkar K, Pacis AS, Maunsell H, Wang YC, Badescu D, et al. Oviduct epithelial cells constitute two developmentally distinct lineages that are spatially separated along the distal-proximal axis. Cell Rep. 2021 Sep 7;36(10):109677.

25. Flesken-Nikitin A, Odai-Afotey AA, Nikitin AY. Role of the stem cell niche in the pathogenesis of epithelial ovarian cancers. Mol Cell Oncol. 2014 Sep;1(3):e963435.

26. Fu D-J, Miller AD, Southard TL, Flesken-Nikitin A, Ellenson LH, Nikitin AY. Stem Cell Pathology. Annu Rev Pathol. 2018 Jan 24;13:71–92.

27. Nassar D, Blanpain C. Cancer stem cells: basic concepts and therapeutic implications. Annu Rev Pathol. 2016 May 23;11:47–76.

28. Fu D-J, Wang L, Chouairi FK, Rose IM, Abetov DA, Miller AD, et al. Gastric squamous-columnar junction contains a large pool of cancer-prone immature osteopontin responsive Lgr5-CD44+ cells. Nat Commun. 2020 Jan 3;11(1):84.

29. Friedmann-Morvinski D, Bushong EA, Ke E, Soda Y, Marumoto T, Singer O, et al. Dedifferentiation of neurons and astrocytes by oncogenes can induce gliomas in mice. Science. 2012 Nov 23;338(6110):1080–4.

30. Schwitalla S, Fingerle AA, Cammareri P, Nebelsiek T, Göktuna SI, Ziegler PK, et al. Intestinal tumorigenesis initiated by dedifferentiation and acquisition of stem-cell-like properties. Cell. 2013 Jan 17;152(1–2):25–38.

31. Rohozinski J, Diaz-Arrastia C, Edwards CL. Do some epithelial ovarian cancers originate from a fallopian tube ciliate cell lineage? Med Hypotheses. 2017 Sep;107:16–21.

32. Xie Y, Park E-S, Xiang D, Li Z. Long-term organoid culture reveals enrichment of organoid-forming epithelial cells in the fimbrial portion of mouse fallopian tube. Stem Cell Res. 2018 Oct;32:51–60.

33. Rose IM, Bidarimath M, Webster A, Godwin AK, Flesken-Nikitin A, Nikitin AY. WNT and inflammatory signaling distinguish human Fallopian tube epithelial cell populations. Sci Rep. 2020 Jun 17;10(1):9837.

34. Cancer Genome Atlas Research Network. Integrated genomic analyses of ovarian carcinoma. Nature. 2011 Jun 29;474(7353):609–15.

35. Flesken-Nikitin A, Choi K-C, Eng JP, Shmidt EN, Nikitin AY. Induction of carcinogenesis by concurrent inactivation of p53 and Rb1 in the mouse ovarian surface epithelium. Cancer Res. 2003 Jul 1;63(13):3459–63.

36. Nikitin AYu, Lee WH. Early loss of the retinoblastoma gene is associated with impaired growth inhibitory innervation during melanotroph carcinogenesis in Rb+/- mice. Genes Dev. 1996 Aug 1;10(15):1870–9.

37. Flesken-Nikitin A, Harlan BA, Nikitin AY. Transplantation into the mouse ovarian fat pad. J Vis Exp. 2016 Sep 7;(115).

Chapter 4: Fine tuning a TE organoid platform to enhance HGSC modeling and improve prognostic value in HGSC

This chapter is focused on briefly summarizing previous studies, future directions for the platform and a discussion on moving the platform into human studies.

4.1 Understanding and identifying new drivers are essential for finding new treatment options of HGSC.

My studies led to two key findings. First, ***Map2k4* as a driver of HGSC (**high-grade serous ovarian carcinoma) **transformation in mouse organoid models.** We further found that *Map2k4* mutations preferentially elicit papillary phenotypes in HGSC. Although both *Nf1* and *Map2k4* are part of the MAPK signaling pathway, cells with *Map2k4* mutations showed resistance to trametinib (a MEK inhibitor), but increased sensitivity to paclitaxel (a chemotherapy drug for HGSC treatment). Second, **SLC1A3 expressing cells are stem cells.** We found that SLC1A3 expressing cells function as a stem cell with organoid forming capacity. These organoids could differentiate into both the ciliated lineage and are predominantly located in the distal region of the mouse oviduct. Notably, these cells are not prone to developing cancer while KRT5 expressing cells are.

Despite progress, there are still gaps in our understanding of the cellular drivers and origins of cancer. For example, in our screen, we observed that certain organoid phenotypes might be predictive of tumor characteristics. Previous studies have suggested that the presentation of organoids can reflect the tumor characteristics in mouse models and patients (1–6). In our screen, we identified five different organoid phenotypes, but only two or three of these were consistently present during our validation studies. To gain deeper insights into how tumor subtypes are linked to specific organoid morphologies, I propose conducting a screen with the goal of separating different phenotypes and identifying the most common genetic alterations associated with each phenotype. This approach would allow us to correlate distinct organoid morphologies and behaviors with specific tumor types, providing a better understanding of how these features relate to HGSC progression.

Furthermore, different tumor presentations might reflect different stages of malignant transformation, which we would need to explore further. Ultimately, by using patient biopsy samples, this approach could help us study organoid transformation and identify potential biomarkers that predict cancer progression.

Through our SLC1A3 organoid lineage tracing experiments, we observed that not only did SLC1A3 expressing cells form organoids, but other cell types were also capable of doing so. In our initial screen, we utilized the heterogeneous population of cells that could form organoids. As shown in our organoid stains, TE organoids consist of a range of differentiated markers. To gain deeper insight into the mechanisms behind cell state and specific drivers, it might be valuable to target each individual organoid forming cell population. Doing so could help us determine if there are specific combinations of drivers within each cell type that might explain the absence of actionable recurrent point mutations in HGSC.

Although we have identified *Map2k4* mutations as important for high-grade serous carcinoma (HGSC), the role of this gene remains unclear. *Map2k4* is generally considered an oncogene due to its involvement in MAPK signaling and combination of MAP2K4 inhibitors with RAS inhibitors show great promise for treatment modalities (7,8) . However, studies in certain cancers, such as ovarian, prostate, and lung carcinomas, have suggested that *Map2k4* may act as a tumor suppressor gene in these contexts (8–12). This discrepancy could be due to cell-specific factors, and further research is needed to understand the conditions that determine whether *Map2k4* functions as an oncogene or as a tumor suppressor in different types of cancer. Additionally, these studies were conducted

in mouse models, and further investigation into human models may be valuable to fully elucidate the role of *Map2k4* in HGSC.

4.2 Correlating molecular subtypes and tumor characteristics

Previous organoid studies have reported various combinations of genes that result in the transformation of TE organoids into different tumor types. However, these studies have not investigated how different gene combinations lead to distinct tumor presentations. In the case of HGSC, known pathological tumor phenotypes include papillary, glandular, solid, and SET (solid, pseudoendometrioid, transitional). Molecularly, HGSC human samples have been classified into four subtypes: mesenchymal, immunoreactive, proliferative, and differentiated. While differentially expressed genes have been identified for each of these subtypes, the key gene drivers that initiate the formation of these subtypes are still unclear. Additionally, while organoid models have been employed to study HGSC, they have not fully explored how distinct gene drivers may lead to different tumor phenotypes. Though some studies have begun to examine the variations between these tumor subtypes, there is still inconclusive data on how these subtypes impact survival and response to common therapies. Our study focuses on a model involving *Map2k4* mutations, which preferentially form papillary tumors. This provides a unique opportunity to compare the impact of *Map2k4* mutations with that of *Nf1* mutations, which tend to form mesenchymal tumors. By combining these models with transcriptomic datasets, we can explore the molecular mechanisms driving the differences between these two tumor presentations. These insights could shed light on how early genetic mutations influence tumor transformation, offering new opportunities for prognostic tools and revealing potential targetable pathways at earlier stages of disease.

4.3 Identifying the minimal combinations of oncogenic drivers of HGSC

The transformation of a healthy cell into a malignant one typically involves both the loss of function of tumor suppressor genes and the gain of function of oncogenes. Our CRISPR knockout (KO) approach has primarily been used to study the role of tumor suppressor genes in malignancy. However, we have not yet explored the role of gene amplification events in high-grade serous carcinoma (HGSC). While our studies have shown that the loss of *Trp53/Nf1* or *Trp53/Pten* can lead to the transformation of organoids and are tumorigenic, further analysis reveals that these genes are involved in regulating *MYC* expression. When we looked at the most amplified genes in HGSC, *MYC* was the top hit (Table 1). This suggests that *MYC* amplification—either directly or via the loss of tumor suppressor genes—could be a key factor in the transformation into HGSC. However, *MYC* amplification is found in only 42% of HGSC cases, indicating that other gene amplification events may also contribute to transformation. We also find that *PIK3CA* and *CCNE1* to be in the list of top amplified genes and are associated with *PTEN* and *RB1* related genes respectively. Therefore, understanding what other amplification events compare to tumor suppressors in our screen are of utmost importance.

To further explore amplification events, we propose conducting a combinatorial CRISPR activation (CRISPRa) screen. This approach would help us identify the key oncogene drivers necessary for tumor transformation. Additionally, research has shown that overexpressing an oncogene or losing tumor suppressor genes in the same pathway can lead to varying chemoresponse profiles. This underscores the complexity of cancer transformation and treatment response, highlighting the need to consider both oncogene

activation and tumor suppressor loss in understanding cancer behavior and therapy outcomes.

4.4 Comparing Serous Carcinomas in the Ovary and Uterine Tube

Serous carcinomas are not limited to the ovary—they may also arise in the uterine tube. Studies suggest that serous endometrial carcinomas share many characteristics with HGSC, including mutations and gene drivers and pathological features. However, important differences exist, such as the absence of BRCA mutations and MDM2 mutations in endometrial carcinomas. These differences may point at various factors such as differences in cell of origin, specific genetic drivers to each cell type, as well as differences in the function and hostility of the tumor microenvironment. This highlights the need for further studies to understand these nuances in cancer origin and progression.

Table 1. Analysis of amplified genes in human HGSC (Firehose legacy dataset)

Gene	Amplification (%)
MYC	42.00%
NDRG1	38.00%
MECOM	36.40%
TERC	35.20%
AGO2	34.90%
RECQL4	34.00%
TONSL	34.00%
PRKCI	32.80%
MAL2	31.10%
EXT1	30.90%
RAD21	29.00%
PIK3CA	28.80%
TBL1XR1	28.70%
SOX2	26.90%
KLHL6	26.80%
DCUN1D1	26.60%
MAP3K13	26.40%
ETV5	25.60%
EIF4A2	24.50%
TFRC	24.20%
FGF12	23.80%
LPP	23.80%
BCL6	23.30%
EIF3E	23.10%
RSPO2	22.80%
TP63	22.60%
CCNE1	21.60%

4.5 The tumor microenvironment impacts HGSC initiation and progression

High-grade serous carcinoma (HGSC) begins with a specific cell of origin, but various factors such as immune cells, fibroblasts, and follicular fluid (FF) work both independently and synergistically to create a hostile, tumor-promoting environment (Figure 1).

Follicular fluid (FF) is a complex mixture that includes hormones, growth factors, cytokines, immune cells, and metabolites. These components can create an environment conducive to cellular transformation. FF is secreted by granulosa cells in the ovary, with additional contributions from theca cells, oocytes, and cumulus cells (12–16). In HGSC, estrogen, progesterone, and androgen receptor expressions vary. Estrogen receptors are most highly expressed (80-95% of HGSC cases) and have been associated with poorer survival outcomes (17–19). This may be due to the cyclic nature of estrogen exposure, which induces inflammation and increases DNA damage in the fallopian tube(19). In contrast, progesterone and androgen receptors are expressed in 20-50% of HGSC cases, with their presence correlating with better survival and chemotherapy response (18). Understanding how FF components transform healthy cells into malignant cells such as driving specific genetic alterations at recurrent sites will aid in more prognostic tools at earlier stages.

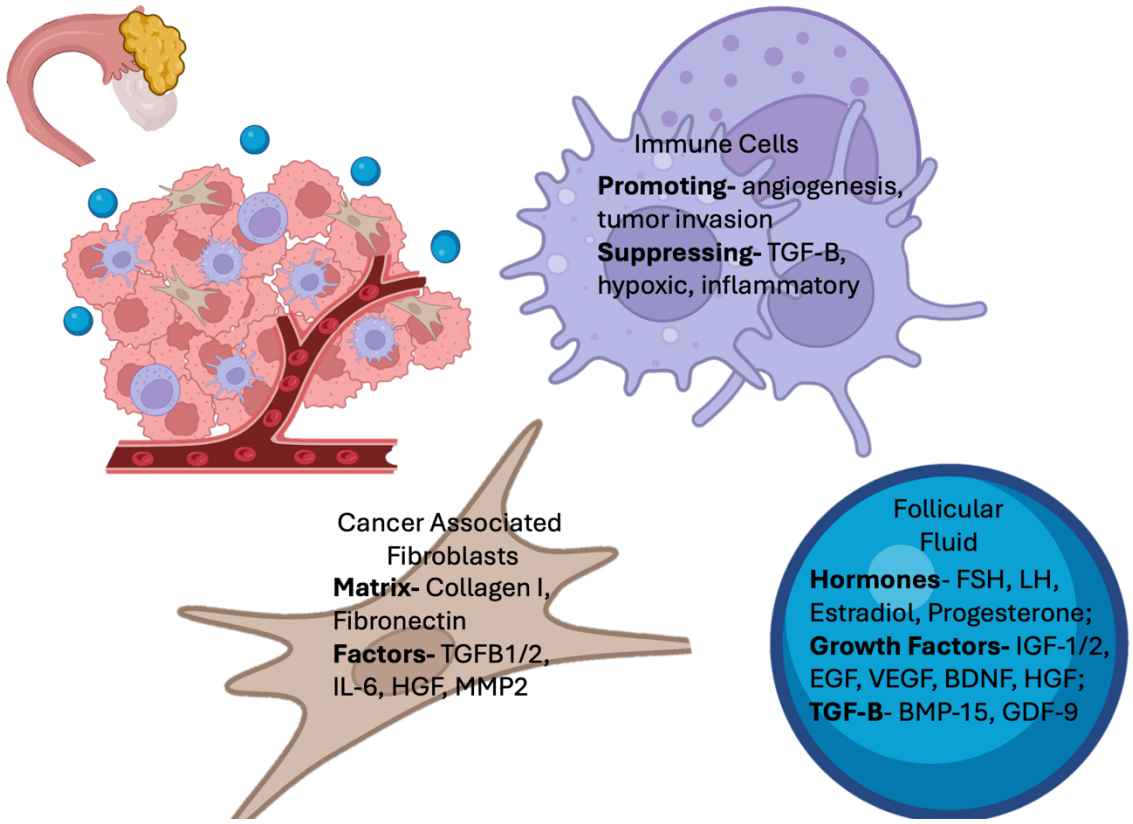

Figure 1. Tumor microenvironment that influences HGSC initiation and progression. Created with help from biorender.com.

Immune cells play a critical role in the evolution of HGSC and its response to chemotherapy. Immature dendritic cells, M2 macrophages, regulatory T cells (Tregs), and myeloid-derived suppressor cells (MDSCs) all contribute to immune tolerance and therapeutic resistance in HGSC (20). Specifically, M2 macrophages secrete TH2 cytokines that promote angiogenesis and tumor invasion (21), while Tregs suppress effector T cells, creating an immunosuppressive environment (21). MDSCs also impair T cell activation and the function of other immune cells (21). Additionally, environmental factors like hypoxia, inflammation, and elevated TGF-B levels can compromise dendritic cell function and T cell activity (21). Moreover, the N-MYC gene, amplified in HGSC, has been shown to inhibit innate immune signaling, contributing to poor responses to immunotherapy (22).

Cancer-associated fibroblasts (CAFs) represent a significant stromal cell population in HGSC tumors and their metastases (23,24). CAFs secrete growth factors, inflammatory cytokines, and extracellular matrix (ECM) proteins, promoting angiogenesis, tumor invasion, and chemoresistance through ECM remodeling (23,25–27). Together, FF, immune cells, and CAFs play vital roles in the HGSC tumor microenvironment, contributing to both initiation and progression. Despite their importance, studies modeling these factors and their tumorigenic potential are still in the early stages.

To study these factors more effectively, we can use co-culture methods that combine immune cells and CAFs or recreate FF-like conditions in vitro. These models will enable us to better understand how different insults impact genome vulnerability and cause changes in the genome landscape. This approach offers a high-throughput way to explore the tumor microenvironment’s influence on cell transformation.

4.6 Developing a Human Organoid Screening Platform for Early HGSC Events

While most studies have focused on mouse models, the establishment of human organoid platforms has now been achieved. However, their application to study early transformation events has not been fully explored. Our platform could serve as a pre-screening tool, allowing us to characterize organoid phenotypes and standardize their malignant potential. Additionally, human-derived tubal organoids could be used to study early initiation events and improve our understanding of targeted therapies.

The development of a platform that combines genetic perturbations with phenotypic analysis could lead to improved screening technologies for HGSC. Historically, studying genetic drivers in HGSC has been challenging, but early detection can significantly improve patient survival outcomes. By isolating cells from patient biopsies, deriving organoids, and performing histological evaluations, disease progression models, treatment response analyses, and multi-omic assessments, we could build more accurate models of HGSC initiation and progression. Traditional PDX-1 models lack the scalability and high throughput capacity of organoid models (29). Organoid approaches could help identify the most effective treatments for individual patients and ultimately improve patient survival. Furthermore, this system could be expanded into a pan-cancer repository, allowing us to compare similarities and differences across various pre-cancerous conditions.

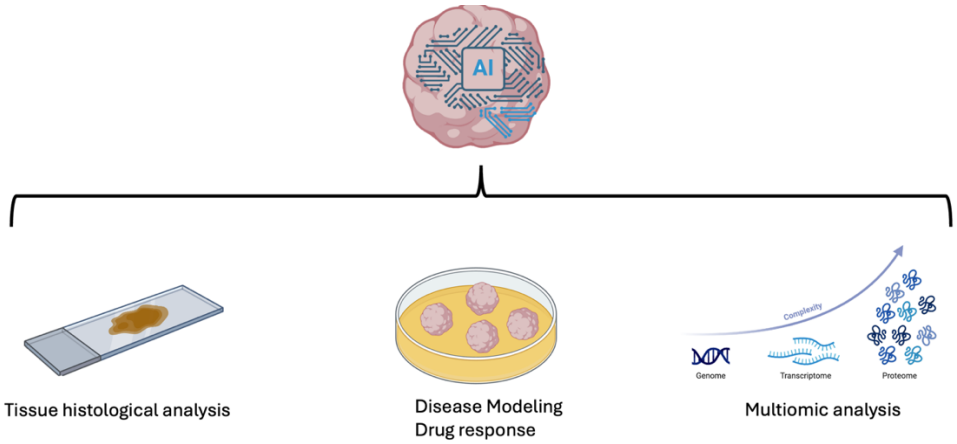

Figure 2. Comprehensive platform for assessing human organoids. Created with help from biorender.com.

4.7 References

1. Jiang X, Oyang L, Peng Q, Liu Q, Xu X, Wu N, et al. Organoids: opportunities and challenges of cancer therapy. Front Cell Dev Biol. 2023 Jul 27;11:1232528.

2. Minoli M, Cantore T, Hanhart D, Kiener M, Fedrizzi T, La Manna F, et al. Bladder cancer organoids as a functional system to model different disease stages and therapy response. Nat Commun. 2023 Apr 18;14(1):2214.

3. Karolak A, Poonja S, Rejniak KA. Morphophenotypic classification of tumor organoids as an indicator of drug exposure and penetration potential. PLoS Comput Biol. 2019 Jul 16;15(7):e1007214.

4. Nanki Y, Chiyoda T, Hirasawa A, Ookubo A, Itoh M, Ueno M, et al. Patient-derived ovarian cancer organoids capture the genomic profiles of primary tumours applicable for drug sensitivity and resistance testing. Sci Rep. 2020 Jul 28;10(1):12581.

5. Hoffmann K, Berger H, Kulbe H, Thillainadarasan S, Mollenkopf H-J, Zemojtel T, et al. Stable expansion of high-grade serous ovarian cancer organoids requires a low-Wnt environment. EMBO J. 2020 Mar 16;39(6):e104013.

6. Vias M, Morrill Gavarró L, Sauer CM, Sanders DA, Piskorz AM, Couturier D-L, et al. High-grade serous ovarian carcinoma organoids as models of chromosomal instability. eLife. 2023 May 11;12.

7. Jansen RA, Mainardi S, Dias MH, Bosma A, van Dijk E, Selig R, et al. Small-molecule inhibition of MAP2K4 is synergistic with RAS inhibitors in KRAS-mutant cancers. Proc Natl Acad Sci USA. 2024 Feb 27;121(9):e2319492121.

8. Xue Z, Vis DJ, Bruna A, Sustic T, van Wageningen S, Batra AS, et al. MAP3K1 and MAP2K4 mutations are associated with sensitivity to MEK inhibitors in multiple cancer models. Cell Res. 2018 Jul;28(7):719–29.

9. Pavese JM, Ogden IM, Voll EA, Huang X, Xu L, Jovanovic B, et al. Mitogen-activated protein kinase kinase 4 (MAP2K4) promotes human prostate cancer metastasis. PLoS ONE. 2014 Jul 14;9(7):e102289.

10. Liu S, Huang J, Zhang Y, Liu Y, Zuo S, Li R. MAP2K4 interacts with Vimentin to activate the PI3K/AKT pathway and promotes breast cancer pathogenesis. Aging (Albany NY). 2019 Nov 25;11(22):10697–710.

11. Huang L, Wu C, Yu D, Wang C, Che X, Miao X, et al. Identification of common variants in BRCA2 and MAP2K4 for susceptibility to sporadic pancreatic cancer. Carcinogenesis. 2013 May;34(5):1001–5.

12. Davis SJ, Choong DYH, Ramakrishna M, Ryland GL, Campbell IG, Gorringe KL. Analysis of the mitogen-activated protein kinase kinase 4 (MAP2K4) tumor suppressor gene in ovarian cancer. BMC Cancer. 2011 May 17;11:173.

13. Liu T, Huang Y, Lin H. Estrogen disorders: Interpreting the abnormal regulation of aromatase in granulosa cells (Review). Int J Mol Med. 2021 May;47(5).

14. Xu X-L, Huang Z-Y, Yu K, Li J, Fu X-W, Deng S-L. Estrogen biosynthesis and signal transduction in ovarian disease. Front Endocrinol (Lausanne). 2022 Mar 1;13:827032.

15. Rodgers RJ, Irving-Rodgers HF. Formation of the ovarian follicular antrum and follicular fluid. Biol Reprod. 2010 Jun;82(6):1021–9.

16. Da Broi MG, Giorgi VSI, Wang F, Keefe DL, Albertini D, Navarro PA. Influence of follicular fluid and cumulus cells on oocyte quality: clinical implications. J Assist Reprod Genet. 2018 May;35(5):735–51.

17. Revelli A, Delle Piane L, Casano S, Molinari E, Massobrio M, Rinaudo P. Follicular fluid content and oocyte quality: from single biochemical markers to metabolomics. Reprod Biol Endocrinol. 2009 May 4;7:40.

18. Osaku D, Oishi T, Kawamura N, Iida Y, Komatsu H, Kudoh A, et al. Differential expression of estrogen receptor subtypes in ovarian high-grade serous carcinoma and clear cell carcinoma. Reprod Med Biol. 2021 Oct;20(4):467–76.

19. Tan J, Song C, Wang D, Hu Y, Liu D, Ma D, et al. Expression of hormone receptors predicts survival and platinum sensitivity of high-grade serous ovarian cancer. Biosci Rep. 2021 May 28;41(5).

20. Dodds LV, Sanchez-Covarrubias AP, Sowamber R, Milea A, Pinto A, Ban Y, et al. Hormone Receptor Expression and Disease Prognosis in High-Grade Serous Ovarian Cancer. medRxiv. 2023 Apr 23;

21. Luo X, Xu J, Yu J, Yi P. Shaping immune responses in the tumor microenvironment of ovarian cancer. Front Immunol. 2021 Jun 23;12:692360.

22. Chen J, Yang L, Ma Y, Zhang Y. Recent advances in understanding the immune microenvironment in ovarian cancer. Front Immunol. 2024 Jun 5;15:1412328.

23. Miranda A, Pattnaik S, Hamilton PT, Fuss MA, Kalaria S, Laumont CM, et al. N-MYC impairs innate immune signaling in high-grade serous ovarian carcinoma. Sci Adv. 2024 May 17;10(20):eadj5428.

24. Xu AM, Haro M, Walts AE, Hu Y, John J, Karlan BY, et al. Spatiotemporal architecture of immune cells and cancer-associated fibroblasts in high-grade serous ovarian carcinoma. Sci Adv. 2024 Apr 19;10(16):eadk8805.

25. Li Y, Tian R, Liu J, Li J, Tan H, Wu Q, et al. Deciphering the immune landscape dominated by cancer-associated fibroblasts to investigate their potential in indicating prognosis and guiding therapeutic regimens in high grade serous ovarian carcinoma. Front Immunol. 2022 Sep 2;13:940801.

26. Zhang M, Chen Z, Wang Y, Zhao H, Du Y. The Role of Cancer-Associated Fibroblasts in Ovarian Cancer. Cancers (Basel). 2022 May 26;14(11).

27. Yang D, Liu J, Qian H, Zhuang Q. Cancer-associated fibroblasts: from basic science to anticancer therapy. Exp Mol Med. 2023 Jul 3;55(7):1322–32.

28. Hansen JM, Coleman RL, Sood AK. Targeting the tumour microenvironment in ovarian cancer. Eur J Cancer. 2016 Mar;56:131–43.

29. Xu H, Jiao D, Liu A, Wu K. Tumor organoids: applications in cancer modeling and potentials in precision medicine. J Hematol Oncol. 2022 May 12;15(1):58.